NASA Contractor Report 3786

An Empirical Method for Predicting the Mixing Noise Levels of Subsonic Circular and Coaxial Jets

James W. Russell

CONTRACT NAS1-16000
FEBRUARY 1984

NASA

NASA Contractor Report 3786

An Empirical Method for Predicting the Mixing Noise Levels of Subsonic Circular and Coaxial Jets

James W. Russell
Kentron International, Inc.
Hampton, Virginia

Prepared for
Langley Research Center
under Contract NAS1-16000

National Aeronautics
and Space Administration

Scientific and Technical
Information Office

1984

TABLE OF CONTENTS

SUMMARY

This report applies the method of Zorumski and Weir (reference 8) to the prediction of static free field source mixing noise levels of subsonic circular and coaxial jet flow streams. An extensive jet noise data base has been developed from nine series of jet noise tests. These series include 214 tests of circular nozzles and 603 tests of coaxial nozzles.

The jet noise, which is a function of frequency and direction, is expressed in terms of four components. These components are the overall power level, the power spectrum level, the overall directivity index, and the relative spectrum level. The relative spectrum is the difference between the sound pressure spectrum level in a fixed direction and the sound power spectrum level.

Sound pressure level data from each test were curve fitted in both the frequency dimension and directivity dimension using bicubic splines. The curve fits, which provide smoothing of the experimental data, are made in the least squares sense. The bicubic splines use a standard grid of seven (7) frequency parameter values and seven (7) directivity angles. The values of the component noise levels at these grid points are referred to as noise level coordinates. These noise level coordinates define the component noise levels for all frequencies and directivities through the bicubic spline function.

Each of the noise level coordinates is a function of the jet flow state. The flow state of a coaxial jet is defined by five (5) independent parameters. The parameters employed here are the equivalent jet velocity, the equivalent jet total temperature, the velocity ratio (of the outer stream to the inner stream), the temperature ratio, and the area ratio. The equivalent flow state variables are defined by equating the values for mass flow, momentum (thrust), and enthalpy of the coaxial jet to an equivalent circular jet.

The noise level coordinates are curve fitted in the five dimensional flow state space by a third order Taylor series. Each jet noise test provides one data point in this five dimensional space for each noise level coordinate. The 817 tests were employed to determine the 56 independent terms in each Taylor series

through the least squares criterion. Because many of the tests were grouped in limited regions of the flow state space while some of the regions of the space were empty, it was possible to determine only 36 unique constants of the 56 constants in the Taylor series.

The empirical method used here reduces the data base of approximately 200,000 sound pressure level measurements to a table of 2,300 constants which can be used to predict the jet mixing noise. Because this prediction method is derived from a least squares approximation to the data base, the mean error is 0 dB. The standard error of the prediction is less than 1.0 dB at the frequencies and directivities where the peak noise levels occur. The peak level frequency parameter (Strouhal number) is near -0.5 and the peak level directivity angles are near 150 degrees (measured from the forward axis of the jet). At high and low frequencies and at directivity angles near the jet axis the estimate of standard error is greater than 2.0 dB. The standard error based on all frequencies and directivity angles is 1.5 dB.

INTRODUCTION

The purpose of this report is to develop an empirical method for predicting the static source noise levels of jet mixing noise from both circular and coaxial subsonic flow jet streams. Supersonic flow jet streams were excluded because of the presence of shock noise in addition to jet mixing noise.

There are currently several empirical methods available for predicting the static source noise levels of both circular and coaxial jets. Usually these methods are restricted to certain jet flow regimes such as subsonic, supersonic, or coaxial jets with inverted flow profiles. Most of the current coaxial jet noise prediction methods, especially those with inverted flow profiles, employ two spectra, one for the outer stream alone and one for the premerged stream. Stone (reference 1), Pao (reference 2), Russell (reference 3), and Jaeck (reference 4) all use the two-spectra methodology. In addition there are several methods available for predicting circular jet noise. Among these is the method of Jaeck (reference 5), Stone (references 1 and 6), and the SAE method (reference 7). In addition Stone (reference 1) predicted noise levels of a wide range of nozzle types including coaxial jets. However, none of these jet noise prediction methods treat the circular jet and coaxial jet together. Therefore, in 1982 Zorumski and Weir (reference 8) developed a curve fitting technique which provided for the empirical static jet source noise prediction for coaxial jets where the circular jet is treated as a special case of the coaxial jet.

The prediction method presented herein applies the empirical curve fitting method developed by Zorumski and Weir (reference 8) to the jet mixing noise, The correlations are based on a different set of jet flow properties than those of reference 8. Furthermore, this report extends both the range of directivity angles and the frequency range employed by Zorumski and Weir. Also additional model test data sets have been included in the prediction method of this report.

The method presented herein equates the coaxial jet to a single stream equivalent jet which has the same mass flow, energy flow, and thrust as the coaxial jet. The coaxial jet noise levels are then defined as functions of the equivalent jet state properties which are velocity, temperature, and three of the ratios of state properties of each jet flow stream. These ratios are velocity (outer stream to inner stream), temperature, and area.

The empirical correlations presented in this report are based on 817 static model jet noise tests from five different industry and government sources in three nations. This data base includes nine separate test series.

LIST OF SYMBOLS

A	Nozzle exit flow area	m^2
A_e	Nozzle exit flow area of single equivalent jet	m^2
A_{ref}	Reference area used in computing normalized overall power level	m^2
A_1	Nozzle exit flow area of inner stream or circular jet	m^2
A_2	Nozzle exit flow area of outer stream	m^2
c_{ISA}	Speed of sound at ISA, SL conditions	m/s
c_p	Specific heat of gas at constant pressure	J/(kg k)
c_∞	Ambient speed of sound	m/s
$D(\theta)$	Directivity Index	dB
$D(\theta_c)$	Directivity Index of coordinate point	dB

$D_{,j}(\theta_c)$	Derivative value for directivity index at coordinate point	
D_e	Nozzle exit flow diameter of single equivalent jet	m
f	One-third octave band center frequency	Hz
f_p	One-third octave band predicted center frequency	Hz
F(f)	One-third octave band normalized power spectrum at center frequency f	dB
$F(\eta)$	One-third octave band normalized power spectrum	dB
$F(\eta_c)$	One-third octave band normalized power spectrum at coordinate point	dB
$F(\eta_p)$	One-third octave band normalized power spectrum at predicted point	dB
$F_{,j}(\eta_c)$	Derivative value of one-third octave band normalized power spectrum at coordinate point	
ISA	International Standard Atmosphere	
j	Index for derivative value	
k_1, k_2, k_3, k_4	Constant terms used in computation of SPL and PWL	dB
$\dot{m}_e$	Mass flow rate of single equivalent jet	kg/s
$\dot{m}_1$	Mass flow rate of inner stream or circular jet	kg/s
$\dot{m}_2$	Mass flow rate of outer stream	kg/s
N	Number of derivatives and derivative multipliers employed in computation of $\overline{OAPWL}$, $D(\theta_c)$, $F(\eta_c)$ and $RSL(\theta_c, \eta_c)$	
OAPWL	Overall acoustic power level	dB
$\overline{OAPWL}$	Normalized overall acoustic power level	dB
$OASPL(\theta)$	Overall sound pressure level	dB
$OASPL(\theta_c)$	Overall sound pressure level at directivity coordinate point	dB
$OASPL(\theta_m)$	Overall sound pressure level at measured directivity angle	dB
$OASPL(\theta_p)$	Overall sound pressure level at predicted directivity angle	dB
$\overline{OASPL}$	Average overall sound pressure level over surface area of sphere at microphone radius	dB
p_{ref}^2	Reference mean square pressure level	N^2/m^4
$PWL(\eta_c)$	One-third octave band power spectrum level at coordinate point	dB
$PWL(f_p)$	One-third octave band power spectrum level at predicted frequency	dB

$PWL_{,j}$	Derivative values for overall acoustic power level	
r	Radial distance from nozzle exit to observer	m
R	Gas constant	J/(kg k)
$RSL(\theta,f)$	Normalized relative spectrum level	dB
$RSL(\theta,\eta)$	Normalized relative spectrum level	dB
$RSL(\theta_c,\eta_c)$	Normalized relative spectrum level at coordinate point	dB
$RSL(\theta_p,\eta_p)$	Normalized relative spectrum level at predicted directivity angle and predicted normalized frequency parameter	dB
$RSL_{,j}(\theta_c,\eta_c)$	Derivative values of normalized relative spectrum level at coordinate point	
$SPL(\theta,f)$	Sound pressure level	dB
$SPL(\theta,\eta)$	Sound pressure level	dB
$SPL(\theta_m,f)$	Measured sound pressure level	dB
$\tilde{SPL}(\theta_c,\eta_c)$	Smoothed sound pressure level at coordinate point	dB
$\tilde{SPL}(\theta_m,\eta_c)$	Smoothed sound pressure level from measured data	dB
$SPL(\theta_p,\eta_p)$	Sound pressure level at predicted directivity angle and predicted frequency	dB
t_∞	Ambient static temperature	k
T_e	Nozzle exit flow equivalent jet total temperature	k
T_1	Nozzle exit flow total temperature of inner stream or circular jet	k
T_2	Nozzle exit flow total temperature of outer stream	k
V	Nozzle exit flow velocity	m/s
V_e	Nozzle exit equivalent flow velocity	m/s
V_1	Nozzle exit flow velocity of inner stream or circular jet	m/s
V_2	Nozzle exit flow velocity of outer stream	m/s
w_{ref}	Reference power level	w
x	Nozzle exit flow parameters	
X_i	Derivative multiplier values	

Greek Symbols:

α_i	Prediction parameter
α_{ir}	Standard value for prediction parameter
γ	Ratio of specific heats
γ_e	Nozzle exit flow specific heat ratio of equivalent jet

γ_1	Nozzle exit flow specific heat ratio of inner stream or circular jet	
γ_2	Nozzle exit flow specific heat ratio of outer stream	
η	Normalized frequency parameter	
η_c	Normalized frequency parameter at coordinate point	
η_p	Normalized frequency parameter at predicted point	
θ	Directivity angle relative to inlet axis	degrees
θ_m	Measured directivity angle relative to inlet axis	degrees
θ_c	Directivity angle at coordinate point	degrees
θ_p	Directivity angle at predicted point	degrees
ρ	Density	kg/m^3
ρ_e	Nozzle exit flow density of single equivalent jet	kg/m^3
ρ_{ISA}	Density of air under ISA, SL conditions	kg/m^3
ρ_∞	Ambient air density	kg/m^3
ϕ	Azimuth directivity angle	degrees

Abbreviations:

GELAC	Lockheed Georgia Company
LeRC	National Aeronautics and Space Administration Lewis Research Center
NGTE	National Gas Turbine Establishment (England)
PWA	Pratt and Whitney Aircraft Company
SNECMA	Societe Nationale d'Etude et de Construction de Motuers d'Aviation (France)

DATA BASE DESCRIPTION

The data base consists of noise and flow state data from nine different model test series listed in Table I. These data are from five different industry and government sources in three nations. They include 603 coaxial jet tests with subsonic flow in both the inner stream and outer stream and 214 subsonic flow circular jet tests. The test data were classified according to the flow state parameters of the jet which are used to define the jet noise levels. These flow state parameters are the equivalent flow velocity (V_e/c_∞), the equivalent total temperature (T_e/t_∞), the ratio of the secondary jet velocity to the primary jet velocity (V_2/V_1), the ratio of the secondary jet total temperature to the primary jet total temperature (T_2/T_1), and the ratio of the secondary jet area to the primary jet area (A_2/A_1). The detailed definitions of the equivalent flow state parameters are presented later in this report. The range of values for each of these flow state parameters was geometrically divided into four subsets with the geometric mean value of each parameter being used to identify the subset of the parameter range. Table II lists the ranges of the subsets and their geometric means for each flow state parameter.

The majority of the data (502 test cases) was supplied by the National Gas Turbine Establishment (NGTE) of England and includes both circular jet data and coaxial jet data from three different test series. The area ratio for the coaxial jet data varied from 2.0 to 6.0 for NGTE Set A and from 1.4 to 8.1 for NGTE Set C. For both coaxial jet data sets, the temperature of the outer stream was maintained near ambient and, because only subsonic jet data were employed, the outer stream velocity was less than the ambient speed of sound. The test data for NGTE Set A are classified graphically in figure 1 and the NGTE Set C test data are classified graphically in figure 2. NGTE Set B was not used. Figure 3 shows the graphical classification of equivalent velocity and equivalent total temperature for the circular jet data of NGTE Set D. The numbers shown on the figures indicate the number of tests which are classified in the particular subset defined by the mean value of the flow parameters.

Pratt and Whitney Aircraft (PWA) provided 50 test points which include both circular and coaxial jet data at area ratios of 0.75 and 1.20. The data obtained from reference 9 includes many tests with high temperature outer stream flow, resulting in higher outer stream velocities. Figure 4 shows the graphical classification of the circular jet and coaxial jet data respectively.

The Societe Nationale d'Etude et de Construction de Moteurs d'Aviation (SNECMA) of France provided 78 test data points from two test series. SNECMA Set A includes 4 circular jet tests and 30 coaxial jet tests at an area ratio of 3.52. These data are classified graphically on figure 5. SNECMA Set B consists of coaxial jet test data at area ratios of 2.25, 3.92, and 6.09. These data are classified graphically on Figures 6. Like the NGTE data, all the SNECMA coaxial jet tests maintain the outer stream flow temperature at or near ambient conditions, whereas for most tests the inner stream flow was heated.

The Lockheed Georgia Company (GELAC) provided two data sets. GELAC Set A (reference 10) consists of 59 circular jet tests which are classified graphically in figure 7. GELAC Set B consists of 32 coaxial jet tests at an area ratio of 2.93. Figure 8 shows the graphical classification of this data. The outer stream velocity of the coaxial jet tests of Set B is less than the ambient speed of sound even though the temperature of the outer stream ranges above the ambient temperature level.

The National Aeronautics and Space Administration Lewis Research Center (LeRC) provided one set of 96 tests (references 11 and 12) including both circular jet and coaxial jet data with area ratios ranging from 1.2 to 3.33. The LeRC coaxial jet data base does include tests with high temperatures and/or high velocity outer streams. Figure 9 shows the graphical classification of the LeRC circular and coaxial jet data.

The graphical classification of all the data is summarized in figure 10 for the circular jet and each of the area ratio subset ranges listed in Table II. The distribution of the test points shown in figure 10 has a significant effect on the data reduction process. It is necessary to have test points in all regions of the classification graphs in order to completely define the constants in the Taylor series for the noise level coordinates. In figure 10(a) the circular jet test points form a banded matrix pattern in the equivalent variables V_e/c_∞ and T_e/t_∞, with the majority of tests on or near the diagonal. The coaxial jet test points with area ratio near unity, figure 10(b), fall in the central region of the graph with a bias toward velocity ratios greater than one and temperature ratios less than one. Many regions of these classification graphs are empty, while other regions have a large number of repeated tests. Note for the circular jet figure 10(a), there are 75 tests in the subset defined by $V_e/c_\infty = 0.707$ and $T_e/t_\infty = 1.414$. Also, figure 10(d) shows 69 tests in the subset defined by $V_e/c_\infty = 0.707$, $T_e/t_\infty = 1.414$, $V_2/V_1 = 0.667$ and $T_2/T_1 = 0.354$. Table I presents the ranges for the directivity angle, frequency, and the normalized velocity and normalized temperatures of both the inner stream and outer stream for each data set at each area ratio.

Also shown in Table I is the amount of protrusion of the primary nozzle for the coaxial jet nozzle data. The NGTE Set C had primary nozzle protrusions varying from 0 to 4.5 primary jet nozzle diameters. The SNECMA data had primary nozzle protrusions of 2.0 and 1.0 primary jet nozzle diameters for Sets A and B respectively. The PWA data had primary nozzle protrusions varying from 0.3 to 0.4 primary jet nozzle diameters. Cursory evaluations of the data have indicated that the effects of primary nozzle protrusion on the measured jet exhaust noise levels are minimal relative to the effects of flow state parameters. Therefore, the effect of primary nozzle protrusion on coaxial jet noise levels is not included in this report.

DATA BASE ORGANIZATION

The jet one-third octave band sound pressure level which is a function of directivity and frequency, $SPL(\theta,f)$, can be expressed as a summation of four components. These are the normalized overall power level, $\overline{OAPWL}$, the power spectrum level, $F(f)$, the directivity index, $D(\theta)$, and the relative spectrum level $RSL(\theta,f)$. Thus the sound pressure level can be expressed as

$$SPL(\theta,f) = \overline{OAPWL} + D(\theta) + F(f) + RSL(\theta,f) + k_1 + k_2 + k_3 , \qquad (1)$$

where k_1, k_2, and k_3 are constants to account for the size of the jet, the microphone distance, the ambient conditions, and the ratio between the reference power level and the reference mean square pressure level.

To correlate the jet noise from different jet flow conditions, a frequency parameter term was used rather than frequency. The frequency parameter, η, is related to frequency, f, by

$$\eta = 10 \log_{10} \frac{fD_e}{V_e} , \qquad (2)$$

where V_e and D_e are the equivalent velocity and equivalent diameter of the coaxial or circular jet. Thus equation 1 can be expressed as

$$SPL(\theta,\eta) = \overline{OAPWL} + D(\theta) + F(\eta) + RSL(\theta,\eta) + k_1 + k_2 + k_3 . \qquad (3)$$

In addition to the $\overline{OAPWL}$, the directivity, $D(\theta)$, the power spectrum level, $F(\eta)$, and the relative spectrum level, $RSL(\theta,\eta)$, were empirically defined as a function of the flow state parameters at seven directivity coordinate points, θ_C, and seven frequency parameter coordinate points, η_C. The directivity coordinate points are 0, 30, 60, 90, 120, 150, and 180 degrees. The frequency parameter coordinate points are -1.5, -1.0, -0.5, 0.0, 0.5, 1.0, and 1.5. Figure 11 shows the coordinate point grid. By defining the four components at each of these coordinate or node points, bicubic spline curves can be fit to the grid and the jet noise characteristics can be defined for all directivities and frequencies.

For each test the measured sound pressure level data were curve fitted first in the frequency direction and then in the directivity direction using cubic splines in a least squares sense to obtain smooth one-third octave-band sound pressure levels. At each directivity angle, the data were smoothed over the frequency range using cubic splines having natural (zero curvature) end conditions. These smoothed sound pressure levels, $\widetilde{SPL}(\theta_m,f)$, were then logarithmically summed to obtain the overall sound pressure levels at the measured directivities as follows:

$$OASPL(\theta_m) = 10 \log_{10} \sum_f 10^{\left(\frac{SPL\ (\theta_m,f)}{10}\right)} \qquad (4)$$

Furthermore the smoothed sound pressure level data were interpolated to obtain sound pressure level data at those frequency parameter coordinate points which lie within the data range $\widetilde{SPL}(\theta_m,\eta_C)$. Because of the limited frequency range, only four or five values of the frequency parameter coordinate points were computed for each test case. Most of the tests provided data for the midrange of the frequency parameter coordinate points. However at the end points (-1.5 and 1.5) there was limited data. The table below shows the number of tests for each frequency parameter coordinate point.

Frequency parameter coordinate point, η_C	-1.5	-1.0	-0.5	0.0	0.5	1.0	1.5
Number of tests	109	570	806	806	806	703	232

Also the test data generally did not cover directivity angles less than 45 degrees or greater than 160 degrees. Figure 12 shows typical examples of the range of test data relative to the grid coordinate points. By using cubic splines which have zero slope at the end points (θ = 0 and 180 degrees), the OASPL(θ_m) values and the SPL(θ_m,η_c) values were curve fit in a least squares sense to obtain smooth OASPL values and smooth sound pressure level values, $\tilde{\text{SPL}}(\theta_m,\eta_c)$, for all directivity angles, θ, at the frequency coordinate points where test data is available. By interpolation, the, OASPL values and the $\tilde{\text{SPL}}$ values at the coordinate points were obtained, OASPL(θ_c) and $\tilde{\text{SPL}}(\theta_c,\eta_c)$.

This is basically the same technique employed by Zorumski and Weir (reference 8) where the use of bicubic splines is discussed in more depth. From the values of OASPL(θ) and the values of $\tilde{\text{SPL}}(\theta,\eta_c)$ for all directivities at the normalized frequency parameter coordinate points, the values of overall power level, OAPWL, and one-third octave band power spectrum level, PWL(η_c), are computed as follows:

$$\text{OAPWL} = 10 \log_{10} \left[\int_A 10^{\left(\frac{\text{OASPL}(\theta)}{10}\right)} dA \right] + k_4 , \qquad (5)$$

and

$$\text{PWL}(\eta_c) = 10 \log_{10} \left[\int_A 10^{\left(\frac{\tilde{\text{SPL}}(\theta,\eta_c)}{10}\right)} dA \right] + k_4 , \qquad (6)$$

where k_4 is a constant to obtain the one-third octave band power spectrum in dB units and is defined by

$$k_4 = 10 \log_{10} \left(\frac{p_{ref}^2}{\rho_\infty c_\infty W_{ref}} \right). \qquad (7)$$

The incremental spherical area, dA, is defined by

$$dA = r^2 \sin \theta \, d\phi . \qquad (8)$$

For an axisymmetric source equations 5 and 6 can be written as

$$\mathrm{OAPWL} = 10\ \log_{10}\left[\ 2\pi r^2 \int_0^{\pi} 10^{\left(\frac{\mathrm{OASPL}(\theta)}{10}\right)} \sin\theta\ d\theta\right] + 10\ \log_{10}\left(\frac{p_{ref}^2}{\rho_\infty c_\infty W_{ref}}\right) \qquad (9)$$

and

$$\mathrm{PWL}(\eta_c) = 10\ \log_{10}\left[\ 2\pi r^2 \int_0^{\pi} 10^{\left(\frac{\widetilde{\mathrm{SPL}}(\theta, \eta_c)}{10}\right)} \sin\theta\ d\theta\right] + 10\ \log_{10}\left(\frac{p_{ref}^2}{\rho_\infty c_\infty W_{ref}}\right). \qquad (10)$$

For this prediction method a normalized overall acoustic power level term was employed, $\overline{\mathrm{OAPWL}}$, which relates the overall power level to the product of the total mass flow and the square of the ambient speed of sound. The normalized overall acoustic power level is computed from the overall power level by

$$\overline{\mathrm{OAPWL}} = \mathrm{OAPWL} + 10\ \log_{10}\left(\frac{W_{ref}}{(\dot{m}_1 + \dot{m}_2)\ c_\infty^{\ 2}}\right). \qquad (11)$$

Similarily a normalized one-third octave band power level, $F(\eta_c)$, was used and is defined from one-third octave band power level and the overall power level by

$$F(\eta_c) = \mathrm{PWL}(\eta_c) - \mathrm{OAPWL}. \qquad (12)$$

The directivity index, $D(\theta)$, is a measure of the relative energy flux in the spherical direction θ. The integral of the energy flux over the spherical area is equal to the overall acoustic power. Thus from the acoustic power an average energy flux can be obtained and at a particular radius this can be related to an average overall sound pressure level, $\overline{\mathrm{OASPL}}$. $\overline{\mathrm{OASPL}}$ is defined from the normalized overall sound power level, $\overline{\mathrm{OAPWL}}$, by

$$\overline{\mathrm{OASPL}} = \overline{\mathrm{OAPWL}} + 10\ \log_{10}\left(\frac{A_{ref}}{4\pi r^2}\right) + 197.0, \qquad (13)$$

where A_{ref} is the area associated with a cold jet at critical conditions which has the same mass flow as the hot jet and is defined as

$$A_{ref} = \left(\frac{\dot{m}_1 + \dot{m}_2}{\rho_\infty \ c_\infty}\right). \tag{14}$$

The 197.0 value in equation 13 is a normalized mean square reference pressure level and is defined by

$$197.0 = -10 \ \log_{10}\left(\frac{p_{ref}^{\ 2}}{\rho_\infty^{\ 2} \ c_\infty^{\ 4}}\right). \tag{15}$$

The directivity index at each coordinate point, $D(\theta_c)$, is then computed by

$$D(\theta_c) = OASPL(\theta_c) - \overline{OASPL} \ . \tag{16}$$

The power spectrum level, $F(\eta)$, is a measure of the distribution of the acoustic power over the one-third frequency bands and satisfies the condition

$$\sum_\eta 10^{\left(\frac{F(\eta)}{10}\right)} = 1. \tag{17}$$

The directivity index, $D(\theta)$, is a measure of the distribution of the energy flux in a given direction and satisfies the condition

$$\frac{1}{2} \int_0^\pi 10^{\left(\frac{D(\theta)}{10}\right)} \sin\theta \ d\theta = 1. \tag{18}$$

The two terms shown in equation 13 represent the k_1 and k_2 terms in equations 1 and 3. Thus equation 3 can be written as

$$SPL(\theta,\eta) = \overline{OAPWL} + D(\theta) + F(\eta) + RSL(\theta,\eta) + 10 \log_{10}\left(\frac{A_{ref}}{4\pi r^2}\right) + 197.0 + k_3 \; . \qquad (19)$$

The k_3 term is a correction term between ambient conditions and ISA conditions and is defined by

$$k_3 = 20 \log_{10}\left(\frac{\rho_\infty c_\infty^{\;2}}{\rho_{ISA} c_{ISA}^{\;2}}\right). \qquad (20)$$

The relative spectrum level at each coordinate point, $RSL(\theta_c,\eta_c)$ is computed by substituting into equation 19 the overall power level term, the directivity term, the power spectrum term, and the smoothed sound pressure level at the coordinate point. Thus the relative spectrum level term is a measure of the deviation in spectrum shift due to directivity and is defined at each coordinate point by

$$RSL(\theta_c,\eta_c) = \widetilde{SPL}(\theta_c,\eta_c) - \overline{OAPWL} - D(\theta_c) - F(\eta_c) - 10 \log_{10}\left(\frac{A_{ref}}{4\pi r^2}\right) - 197.0 \; . \qquad (21)$$

The relative spectrum must satisfy the constraints in both the directivity direction and the frequency direction such that

$$\frac{1}{2}\int_0^\pi 10^{\left(\frac{D(\theta) + RSL(\theta,\eta)}{10}\right)} \sin\theta \, d\theta = 1 \text{ for all } \eta . \qquad (22)$$

and

$$\sum_\eta 10^{\left(\frac{F(\eta) + RSL(\theta,\eta)}{10}\right)} = 1 \text{ for all } \theta . \qquad (23)$$

JET FLOW STATE PROPERTIES

At each of the noise level coordinate points, the noise level components or variables have been defined for each test point where data is available. At each coordinate point each noise level variable can be defined as a function of the jet flow state properties. An empirical fit for each of these noise level variables was obtained by employing a multidimensional Taylor series in terms of the jet flow state parameters. For this prediction the jet flow state parameters employed for the circular jet were the normalized jet velocity, V_1/c_∞, and the normalized jet total temperature, T_1/t_∞. Since only subsonic jet tests were employed, the jet exit static pressure is equal to the ambient pressure. Thus the jet velocity and jet total temperature are sufficient for the circular jet. For the coaxial jet the equivalent single jet velocity and equivalent jet total temperature were employed. The equivalent jet has the same mass flow, thrust, and energy flow as the coaxial jet. Also the coaxial jet requires three additional jet flow state parameters to define the noise level variables at the coordinate points. These parameters are (1) the ratio of the secondary jet velocity to the primary jet velocity, V_2/V_1, (2) the ratio of the secondary jet total temperature to the primary jet total temperature, T_2/T_1, and (3) the ratio of the secondary jet area to the primary jet area, A_2/A_1. These flow state parameters were selected rather than the total pressures and total temperatures of Zorumski and Weir (reference 8) because they readily provide a means of examining the effects of velocity ratio and/or temperature ratio on the noise levels of a coaxial jet. Because of the limitations of the test data, there is a limited range of operation for each of the jet flow parameters. The operating range for each of the jet flow state parameters is tabulated below.

Flow State Parameter	Operating Range
Normalized equivalent jet velocity, V_e/c_∞	0.3 to 2.0
Normalized equivalent jet total temperature, T_e/t_∞	0.7 to 4.5
Ratio of secondary jet velocity to primary jet velocity, V_2/V_1	0.02 to 2.5
Ratio of secondary jet total temperature to primary jet total temperature, T_2/T_1	0.2 to 4.0
Ratio of secondary jet area to primary jet area, A_2/A_1	0.5 to 10.0

EQUIVALENT JET FLOW PROPERTIES

The single equivalent jet has the same mass flow, energy flow, and thrust as the coaxial jet as shown on figure 13. The mass flow of the single equivalent jet is related to the mass flow of the coaxial jet by

$$\dot{m}_e = \dot{m}_1 + \dot{m}_2 \tag{24}$$

where $\dot{m} = \rho AV$.

The velocity of the single equivalent jet is obtained by equivalencing the mass flow and thrust of the coannular jet to the single jet by

$$V_e = \frac{\dot{m}_1 V_1 + \dot{m}_2 V_2}{\dot{m}_1 + \dot{m}_2} . \tag{25}$$

Since the gas constant of air is not significantly changed by the addition of a small amount of hydrocarbon fuel combustion products, the equivalent temperature is defined by

$$T_e = \frac{\dot{m}_1\left(\frac{\gamma_1}{\gamma_1 - 1}\right)T_1 + \dot{m}_2\left(\frac{\gamma_2}{\gamma_2 - 1}\right)T_2}{\dot{m}_1\left(\frac{\gamma_1}{\gamma_1 - 1}\right) + \dot{m}_2\ \frac{\gamma_2}{\gamma_2 - 1}} , \tag{26}$$

where $\frac{\gamma}{\gamma - 1} = \frac{c_p}{R}$.

The specific heat ratio of the equivalent jet is defined by

$$\frac{\gamma_e}{\gamma_e - 1} = \frac{\dot{m}_1\left(\frac{\gamma_1}{\gamma_1 - 1}\right) + \dot{m}_2\left(\frac{\gamma_2}{\gamma_2 - 1}\right)}{\dot{m}_1 + \dot{m}_2} . \tag{27}$$

Because the jet static pressure is equal to the ambient static pressure, the jet exhaust density of the equivalent jet can be defined by

$$\rho_e = \rho_\infty \left[\frac{T_e}{t_\infty} - \frac{\gamma_e - 1}{2} \left(\frac{V_e}{c_\infty} \right)^2 \right]^{-1} . \tag{28}$$

The equivalent jet area for the coaxial jet is defined from the mass flow as

$$A_e = \frac{\dot{m}_e}{\rho_e V_e} , \tag{29}$$

and the equivalent diameter is

$$D_e = \sqrt{\frac{4 A_e}{\pi}} . \tag{30}$$

TAYLOR SERIES

The Taylor Series is a multidimensional function for expressing the jet noise variables at each of the noise level coordinate points as a function of the flow state parameters. The Taylor series depends on assigning a standard condition to each of the prediction parameters and then operating on values which are not far removed from the standard condition. The operating range for some of the prediction parameters such as velocity ratio (V_2/V_1) vary by a factor greater than 100. To minimize the range of operation the logarithmic values of the prediction parameters were employed rather than the actual values. If we define the parameter α_i to represent the i_{th} prediction parameter, and α_{ir} to represent the standard value for the i_{th} prediction parameter, the parameter value (x_i) for the i_{th} source prediction parameter is defined by

$$x_i = \log_{10} \left(\frac{\alpha_i}{\alpha_{ir}} \right) . \tag{31}$$

For this study the five source parameter values are defined as follows

$$x_1 = \log_{10} \frac{V_e/c_\infty}{1.0} \tag{32}$$

$$x_2 = \log_{10} \frac{T_e/t_\infty}{2.0} \tag{33}$$

$$x_3 = \log_{10} \frac{V_2/V_1}{1.0} \tag{34}$$

$$x_4 = \log_{10} \frac{T_2/T_1}{1.0} \tag{35}$$

$$x_5 = \log_{10} \frac{A_2/A_1}{1.0} \tag{36}$$

Note that the standard values are 1.0 except for α_2 which has a standard value of 2.0.

With the five source prediction parameters, the third order Taylor series has a constant plus 55 possible independent derivatives as presented in Table I of reference 8. Zorumski and Weir (reference 8) present a more detailed description of the Taylor series which was employed in this report.

Using the data base of 817 test points for which the source prediction parameters and the noise level coordinate values are defined, numerical values for the derivatives were obtained using a least squares fit. This is repeated for each of the noise level coordinates including the normalized overall power level, $\overline{OAPWL}$, the seven directivity index coordinates, $D(\theta_c)$, the seven normalized power spectra coordinates, $F(\eta_c)$ and the forty nine normalized relative spectra coordinates, $RSL(\theta_c, \eta_c)$.

Due to the distribution of the source prediction parameters not all of the third order derivative values were determined. In addition, for the coaxial jet, the area ratio prediction parameter, x_5, was not considered to be an independent first, second, or third order derivative by itself, but was used as part of a second or third order derivative chain with derivatives from other source prediction parameters. For the circular and coaxial jet the least squares fit with the Taylor series obtained constant values for 36 derivative terms including the constant term. Table III shows the derivative terms and the derivative multiplier term for each of the 36 non-zero terms used for the coaxial jet. Since the values of x_3, x_4, x_5 are set equal to 0 for the circular jet, only the first eight derivative terms apply to the circular jet as shown in Table III. For the normalized power spectra level, $F(\eta_c)$, and the normalized relative spectra, $RSL(\theta_c, \eta_c)$, there are fewer data cases at the low normalized frequency parameter coordinate points (η_c = -1.5 and -1.0) and the highest normalized frequency parameter coordinate point (η_c = $\pm$1.5) and hence there were fewer derivative values obtained from the least squares fit of the Taylor series at these coordinates.

The values for each of the 36 normalized overall power level derivative terms, $PWL_{,j}$, and the directivity index derivative term, $D_{,j}(\theta_c)$, at the directivity angle coordinate points of 0, 30, 60, 90, 120, 150, and 180 degrees are presented in Table IV. Table V presents the values for each of the 36 normalized power spectra level derivative terms, $F_{,j}(\eta_c)$ at the normalized frequency parameter coordinate values, η_c, of -1.5, -1.0, -0.5, 0.0, 0.5, 1.0, 1.5. It should be noted that there are several derivative values of 0.0 at η_c values of -1.5, -1.0, and +1.5 because the limited amount of data available at these normalized frequency parameter values was not sufficient to define all 36 derivative terms. Table VI presents the values for the 36 derivative terms for each of the relative spectral level coordinates, $RSL(\theta_c, \eta_c)$, at the directivity angle coordinate points, θ_c, of 0, 30, 60, 90, 120, 150, 180 degrees and at the normalized frequency parameter coordinate points, η_c, of -1.5, -1.0, -0.5, 0.0, 0.5, 1.0, and 1.5.

PREDICTION METHOD

For a circular or coaxial jet, the noise levels at predicted directivity angles, θ_p, and predicted one-third octave center band frequencies, f_p, are obtained by a step procedure method. This step procedure method provides for the computation of the overall sound pressure level, $OASPL(\theta_p)$, the one-third octave band power spectrum level, $PWL(f_p)$, and the one-third octave band sound pressure levels, $SPL(\theta_p, f_p)$, at the directivity angles, θ_p, and the one-third octave center band frequencies, f_p.

To obtain the values at the predicted frequencies or directivity angles, the known values of the directivity coordinates or normalized frequency parameter coordinates are interpolated using a cubic spline. The cubic spline is composed of a set of continuous third order polynomial basis functions over a number of subintervals which have continuous first and second order derivatives over the total interval. These continuous conditions relate the constants of the cubic polynomial for each subinterval provided that the magnitudes are defined at the ends of each subinterval, and either the slope or curvature is defined at the ends of the total interval.

The circular or coaxial jet noise levels are obtained from the following fourteen step prediction method.

Step 1. Compute the equivalent flow state properties including the equivalent velocity, V_e, equivalent total temperature, T_e, equivalent mass flow rate, m_e, and equivalent diameter, D_e, using equations 24 through 30.

Step 2. Compute the values of the exit flow parameter, x_1 to x_5 using the equivalent jet flow properties obtained from Step 1 and the jet flow property ratios in equations 32 through 36. For the circular jet where $A_2 = 0$, V_e is set equal to V_1, T_e is set equal to T_1, and the values of x_3, x_4, and x_5 are set equal to 0.0.

Step 3. Compute the values of the derivative multipliers X_1 to X_N as listed in Table III using the values of x_1 to x_5 obtained from Step 2. N has a value of 8 for the circular jet and a value of 36 for the coaxial jet.

Step 4. Compute the value of the normalized overall power level, $\overline{OAPWL}$, from the derivative multiplier values, X_j, obtained in Step 3 and the corresponding N number of $\overline{OAPWL}$ derivative values, $PWL_{,j}$, listed in Table IV, where N is equal to 8 for the circular jet and 36 for the coaxial jet, using equation 37.

$$\overline{OAPWL} = \sum_{j=1}^{N} PWL,_j \; X_j \qquad (37)$$

Step 5. Compute the values of the directivity index, $D(\theta_c)$, at each of the directivity angle coordinate points of 0, 30, 60, 90, 120, 150, and 180 degrees, from the derivative multiplier values, X_j, obtained in Step 2 and the corresponding N number of directivity index derivative values, $D,_j(\theta_c)$, presented in Table IV using equation 38.

$$D(\theta_c) = \sum_{j=1}^{N} D,_j \, (\theta_c) \; X_j \qquad (38)$$

Step 6. Compute the values of the normalized power spectra, $F(\eta_c)$ at each of the normalized frequency parameter coordinate points of -1.5, -1.0, -0.5, 0.0, 0.5, 1.0, and 1.5 from the derivative multipliers, X_j, and the corresponding N number of normalized power spectra derivative values, $F,_j(\eta_c)$, presented in Table V using equation 39.

$$F(\eta_c) = \sum_{j=1}^{N} F,_j(\eta_c) \; X_j \qquad (39)$$

Step 7. Compute the values of the normalized relative spectrum, $RSL(\theta_c, \eta_c)$, at each of the 49 coordinate points shown on Figure 11 including the the directivity angle coordinate points of 0, 30, 60, 90, 120, 150, and 180 degrees corresponding to each of the normalized frequency parameter coordinate points of -1.5, -1.0, -0.5, 0.0, 0.5, 1.0, and 1.5, from the derivative values, $RSL,_j \, (\theta_c, \eta_c)$, presented in Table VI, using equation 40.

$$RSL \, (\theta_c, \eta_c) = \sum_{j=1}^{N} RSL,_j \, (\theta_c, \eta_c) \; X_j \qquad (40)$$

Step 8. Compute the values of overall sound pressure level, $OASPL(\theta_c)$, at each of the directivity angle coordinate points of 0, 30, 60, 90, 120, 150, and 180 degrees from the $\overline{OAPWL}$ value obtained from Step 4, and the values of $D(\theta_c)$ obtained from Step 5 using equation 41.

$$OASPL(\theta_c) = \overline{OAPWL} + D(\theta_c) + 20 \log_{10} \left(\frac{\rho_\infty c_\infty^2}{\rho_{ISA} c_{ISA}^2} \right) +$$

$$10 \log_{10} \left(\frac{A_{ref}}{4\pi r^2} \right) + 197.0, \quad (41)$$

where A_{ref} is defined from equation 14 as follows:

$$A_{ref} = \frac{\dot{m}_e}{\rho_\infty c_\infty}, \quad (14)$$

and r is the distance between the center of the nozzle exit plane and the observer position.

Step 9. Compute the OASPL values at the particular directivity angles at which noise levels are desired, θ_p, by interpolating the OASPL(θ_c) values obtained in Step 8 using a cubic spline which has zero slope end conditions (directivity angles of 0 and 180° degrees) to obtain the values for OASPL(θ_p). The cubic spline is a piecewise third order polynomial with continuous slope and curvature at the node points which are the directivity angle coordinate points of 0, 30, 60, 90, 120, 150, and 180 degrees.

Step 10. Compute the relative spectrum level values at the particular directivity angles, θ_p, by interpolating the RSL(θ_c, η_c) values obtained in Step 7 using a cubic spline which has zero slope end conditions to obtain the values of RSL(θ_p, η_c). See figure 14.

Step 11. For the particular one-third octave center band frequencies, f_p, compute the values of the particular normalized frequency parameters, η_p, using equation 2.

$$\eta_p = f_p D_e/V_e , \quad (2)$$

where D_e and V_e are the values of the equivalent jet diameter and equivalent jet velocity obtained in Step 1.

Step 12. Compute the values of the normalized one-third octave band power spectrum levels and the relative spectrum levels at the particular normalized frequency parameter values, η_p, obtained in Step 11 and at the particular directivity angles, θ_p, by interpolating the $F(\eta_c)$ values obtained in Step 6 and the $RSL(\theta_p, \eta_c)$ values obtained in Step 10 using a cubic spline which has zero curvature end conditions (η_c = -1.5 and +1.5) to obtain values of $F(\eta_p)$ and $RSL(\theta_p, \eta_p)$. See figure 15.

Step 13. Compute sound pressure levels at the particular directivity angles, θ_p, and the particular frequency levels, f_p, from the $OASPL(\theta_p)$ values obtained in Step 9, and the values of $F(\eta_p)$ and $RSL(\theta_p, \eta_p)$ obtained in Step 12 to obtain the values of $SPL(\theta_p, f_p)$ using equation 42.

$$SPL(\theta_p, f_p) = OASPL(\theta_p) + F(\eta_p) + RSL(\theta_p, \eta_p). \tag{42}$$

Step 14. Compute the one third octave band power spectrum level at the particular frequency levels, f_p, for which noise levels are desired from the $\overline{OAPWL}$ value obtained in Step 4 and the $F(\eta_p)$ values obtained in Step 12 to obtain the values of $PWL(\eta_p)$ using equation 43.

$$PWL(\eta_p) = \overline{OAPWL} + F(\eta_p) + 20 \log_{10}\left(\frac{\rho_\infty \; c_\infty^2}{\rho_{ISA} \; c_{ISA}^2}\right)$$

$$+ 10 \log_{10} (\dot{m}_e \; c_\infty^2 / w_{ref}) \; . \tag{43}$$

ERROR ANALYSIS

The application of the empirical prediction method developed by Zorumski and Weir (reference 8) which employs a Taylor series is a powerful and efficient method, in that it reduces a large data base with almost 200,000 elements to a table of about 2300 constants. Table VII presents a summary of the number of directivity angles, the number of frequencies, the number of tests, and the total number of sound pressure levels in the data base. Table VIII shows that for the circular jet there are 512 constants and for the coaxial jet there are 2304 constants used to define the node points for prediction of the jet noise levels.

Associated with the Taylor series fit to each of the 49 coordinate points is a prediction error. These errors can be combined to obtain a standard error value for each of the noise variables which make up the noise prediction. The variables and the standard error are listed below.

NOISE VARIABLE	STANDARD ERROR dB
Normalized Overall Power Level	1.381
Directivity	1.623
Power Spectra	1.385
Relative Spectra	2.710

In addition, for each coordinate point, θ_C, η_C, the standard errors associated with the normalized overall power level, the directivity, the power spectra, and the relative spectra can be combined to obtain a standard error of the predicted sound pressure level at the coordinate point, SPL(θ_C,η_C). Table IX summarizes the standard error for the sound pressure levels at each of the coordinate points. Figure 16 presents a contour plot of the standard error of the predicted sound pressure levels as a function of the directivity angle and normalized frequency parameter. From the table and the plot it can be seen that the greatest errors are at directivity angles below 20 degrees and above 165 degrees. The standard deviation is greatest at directivity angles of 0 degrees and 180 degrees. Also because of the available frequency range limitations of the data, there is less data available at the normalized frequency parameter values of -1.5 and +1.5 than there is at the other normalized frequency range parameter values. Again this reduction in the amount of available data acts to increase the value of the standard deviation in these regions.

VALIDATION OF PREDICTION METHOD

Comparisons were made between the prediction method and the measured one-third octave band sound pressure level data for both circular jet test cases and coaxial jet test cases at three directivity angles nearest 90, 120, and 150 degrees where measurements were taken. Figures 17 thru 28 present comparisons between the measured and predicted one-third octave band sound pressure levels for twelve circular jet tests. These tests were selected to cover a wide range of normalized equivalent velocities, V_e/c_∞, and normalized equivalent total temperatures, T_e/t_∞, and include at least one test case from each of the seven data sets. The normalized equivalent velocities covered in these tests range from 0.58 to 1.78. Similarily the normalized total temperature ranges from 1.00 to 4.13. For each test at each angle a standard error was computed to show the difference between the measured and predicted SPL level over the frequency range. Table X shows the minimum, maximum, and average standard error value for the twelve circular jet tests at each of the three directivity angles closest to 90, 120, and 150 degrees where measured data are available.

From Table X it can be seen that the average standard error increases from 1.6 to 1.9 dB as the directivity angle increases from 90 to 150 degrees. These standard errors may or may not be representative of the 214 circular jet tests, since they represent less than six percent of the tests. Furthermore, the prediction method is based on smooth data, whereas the standard error for each test is computed from the actual data. The data shown at 90 degrees and 120 degrees on figure 22 has several data points which are considerably displaced from the smooth broad band spectra. Also there are other tests that have unsmooth spectra distributions. Figures 17 thru 28 show that at directivity angles of 150 degrees, the predicted SPL values at the peak frequency are either less than or equal to the measured values. It is expected that other tests will show the predicted SPL value at the peak to be higher than the measured values. In general the measured and predicted peak noise levels occur at the same frequency.

Figures 29 thru 54 present comparisons between the measured and predicted one-third octave band sound pressure levels for 26 coaxial jet tests. These tests were selected to cover a wide range of normalized equivalent velocities, V_e/c_∞, and normalized equivalent total temperatures, T_e/t_∞, as well as different velocity ratios, V_2/V_1, temperature ratios, T_2/T_1, and area ratios, A_2/A_1.

Table X presents the minimum, maximum and average standard error values for the 26 coaxial jet tests at each of the three directivity angles closest to 90, 120, and 150 degrees where measured data are available. Table X shows that the coaxial jet like the circular jet has the largest average standard error which is 2.5 dB at the directivity angle of 150 degrees. Again these standard error values represent only 26 tests or less than 5 percent of the 603 coaxial jet tests in the data base, and therefore may not be representative of all the tests. For the 26 tests, figures 29 thru 54 show at the directivity angle nearest 150 degrees, the peak SPL values are underpredicted in 13 tests and overpredicted in 6 of the tests. The predicted peak frequency appeared to be within one-third octave band of the measured peak frequency at a directivity angle of 150 degrees.

CONCLUSIONS

The empirical method presented in this report is an acceptable method for predicting the static free field source noise levels of subsonic circular and coaxial jet flow streams. It provides for defining the jet mixing noise levels of a coaxial jet using approximately 2300 constants, whereas for a single jet only 512 constants are required. In the actual data base there are approximately 200,000 sound pressure level values.

The technique employed is based on the method of Zorumski and Weir (reference 8). The prediction method employs different flow state properties than Zorumski and Weir to provide for direct examination of the effects of velocity ratio and temperature ratio on the noise level of a coaxial jet. Also the method of this report provides a greater range of predictions than reference 8 in that it predicts noise levels at directivities ranging from 0 to 180 degrees and frequency parameters ranging from -1.5 to 1.5.

At directivity angles of 120 and 150 degrees where the peak jet noise occurs, the standard error on the smoothed data is less than 1.5 dB as shown in Table IX and figure 15. For the 12 circular jet tests of figures 17 thru 28, the average standard error over the range of one-third octave band frequencies at a directivity angle of 120 degrees is 1.8 dB and at 150 degrees is 1.9 dB. For the 26 coaxial jet tests of Figures 29 thru 54, the average standard error over the range of one-third octave band frequencies at a directivity angle of 120 degrees is 1.5 dB and at 150 degrees is 2.5 dB. Table X summarizes the maximum, minimum, and average standard errors for the circular and coaxial jet tests of figures 17 thru 54 at directivity angles near 90, 120, and 150 degrees. The actual data in the figures are unsmoothed and therefore the standard errors are greater than the standard errors obtained with the smoothed data. Also the actual data represents less than 6 percent of the circular jet tests and less than 5 percent of the coaxial jet tests and therefore may not be representative of the total data set.

The prediction method is limited to subsonic jets which have equivalent jet velocities ranging from 0.3 to 2.0 times the ambient speed of sound and equivalent total temperatures ranging from 0.7 to 4.5 times the ambient speed of sound. The table below shows the operating range for each of the five jet flow parameters employed in the empirical prediction.

Prediction Parameter	V_e/c_∞	T_e/t_∞	V_2/V_1	T_2/T_1	A_2/A_1
Range of Operation	0.3-2.0	0.7-4.5	0.02-2.5	0.2-4.0	0.5-10.0

Also the coaxial jet prediction is valid for primary nozzle protrusions varying from 0.0 to 4.3 primary jet nozzle diameters.

REFERENCES

1. Stone, J. R.: Interim Prediction Method for Jet Noise. NASA TM X-71618, 1974.

2. Pao, S. P.: A Correlation of Mixing Noise From Coannular Jets With Inverted Flow Profiles. NASA TP-1301, 1979.

3. Russell, J. W.: A Method for Predicting the Noise Levels of Coannular Jets with Inverted Velocity Profiles. NASA CR-3176, 1979.

4. Jaeck, C. L.: Empirical Jet Noise Predictions for Single and Dual Flow Jets With and Without Suppressor Nozzles. Volume II - Dual Flow Subsonic and Supersonic Jets. Doc. No. D6-42929-2, Boeing Company, August 1977.

5. Jaeck, C. L.: Empirical Jet Noise Predictions for Single and Dual Flow Jets With and Without Suppressor Nozzles. Volume I - Single Flow Subsonic and Supersonic Jets. Doc. No. D6-42929-1, Boeing Company, April 1976.

6. Stone, J. R.: An Empirical Model for Inverted-Velocity-Profile Jet Noise Prediction. NASA TM-73838, 1977.

7. Gas Turbine Jet Exhaust Noise Prediction, Appendix A. Society of Automotive Engineers Aerospace Recommended Practice 876C. September 1982.

8. Zorumski, W. E.; and Weir, D. S.: Empirical Source Noise Prediction Method With Application to Subsonic Coaxial Jet Mixing Noise. NASA TP-2084, 1982.

9. Kozlowski, H.; and Packman, A. B.: Aerodynamic and Acoustic Tests of Duct-Burning Turbofan Exhaust Nozzles. NASA CR-2628, 1976.

10. Tanna, H. K.; Dean, P. D.; and Burrin, R. H.: The Generation and Radiation of Supersonic Jet Noise. Volume III, Turbulent Mixing Noise Data. AFAPL-TR-76-65-VOL III, Lockheed Georgia Company, 1976.

11. Goodykoontz, J. H.; and Stone, J. R.: Experimental Study of Coaxial Nozzle Exhaust Noise. NASA TM-79090, 1979.

12. Stone, J. R.; Goodykoontz, J. H.; and Gutierrez, O. A.: Effects of Geometric and Flow-Field Variables on Inverted-Velocity-Profile Coaxial Jet Noise and Source Distributions. NASA TM-79095, 1979.

TABLE I. - SUMMARY OF DATA BASE RANGE OF VARIABLES

SOURCE	TEST SERIES	NO. OF TESTS	GEOMETRIC VARIABLES		ACOUSTIC MEASUREMENT RANGES		FLOW STATE PARAMETER RANGES			
							INNER STREAM		OUTER STREAM	
			AREA RATIO	PRIMARY NOZZLE PROTRUSION	DIRECTIVITY ANGLE (DEGREES)	FREQUENCY (Hz)	NORMALIZED VELOCITY V_1/c_∞	NORMALIZED TEMPERATURE T_1/t_∞	NORMALIZED VELOCITY V_2/c_∞	NORMALIZED TEMPERATURE T_2/t_∞
NGTE	A	32	1.0	—	60-160	250-40000	0.530-1.441	0.827-2.649	—	—
	A	58	2.0	0.0	60-160	250-40000	0.582-1.120	1.004-3.125	0.119-0.899	1.000-1.011
	A	58	4.0	0.0	60-160	250-40000	0.580-1.119	1.000-3.125	0.110-0.903	1.000-1.018
	A	56	6.0	0.0	60-160	250-40000	0.582-1.121	1.000-3.125	0.119-0.906	1.000-1.018
NGTE	C	51	1.0	—	45-150	100-40000	0.553-1.516	2.678-2.875	—	—
	C	19	1.4	3.0	45-150	100-40000	0.559-1.475	2.665-2.765	0.341-0.881	1.021-1.059
	C	36	1.5	0.0,1.7	45-150	100-40000	0.549-1.504	2.782-2.927	0.032-0.907	1.031-1.289
	C	14	1.6	4.4	45-150	100-40000	0.552-1.501	2.809-2.854	0.073-0.893	1.035-1.301
	C	54	1.9	1.5,3.0,4.5	45-150	100-40000	0.555-1.4768	2.6619-2.806	0.206-0.901	1.017-1.106
	C	20	2.0	0.0	45-150	100-40000	0.559-1.516	2.751-2.887	0.028-0.913	1.024-1.141
	C	23	4.0	3.0,4.4	45-150	100-40000	0.553-1.503	2.796-2.867	0.013-0.908	1.024-1.092
	C	14	4.1	1.7	45-150	100-40000	0.552-1.504	2.802-2.876	0.107-0.904	1.027-1.066
	C	16	4.3	0.0	45-150	100-40000	0.566-1.521	2.872-2.906	0.307-0.908	1.020-1.044
	C	15	7.9	3.0	45-150	100-40000	0.552-1.135	2.833-2.854	0.093-0.711	1.027-1.270
	C	22	8.0	0.0,4.3	45-150	100-40000	0.550-1.514	2.813-2.886	0.038-0.903	1.020-1.171
	C	3	8.1	3.1	45-150	100-40000	1.155-1.523	2.886-2.913	0.075-0.356	1.028-1.336
NGTE	D	21	1.0	—	60-160	250-80000	0.530-1.441	0.8269-2.672	—	—

TABLE I. - Concluded.

SOURCE	TEST SERIES	NO. OF TESTS	AREA RATIO	PRIMARY NOZZLE PROTRUSION	DIRECTIVITY ANGLE RANGE (DEGREES)	FREQUENCY RANGE (Hz)	INNER STREAM NORMALIZED VELOCITY V_1/c_∞	INNER STREAM NORMALIZED TEMPERATURE T_1/t_∞	OUTER STREAM NORMALIZED VELOCITY V_2/c_∞	OUTER STREAM NORMALIZED TEMPERATURE T_2/t_∞
PWA	A	15	1.0	—	60-165	100-80000	0.502-1.676	1.304-3.661	—	—
	A	29	0.75	0.3	60-165	100-80000	0.518-1.466	1.278-3.671	0.485-1.685	1.267-3.674
	A	6	1.20	0.4	60-165	100-80000	0.864-1.259	1.306-2.726	0.921-1.697	2.344-3.639
SNECMA	A	4	1.0	—	20-160	200-100000	1.067-1.179	2.821-3.046	—	—
	A	30	3.52	2.0	20-160	200-100000	0.555-1.270	1.000-3.046	0.482-0.833	0.983-1.157
SNECMA	B	11	2.25	1.0	20-160	200-100000	0.721-1.309	2.368-2.992	0.366-0.921	1.078-1.174
	B	16	3.92	1.0	20-160	200-100000	0.721-1.302	2.365-2.984	0.374-0.922	1.091-1.179
	B	17	6.09	1.0	20-160	200-100000	0.716-1.304	2.363-2.990	0.366-0.912	1.077-1.168
GELAC	A	59	1.0	—	30-165	200-40000	0.347-1.483	0.992-3.649	—	—
GELAC	B	32	2.93	0.0	70-160	250-31500	0.629-1.174	1.362-2.853	0.291-0.660	1.031-1.687
LERC	A	32	1.0	—	47-155	100-50000	0.857-1.788	0.989-4.154	—	—
	A	16	1.20	0.0	47-155	100-50000	0.655-1.786	0.989-4.142	0.647-1.740	1.027-4.036
	A	16	1.50	0.0	47-155	100-50000	0.685-1.783	0.995-3.989	0.677-1.720	1.005-3.800
	A	16	2.00	0.0	47-155	100-50000	0.653-1.771	0.974-4.096	0.644-1.702	0.986-3.878
	A	16	3.33	0.0	47-155	100-50000	0.658-1.788	1.005-4.152	0.647-1.720	1.011-3.958

TABLE II. - SUBSET VALUE RANGE AND GEOMETRIC MEAN FOR FLOW STATE PARAMETERS

Subset		Flow State Parameters				
		V_e/c_∞	T_e/t_∞	V_2/V_1	T_2/T_1	A_2/A_1
1	Range	0.25-0.5	0.5-1.0	0.088-0.198	0.25-0.5	0.707-1.414
	Mean Value	0.354	0.707	0.132	0.354	1.0
2	Range	0.5-1.0	1.0-2.0	0.198-0.444	0.5-1.0	1.414-2.828
	Mean Value	0.707	1.414	0.296	0.707	2.0
3	Range	1.0-2.0	2.0-4.0	0.444-1.0	1.0-2.0	2.828-5.656
	Mean Value	1.414	2.282	0.667	1.414	4.0
4	Range	2.0-4.0	4.0-8.0	1.0-2.25	2.0-4.0	5.656-11.312
	Mean Value	2.828	5.656	1.50	2.828	8.0

TABLE III. - NON-ZERO DERIVATIVE TERMS FOR TAYLOR SERIES FIT TO CIRCULAR AND COAXIAL JET

Derivative	Derivative	Derivative Multiplier
	Circular and Coannular Jet	
1	1	1
2	$\Delta_{,1}$	x_1
3	$\Delta_{,2}$	x_2
4	$\Delta_{,11}$	$x_1^2/2$
5	$\Delta_{,12}$	$x_1 x_2$
6	$\Delta_{,22}$	$x_2^2/2$
7	$\Delta_{,112}$	$x_1^2 x_2/2$
8	$\Delta_{,122}$	$x_1 x_2^2/2$
	Coannular Jet Only	
9	$\Delta_{,3}$	x_3
10	$\Delta_{,4}$	x_4
11	$\Delta_{,13}$	$x_1 x_3$
12	$\Delta_{,14}$	$x_1 x_4$
13	$\Delta_{,15}$	$x_1 x_5$
14	$\Delta_{,23}$	$x_2 x_3$
15	$\Delta_{,24}$	$x_2 x_4$
16	$\Delta_{,25}$	$x_2 x_5$
17	$\Delta_{,33}$	$x_3^2/2$
18	$\Delta_{,34}$	$x_3 x_4$
19	$\Delta_{,35}$	$x_3 x_5$
20	$\Delta_{,44}$	$x_4^2/2$

TABLE III. - Continued.

Derivative	Derivative	Derivative Multiplier
	Coannular Jet Only	
21	$\Delta_{,45}$	$x_4 x_5$
22	$\Delta_{,113}$	$x_1^2 x_3 /2$
23	$\Delta_{,115}$	$x_1^2 x_5 /2$
24	$\Delta_{,133}$	$x_1 x_3^2 /2$
25	$\Delta_{,134}$	$x_1 x_3 x_4$
26	$\Delta_{,135}$	$x_1 x_3 x_5$
27	$\Delta_{,145}$	$x_1 x_4 x_5$
28	$\Delta_{,155}$	$x_1 x_5^2 /2$
29	$\Delta_{,333}$	$x_3^3 /6$
30	$\Delta_{,334}$	$x_3^2 x_4 /2$
31	$\Delta_{,335}$	$x_3^2 x_5 /2$
32	$\Delta_{,344}$	$x_3 x_4^2 /2$
33	$\Delta_{,345}$	$x_3 x_4 x_5$
34	$\Delta_{,355}$	$x_3 x_5^2 /2$
35	$\Delta_{,445}$	$x_4^2 x_5 /2$
36	$\Delta_{,455}$	$x_4 x_5^2 /2$

where Δ represents the noise coordinate and the source noise parameters, x_i, are

$$x_1 = \log_{10} (V_e/c_\infty)$$

$$x_2 = \log_{10} (T_e/(2t_\infty))$$

$$x_3 = \log_{10} (V_2/V_1)$$

$$x_4 = \log_{10} (T_2/T_1)$$

$$x_5 = \log_{10} (A_2/A_1)$$

TABLE IV. - DERIVATIVE VALUES FOR NORMALIZED OVERALL POWER LEVEL AND DIRECTIVITY INDEX COORDINATE POINTS, $D(\theta_c)$

Derivative Index, j	Derivative Multiplier, X_j	Derivative Values for $\overline{OAPWL}$	Derivative Values for Directivity Index $(D_{,j}(\theta_c))$						
		$PWL_{,j}$	$D_{,j}(0)$	$D_{,j}(30)$	$D_{,j}(60)$	$D_{,j}(90)$	$D_{,j}(120)$	$D_{,j}(150)$	$D_{,j}(180)$
				CIRCULAR JET AND COAXIAL JET					
1	1	-41.64	-12.43	-10.57	-7.84	-4.54	.44	6.29	6.38
2	x_1	64.84	-17.35	-16.34	-16.71	-12.48	-4.83	6.87	4.36
3	x_2	5.85	3.35	.54	1.26	.20	2.24	-.20	-12.57
4	$x_1\ x_1/2$	45.66	5.25	-6.42	11.35	-28.69	-21.59	-19.65	-51.73
5	$x_1\ x_2$	-45.95	-75.93	-56.72	-47.74	-14.32	2.43	8.96	-14.87
6	$x_2\ x_2/2$	28.98	142.80	107.84	76.07	28.13	13.19	-24.37	-69.90
7	$x_1\ x_1\ x_2/2$	-67.28	-147.56	-178.07	-192.58	-137.39	-83.21	21.51	102.77
8	$x_1\ x_2\ x_2/2$	65.60	180.53	168.22	119.55	43.89	55.58	-30.98	-179.12
					Coaxial Jet Only				
9	x_3	-3.78	10.22	13.12	13.54	9.91	5.39	-4.83	-12.40
10	x_4	-3.81	-2.33	-3.30	-3.39	-.83	-1.46	-.42	9.62
11	$x_1\ x_3$	-12.14	9.26	8.54	3.45	-2.45	-1.91	2.45	60.26
12	$x_1\ x_4$	-6.75	15.17	14.35	5.40	15.72	10.19	-1.38	9.77
13	$x_1\ x_5$	14.77	-11.61	-1.72	13.00	8.69	9.09	-14.63	-1.29
14	$x_2\ x_3$	37.95	.47	-1.10	.91	3.07	5.28	-4.27	-19.71
15	$x_2\ x_4$	.75	-53.84	-52.80	-39.79	-14.75	-20.67	17.42	56.67
16	$x_2\ x_5$	-11.83	3.31	3.71	1.46	1.27	2.11	-1.23	-19.54
17	$x_3\ x_3/2$	-6.53	43.94	46.06	42.20	33.04	16.57	-18.83	-24.69
18	$x_3\ x_4$	12.77	-43.15	-34.62	-24.48	-11.60	.30	12.34	16.01
19	$x_3\ x_5$	-17.63	3.14	3.37	4.10	9.30	5.16	-4.12	31.81
20	$x_4\ x_4/2$	5.05	44.33	25.17	6.61	-1.50	1.27	-14.60	-44.19
21	$x_4\ x_5$	-.12	-4.68	-2.74	-4.62	-2.88	-11.52	9.39	-5.09
22	$x_1\ x_1\ x_3/2$	11.86	37.70	13.31	5.29	-17.63	-30.21	5.37	148.29
23	$x_1\ x_1\ x_5/2$	-41.33	-1.70	-19.93	-59.88	-16.95	-22.64	30.05	111.51
24	$x_1\ x_3\ x_3/2$	40.51	18.73	18.16	12.75	9.76	2.25	7.51	105.11
25	$x_1\ x_3\ x_4$	-37.63	-23.67	-28.99	-27.16	-35.00	-11.17	-2.11	-14.68
26	$x_1\ x_3\ x_5$	29.26	-.44	-2.44	.44	-1.72	-8.14	7.46	69.81
27	$x_1\ x_4\ x_5$	33.74	-43.67	-32.07	-13.20	-29.24	-21.80	6.99	52.26
28	$x_1\ x_5\ x_5/2$	-12.19	-13.22	-27.97	-54.74	-37.21	-48.71	52.23	111.33
29	$x_3\ x_3\ x_3/6$	68.07	19.20	20.33	23.72	23.68	11.00	-20.08	-13.36
30	$x_3\ x_3\ x_4/2$	-69.25	-7.82	.94	-1.97	-4.61	6.05	8.12	-8.01
31	$x_3\ x_3\ x_5/2$	23.03	-17.62	-12.62	-5.29	3.08	1.40	-.34	49.66
32	$x_3\ x_4\ x_4/2$	10.90	50.11	32.54	26.46	15.57	26.99	-8.18	-20.66
33	$x_3\ x_4\ x_5$	-1.15	23.04	11.21	4.20	-4.62	9.05	-14.19	-69.82
34	$x_3\ x_5\ x_5/2$	34.02	-2.11	-4.00	-1.86	-6.54	-.49	-3.57	-25.51
35	$x_4\ x_4\ x_5/2$	8.42	3.65	19.64	27.43	10.65	3.77	10.43	-44.59
36	$x_4\ x_5\ x_5/2$	43.73	-8.43	-6.21	7.00	-2.40	21.33	-14.97	-11.41

TABLE V. - DERIVATIVE VALUES FOR ONE-THIRD OCTAVE BAND NORMALIZED POWER SPECTRUM AT COORDINATE POINTS, $F(n_c)$

Derivative Index, j	Derivative Multiplier, X_j	$F_{,j}(-1.5)$	$F_{,j}(-1.0)$	$F_{,j}(-0.5)$	$F_{,j}(0.0)$	$F_{,j}(0.5)$	$F_{,j}(1.0)$	$F_{,j}(1.5)$
				Circular and Coaxial Jet				
1	1	-27.59	-14.16	-10.17	-13.97	-17.56	-23.89	-29.75
2	x_1	-8.46	8.44	1.49	-4.45	-6.33	-20.25	-44.32
3	x_2	19.20	-.12	-.77	-1.52	-8.44	-1.12	-20.97
4	$x_1\ x_1/2$	0.00	25.92	-3.57	-4.99	2.30	-24.48	0.00
5	$x_1\ x_2$	0.00	-47.71	-7.41	27.91	21.08	-6.53	-51.27
6	$x_2\ x_2/2$	-40.02	15.36	-3.01	-16.45	-.99	81.36	0.00
7	$x_1\ x_1\ x_2/2$	0.00	-138.82	56.76	113.51	148.84	-87.26	0.00
8	$x_1\ x_2\ x_2/2$	0.00	103.69	46.69	-28.24	60.35	308.24	0.00
				Coaxial Jet Only				
9	x_3	13.65	2.61	-12.30	-1.04	11.00	15.90	10.24
10	x_4	-10.32	2.16	1.81	1.38	3.47	1.82	2.51
11	$x_1\ x_3$	0.00	10.82	-24.04	-5.18	38.23	5.54	-25.51
12	$x_1\ x_4$	0.00	8.90	12.25	6.03	-12.64	-22.06	0.00
13	$x_1\ x_5$	0.00	-19.14	-4.07	5.56	8.09	4.88	60.14
14	$x_2\ x_3$	0.00	-15.81	-17.73	-10.58	-19.32	-6.16	0.00
15	$x_2\ x_4$	0.00	-6.02	19.18	12.39	5.69	18.48	0.00
16	$x_2\ x_5$	0.00	2.97	.77	-1.34	2.86	6.38	-1.02
17	$x_3\ x_3/2$	0.00	17.79	-35.24	-10.08	29.79	83.56	189.29
18	$x_3\ x_4$	19.06	-11.70	15.35	15.94	-8.78	-39.83	-51.46
19	$x_3\ x_5$	4.30	42.09	1.49	-22.60	-28.44	-9.27	25.99
20	$x_4\ x_4/2$	-9.09	-27.74	-21.10	-9.46	24.30	36.32	17.11
21	$x_4\ x_5$	-36.86	-5.00	6.32	.04	3.37	3.23	35.87
22	$x_1\ x_1\ x_3/2$	0.00	0.00	-14.08	-30.83	11.15	-67.15	0.00
23	$x_1\ x_1\ x_5/2$	0.00	2.81	57.68	11.72	14.29	-48.23	0.00
24	$x_1\ x_3\ x_3/2$	0.00	0.00	-48.21	-14.29	40.54	72.22	83.44
25	$x_1\ x_3\ x_4$	0.00	0.00	9.70	39.73	63.43	-13.79	0.00
26	$x_1\ x_3\ x_5$	0.00	0.00	-8.41	-8.39	-1.51	5.93	57.28
27	$x_1\ x_4\ x_5$	0.00	0.00	-6.49	5.86	-1.82	-40.51	0.00
28	$x_1\ x_5\ x_5/2$	0.00	0.00	27.94	-6.40	-35.42	-78.46	-57.85
29	$x_3\ x_3\ x_3/6$	0.00	-72.96	-64.83	7.96	81.68	116.27	187.73
30	$x_3\ x_3\ x_4/2$	0.00	98.39	52.29	5.73	-32.15	-35.47	0.00
31	$x_3\ x_3\ x_5/2$	0.00	-18.80	12.53	4.15	12.02	-3.24	-42.41
32	$x_3\ x_4\ x_4/2$	0.00	-74.92	-8.12	-8.41	-42.27	-33.64	0.00
33	$x_3\ x_4\ x_5$	0.00	-6.34	-41.86	-5.54	15.64	42.59	0.00
34	$x_3\ x_5\ x_5/2$	0.00	-75.38	-5.52	32.27	62.84	44.41	-51.21
35	$x_4\ x_4\ x_5/2$	0.00	13.14	25.61	16.43	-34.37	-27.71	211.60
36	$x_4\ x_5\ x_5/2$	0.00	-1.47	-13.69	12.21	-18.90	-17.02	0.00

TABLE VI. - DERIVATIVE VALUES FOR RELATIVE SPECTRA LEVELS AT COORDINATE POINTS, RSL(θ_c, η_c)

Derivative Index, j	Derivative Multiplier, X_j	$RSL_{,j}$ (0,-1.5)	$RSL_{,j}$ (0,-1.0)	$RSL_{,j}$ (0,-0.5)	$RSL_{,j}$ (0,0.0)	$RSL_{,j}$ (0,0.5)	$RSL_{,j}$ (0,1.0)	$RSL_{,j}$ (0,1.5)
				Circular and Coaxial Jet				
1	1	3.70	-2.47	-1.86	2.47	3.43	3.09	.79
2	x_1	7.34	-23.49	1.68	3.78	-7.11	-3.09	-5.46
3	x_2	-10.40	12.67	3.69	-2.71	-1.73	7.00	10.52
4	$x_1\ x_1/2$	0.00	-4.52	45.78	-58.04	-134.84	-144.66	0.00
5	$x_1\ x_2$	0.00	79.23	1.83	13.59	30.92	19.66	145.06
6	$x_2\ x_2/2$	-18.95	-80.04	-26.44	-13.19	-11.66	48.07	0.00
7	$x_1\ x_1\ x_2/2$	0.00	129.39	-56.85	-13.42	-148.64	-310.26	0.00
8	$x_1\ x_2\ x_2/2$	0.00	-110.57	-133.33	50.04	517.96	444.11	0.00
				Coaxial Jet Only				
9	x_3	-14.34	5.46	11.36	-7.62	-27.22	-35.73	-16.11
10	x_4	7.58	-8.73	-6.40	7.93	13.60	15.86	9.31
11	$x_1\ x_3$	0.00	-1.96	-6.81	4.70	-10.47	-32.32	21.79
12	$x_1\ x_4$	0.00	-41.58	29.32	13.68	-21.77	-34.43	0.00
13	$x_1\ x_5$	0.00	-3.23	61.90	-17.86	-75.31	-82.60	55.93
14	$x_2\ x_3$	0.00	.99	46.61	-18.29	-68.09	-46.64	0.00
15	$x_2\ x_4$	0.00	4.78	-90.89	17.67	100.51	145.35	0.00
16	$x_2\ x_5$	0.00	11.20	-14.99	7.15	22.38	19.47	35.58
17	$x_3\ x_3/2$	0.00	-30.45	13.60	-24.54	-57.11	-93.90	46.63
18	$x_3\ x_4$	-56.30	72.74	29.52	2.09	-20.12	-23.78	-42.10
19	$x_3\ x_5$	23.01	-20.76	28.84	3.56	-37.31	-39.03	17.53
20	$x_4\ x_4/2$	116.22	-68.87	-49.73	-.92	34.58	75.72	6.62
21	$x_4\ x_5$	-153.51	-14.73	-52.93	5.43	65.15	87.70	24.43
22	$x_1\ x_1\ x_3/2$	0.00	0.00	-5.21	-7.88	-27.75	-91.66	0.00
23	$x_1\ x_1\ x_5/2$	0.00	-52.60	-32.86	34.90	78.78	6.24	0.00
24	$x_1\ x_3\ x_3/2$	0.00	0.00	-24.66	1.03	11.79	-24.29	11.27
25	$x_1\ x_3\ x_4$	0.00	0.00	30.99	4.62	-51.20	-101.39	0.00
26	$x_1\ x_3\ x_5$	0.00	0.00	-.45	9.05	5.80	-38.76	-27.01
27	$x_1\ x_4\ x_5$	0.00	0.00	8.72	3.72	1.63	42.76	0.00
28	$x_1\ x_5\ x_5/2$	0.00	0.00	-112.81	54.06	155.31	144.63	-58.70
29	$x_3\ x_3\ x_3/6$	0.00	-40.89	3.99	-18.37	-43.95	-41.88	118.17
30	$x_3\ x_3\ x_4/2$	0.00	28.94	-10.23	-6.37	11.03	-57.54	0.00
31	$x_3\ x_3\ x_5/2$	0.00	-14.94	-6.12	16.18	16.62	25.73	40.40
32	$x_3\ x_4\ x_4/2$	0.00	97.14	89.70	-30.99	-50.66	-67.03	0.00
33	$x_3\ x_4\ x_5$	0.00	-28.07	27.76	-38.71	-55.94	-78.03	0.00
34	$x_3\ x_5\ x_5/2$	0.00	-1.42	-37.32	-3.53	54.04	26.98	-10.95
35	$x_4\ x_4\ x_5/2$	0.00	52.79	43.89	-10.51	-3.60	-27.94	253.16
36	$x_4\ x_5\ x_5/2$	0.00	16.83	114.16	-27.20	-133.30	-135.23	0.00

TABLE VI. - Continued.

Derivative Index, j	Derivative Multiplier, X_j	RSL,$_j$ (30,-1.5)	RSL,$_j$ (30,-1.0)	RSL,$_j$ (30,-0.5)	RSL,$_j$ (30,0.0)	RSL,$_j$ (30,0.5)	RSL,$_j$ (30,1.0)	RSL,$_j$ (30,1.5)
					Circular and Coaxial Jet			
1	1	1.22	-3.65	-2.37	2.62	4.47	4.41	1.94
2	x_1	3.17	-12.44	1.37	2.62	-2.10	.79	-3.77
3	x_2	-.48	11.92	5.55	-1.35	-4.34	4.23	1.59
4	$x_1\ x_1/2$	0.00	16.82	31.26	-26.27	-60.59	-78.79	0.00
5	$x_1\ x_2$	0.00	29.00	-6.71	-2.08	21.60	29.71	48.83
6	$x_2\ x_2/2$	-26.42	-24.89	-1.74	-8.55	-50.63	-18.07	0.00
7	$x_1\ x_1\ x_2/2$	0.00	-65.02	-98.78	-21.59	73.99	-88.84	0.00
8	$x_1\ x_2\ x_2/2$	0.00	-61.09	-90.94	38.34	266.55	177.25	0.00
					Coaxial Jet Only			
9	x_3	-9.00	-1.28	9.15	-6.66	-23.97	-30.07	-14.78
10	x_4	3.40	-3.79	-5.02	6.10	7.71	8.90	4.99
11	$x_1\ x_3$	0.00	-9.73	-9.05	5.80	11.00	-14.57	7.99
12	$x_1\ x_4$	0.00	-35.24	30.51	5.86	-25.85	-35.86	0.00
13	$x_1\ x_5$	0.00	-23.90	42.28	-9.11	-58.50	-47.12	25.90
14	$x_2\ x_3$	0.00	-10.10	43.55	-14.30	-60.97	-41.78	0.00
15	$x_2\ x_4$	0.00	26.77	-77.65	11.22	54.51	92.39	0.00
16	$x_2\ x_5$	0.00	16.09	-10.81	2.55	18.98	9.40	28.87
17	$x_3\ x_3/2$	0.00	-37.30	9.24	-23.27	-57.94	-84.83	18.83
18	$x_3\ x_4$	-40.64	52.12	24.29	2.35	-6.73	-7.98	-35.89
19	$x_3\ x_5$	21.42	-32.66	25.96	4.99	-27.44	-29.21	-.04
20	$x_4\ x_4/2$	110.97	-36.49	-37.40	-5.28	8.84	41.15	1.35
21	$x_4\ x_5$	-134.11	-9.04	-45.04	2.02	36.34	53.58	8.25
22	$x_1\ x_1\ x_3/2$	0.00	0.00	-15.31	15.41	45.05	-46.19	0.00
23	$x_1\ x_1\ x_5/2$	0.00	40.74	-35.61	16.35	66.24	1.65	0.00
24	$x_1\ x_3\ x_3/2$	0.00	0.00	-27.28	1.25	22.95	-11.08	26.79
25	$x_1\ x_3\ x_4$	0.00	0.00	32.81	7.86	-11.47	-62.92	0.00
26	$x_1\ x_3\ x_5$	0.00	0.00	-2.58	15.43	24.57	-17.51	-3.62
27	$x_1\ x_4\ x_5$	0.00	0.00	3.39	14.65	12.79	52.01	0.00
28	$x_1\ x_5\ x_5/2$	0.00	0.00	-82.90	44.36	134.04	103.78	-25.88
29	$x_3\ x_3\ x_3/6$	0.00	-10.65	.48	-20.26	-60.13	-56.46	37.24
30	$x_3\ x_3\ x_4/2$	0.00	-6.73	-15.65	-7.14	20.79	-30.57	0.00
31	$x_3\ x_3\ x_5/2$	0.00	7.83	-9.92	15.08	9.36	14.24	7.52
32	$x_3\ x_4\ x_4/2$	0.00	79.16	82.58	-16.82	19.56	.54	0.00
33	$x_3\ x_4\ x_5$	0.00	-33.59	27.01	-35.62	-40.64	-55.15	0.00
34	$x_3\ x_5\ x_5/2$	0.00	34.85	-37.25	-4.91	41.64	15.97	3.23
35	$x_4\ x_4\ x_5/2$	0.00	29.77	28.51	-.75	16.14	-2.06	140.03
36	$x_4\ x_5\ x_5/2$	0.00	38.85	93.89	-14.88	-82.56	-73.93	0.00

TABLE VI. - Continued.

Derivative Index, j	Derivative Multiplier, X_j	RSL,j (60,-1.5)	RSL,j (60,-1.0)	RSL,j (60,-0.5)	RSL,j (60,0.0)	RSL,j (60,0.5)	RSL,j (60,1.0)	RSL,j (60,1.5)
				Circular and Coaxial Jet				
1	1	-1.04	-4.01	-2.59	2.49	4.71	5.31	5.70
2	x_1	1.68	-10.40	.82	3.27	2.65	4.65	13.61
3	x_2	8.40	8.03	5.49	-.05	-2.26	.86	-1.43
4	$x_1\ x_1/2$	0.00	-15.22	15.47	-10.56	-16.55	-10.41	0.00
5	$x_1\ x_2$	0.00	32.16	-10.11	-10.91	4.78	24.80	-18.04
6	$x_2\ x_2/2$	-54.75	-22.01	11.27	-3.47	-40.41	-60.99	0.00
7	$x_1\ x_1\ x_2/2$	0.00	67.03	-98.32	-37.55	78.35	104.97	0.00
8	$x_1\ x_2\ x_2/2$	0.00	-63.85	-73.38	15.96	127.54	-46.86	0.00
				Coaxial Jet Only				
9	x_3	-8.24	-3.07	7.45	-7.22	-21.48	-21.52	-3.63
10	x_4	1.85	-4.67	-3.65	5.41	5.29	3.11	-5.95
11	$x_1\ x_3$	0.00	-8.12	-10.09	1.40	8.36	3.94	15.90
12	$x_1\ x_4$	0.00	-21.02	26.33	3.39	-20.13	-32.52	0.00
13	$x_1\ x_5$	0.00	-17.50	23.21	-13.25	-46.79	-11.60	-13.52
14	$x_2\ x_3$	0.00	-6.67	33.87	-14.76	-48.93	-29.83	0.00
15	$x_2\ x_4$	0.00	3.70	-56.95	16.79	36.10	50.35	0.00
16	$x_2\ x_5$	0.00	11.84	-7.34	2.45	16.31	.34	22.72
17	$x_3\ x_3/2$	0.00	-34.77	9.51	-22.56	-54.45	-71.08	-30.83
18	$x_3\ x_4$	-34.67	43.27	12.71	-.88	-1.44	8.36	-10.62
19	$x_3\ x_5$	15.08	-27.72	19.30	4.08	-20.55	-20.51	-27.21
20	$x_4\ x_4/2$	90.30	-25.73	-22.37	-3.00	-.65	10.03	-9.68
21	$x_4\ x_5$	-94.68	-6.51	-28.63	6.53	21.71	23.89	-5.39
22	$x_1\ x_1\ x_3/2$	0.00	0.00	-19.09	19.66	52.86	14.42	0.00
23	$x_1\ x_1\ x_5/2$	0.00	84.30	-17.47	-.33	18.33	18.42	0.00
24	$x_1\ x_3\ x_3/2$	0.00	0.00	-24.30	-2.10	19.39	-7.09	8.13
25	$x_1\ x_3\ x_4$	0.00	0.00	21.20	-.69	-7.37	-13.42	0.00
26	$x_1\ x_3\ x_5$	0.00	0.00	-5.30	15.67	29.17	-2.62	-23.46
27	$x_1\ x_4\ x_5$	0.00	0.00	-2.59	14.39	10.40	55.69	0.00
28	$x_1\ x_5\ x_5/2$	0.00	0.00	-46.18	47.14	97.73	59.63	-7.09
29	$x_3\ x_3\ x_3/6$	0.00	-28.94	-.50	-25.94	-62.34	-56.14	-30.64
30	$x_3\ x_3\ x_4/2$	0.00	8.84	-13.79	-.10	23.46	-14.60	0.00
31	$x_3\ x_3\ x_5/2$	0.00	-5.87	-12.63	12.37	7.23	7.76	-3.71
32	$x_3\ x_4\ x_4/2$	0.00	94.57	56.22	-20.01	38.75	33.84	0.00
33	$x_3\ x_4\ x_5$	0.00	-18.78	24.01	-33.64	-31.31	-36.27	0.00
34	$x_3\ x_5\ x_5/2$	0.00	25.00	-31.07	-5.05	33.85	9.21	24.65
35	$x_4\ x_4\ x_5/2$	0.00	22.52	15.73	-.36	18.51	8.29	-23.59
36	$x_4\ x_5\ x_5/2$	0.00	15.45	59.52	-20.12	-52.72	-22.75	0.00

TABLE VI. - Continued.

Derivative Index, j	Derivative Multiplier, X_j	RSL,$_j$ (90,-1.5)	RSL,$_j$ (90,-1.0)	RSL,$_j$ (90,-0.5)	RSL,$_j$ (90,0.0)	RSL,$_j$ (90,0.5)	RSL,$_j$ (90,1.0)	RSL,$_j$ (90,1.5)
					Circular and Coaxial Jet			
1	1	-1.64	-5.07	-2.41	2.46	4.07	5.42	5.12
2	x_1	.01	-5.84	-1.71	4.05	8.19	7.07	19.60
3	x_2	-10.22	2.57	4.45	1.99	2.55	.41	8.46
4	$x_1\ x_1/2$	0.00	-3.41	-.09	-5.26	4.20	-16.48	0.00
5	$x_1\ x_2$	0.00	24.45	-5.45	-17.12	-3.89	6.16	29.34
6	$x_2\ x_2/2$	55.56	-4.72	9.32	1.67	-11.66	-35.36	0.00
7	$x_1\ x_1\ x_2/2$	0.00	121.57	-71.18	-90.44	-28.79	20.68	0.00
8	$x_1\ x_2\ x_2/2$	0.00	-115.10	-44.51	-4.80	-9.91	-70.58	0.00
					Coaxial Jet Only			
9	x_3	-9.26	-7.37	4.64	-5.91	-11.96	-8.03	8.45
10	x_4	2.52	-2.83	-2.47	2.04	1.12	.34	-6.16
11	$x_1\ x_3$	0.00	-6.49	-3.32	-2.26	-11.98	6.59	23.63
12	$x_1\ x_4$	0.00	-7.52	9.00	3.32	-1.24	-6.76	0.00
13	$x_1\ x_5$	0.00	.15	2.08	-13.37	-14.77	11.29	-8.09
14	$x_2\ x_3$	0.00	-6.25	11.58	-10.70	-12.29	-2.58	0.00
15	$x_2\ x_4$	0.00	-9.20	-28.32	10.92	16.60	30.37	0.00
16	$x_2\ x_5$	0.00	6.09	-3.78	1.41	1.65	-4.28	-7.00
17	$x_3\ x_3/2$	0.00	-34.43	6.60	-17.84	-29.55	-49.04	-55.14
18	$x_3\ x_4$	-24.61	14.69	-1.76	-.14	10.36	23.52	28.75
19	$x_3 \cdot x_5$	2.26	-29.04	8.14	9.82	5.10	-13.15	-35.69
20	$x_4\ x_4/2$	30.25	7.18	-8.14	-9.00	-17.37	-10.68	3.12
21	$x_4\ x_5$	-13.68	7.44	-9.72	4.43	.43	10.26	-.50
22	$x_1\ x_1\ x_3/2$	0.00	0.00	-20.17	9.20	7.91	17.34	0.00
23	$x_1\ x_1\ x_5/2$	0.00	52.85	-9.48	-16.29	-19.67	57.36	0.00
24	$x_1\ x_3\ x_3/2$	0.00	0.00	-16.28	-5.91	-1.19	-30.38	-48.93
25	$x_1\ x_3\ x_4$	0.00	0.00	14.87	-15.15	-35.69	18.35	0.00
26	$x_1\ x_3\ x_5$	0.00	0.00	-6.62	11.31	16.32	-13.90	-56.75
27	$x_1\ x_4\ x_5$	0.00	0.00	5.94	9.25	1.63	30.34	0.00
28	$x_1\ x_5\ x_5/2$	0.00	0.00	-.69	38.42	28.92	19.82	-6.66
29	$x_3\ x_3\ x_3/6$	0.00	-14.76	-9.06	-40.22	-56.62	-34.81	-8.59
30	$x_3\ x_3\ x_4/2$	0.00	-27.12	-3.05	21.81	46.23	-11.04	0.00
31	$x_3\ x_3\ x_5/2$	0.00	-7.97	-16.56	7.49	7.59	9.20	22.75
32	$x_3\ x_4\ x_4/2$	0.00	97.36	29.94	-12.12	6.42	-9.61	0.00
33	$x_3\ x_4\ x_5$	0.00	-5.12	19.28	-27.67	-19.83	-30.84	0.00
34	$x_3\ x_5\ x_5/2$	0.00	32.30	-20.86	-16.58	-5.19	2.62	33.55
35	$x_4\ x_4\ x_5/2$	0.00	9.93	8.12	8.77	12.36	-.88	-64.11
36	$x_4\ x_5\ x_5/2$	0.00	-17.83	26.20	-9.70	1.61	-6.07	0.00

TABLE VI. - Continued.

Derivative Index, j	Derivative Multiplier, X_j	$RSL_{,j}$ (120,-1.5)	$RSL_{,j}$ (120,-1.0)	$RSL_{,j}$ (120,-0.5)	$RSL_{,j}$ (120,0.0)	$RSL_{,j}$ (120,0.5)	$RSL_{,j}$ (120,1.0)	$RSL_{,j}$ (120,1.5)
				Circular and Coaxial Jet				
1	1	-3.75	-5.07	-1.38	2.84	2.78	2.90	2.00
2	x_1	-10.99	-5.83	-.71	5.74	8.91	8.99	22.10
3	x_2	6.77	6.36	4.60	-.15	-1.05	-5.86	8.12
4	$x_1\ x_1/2$	0.00	-1.46	5.42	-1.37	9.15	9.47	0.00
5	$x_1\ x_2$	0.00	8.00	-5.25	-23.25	-.79	23.37	74.06
6	$x_2\ x_2/2$	-27.09	20.42	4.04	-3.05	-23.47	-60.23	0.00
7	$x_1\ x_1\ x_2/2$	0.00	-17.17	-79.12	-92.67	13.61	219.91	0.00
8	$x_1\ x_2\ x_2/2$	0.00	-82.36	-4.86	-1.39	-116.57	-264.53	0.00
				Coaxial Jet Only				
9	x_3	-1.58	-4.94	.77	-3.71	-4.01	3.44	9.85
10	x_4	-.66	-3.83	-1.68	-.59	-2.15	-3.59	-7.35
11	$x_1\ x_3$	0.00	-.15	-16.01	1.83	-7.76	23.14	30.71
12	$x_1\ x_4$	0.00	9.98	9.60	.45	-2.78	-4.94	0.00
13	$x_1\ x_5$	0.00	18.91	-1.24	-9.72	3.39	14.36	-9.17
14	$x_2\ x_3$	0.00	-.31	2.47	-4.45	9.74	11.03	0.00
15	$x_2\ x_4$	0.00	-9.64	-9.53	-1.42	4.99	14.15	0.00
16	$x_2\ x_5$	0.00	-7.50	4.34	2.51	-7.77	-12.63	-12.49
17	$x_3\ x_3/2$	0.00	-23.61	3.52	-12.23	-12.54	-20.67	-34.22
18	$x_3\ x_4$	3.96	1.57	-2.95	3.88	19.95	25.73	32.38
19	$x_3\ x_5$	-3.56	-14.05	6.19	14.59	16.09	-5.74	-12.25
20	$x_4\ x_4/2$	-28.10	6.69	-6.91	-7.38	-26.65	-26.72	-20.14
21	$x_4\ x_5$	28.47	3.23	-.63	.65	-3.58	7.60	-2.19
22	$x_1\ x_1\ x_3/2$	0.00	0.00	-39.90	14.80	35.21	74.22	0.00
23	$x_1\ x_1\ x_5/2$	0.00	-13.92	-18.90	2.66	16.38	80.70	0.00
24	$x_1\ x_3\ x_3/2$	0.00	0.00	-24.09	-4.64	5.10	-2.84	-44.56
25	$x_1\ x_3\ x_4$	0.00	0.00	-1.02	-16.51	-54.63	23.63	0.00
26	$x_1\ x_3\ x_5$	0.00	0.00	-15.83	4.07	16.82	6.56	-50.69
27	$x_1\ x_4\ x_5$	0.00	0.00	-8.10	4.35	13.98	33.27	0.00
28	$x_1\ x_5\ x_5/2$	0.00	0.00	-25.06	28.55	31.90	45.37	20.46
29	$x_3\ x_3\ x_3/6$	0.00	2.05	-5.22	-37.38	-47.57	-7.72	32.20
30	$x_3\ x_3\ x_4/2$	0.00	-62.76	-5.59	23.58	54.21	-7.63	0.00
31	$x_3\ x_3\ x_5/2$	0.00	-10.84	-8.15	5.74	6.65	10.65	35.61
32	$x_3\ x_4\ x_4/2$	0.00	97.85	43.33	10.87	-15.19	-46.29	0.00
33	$x_3\ x_4\ x_5$	0.00	-2.13	8.79	-20.43	-18.55	-24.10	0.00
34	$x_3\ x_5\ x_5/2$	0.00	-1.19	-14.11	-24.01	-25.52	-.60	6.02
35	$x_4\ x_4\ x_5/2$	0.00	-2.44	14.15	3.45	9.84	-3.12	-40.05
36	$x_4\ x_5\ x_5/2$	0.00	11.61	10.29	-6.60	10.36	-6.70	0.00

TABLE VI. - Continued.

Derivative Index, j	Derivative Multiplier, X_j	$RSL_{,j}$ (150,-1.5)	$RSL_{,j}$ (150,-1.0)	$RSL_{,j}$ (150,-0.5)	$RSL_{,j}$ (150,0.0)	$RSL_{,j}$ (150,0.5)	$RSL_{,j}$ (150,1.0)	$RSL_{,j}$ (150,1.5)
					Circular and Coaxial Jet			
1	1	.57	1.48	1.16	-4.05	-8.48	-9.64	-6.38
2	x_1	-3.13	-3.25	-1.81	3.84	11.45	8.21	-.40
3	x_2	-7.24	3.72	-.78	-9.83	-7.76	-3.31	10.60
4	$x_1\ x_1/2$	0.00	-20.25	-1.80	43.37	69.04	48.36	0.00
5	$x_1\ x_2$	0.00	11.92	11.21	41.01	40.45	46.86	45.50
6	$x_2\ x_2/2$	68.97	-4.15	-22.85	-30.81	-25.27	18.50	0.00
7	$x_1\ x_1\ x_2/2$	0.00	12.63	31.88	242.06	152.09	115.90	0.00
8	$x_1\ x_2\ x_2/2$	0.00	-67.21	-44.76	-99.58	-224.10	-68.30	0.00
					Coaxial Jet Only			
9	x_3	1.92	1.97	1.92	.41	23.11	16.02	-2.13
10	x_4	2.55	-2.33	-1.43	-.21	-6.60	-.98	-1.19
11	$x_1\ x_3$	0.00	2.84	-2.80	16.32	-10.12	-18.37	-19.07
12	$x_1\ x_4$	0.00	-4.78	3.29	-5.57	10.57	7.82	0.00
13	$x_1\ x_5$	0.00	15.12	2.02	31.06	34.53	10.95	10.60
14	$x_2\ x_3$	0.00	.80	-4.05	-2.26	53.96	20.53	0.00
15	$x_2\ x_4$	0.00	-11.26	-9.27	7.92	-21.05	7.66	0.00
16	$x_2\ x_5$	0.00	.62	2.58	-13.42	-25.25	-22.41	-5.96
17	$x_3\ x_3/2$	0.00	-3.72	11.77	-3.41	56.88	22.00	14.92
18	$x_3\ x_4$	7.66	-.22	-4.35	11.95	9.86	19.70	-21.98
19	$x_3\ x_5$	7.72	-10.19	.37	-6.48	13.93	5.61	-1.69
20	$x_4\ x_4/2$	1.75	14.22	2.96	9.16	-6.88	.10	10.68
21	$x_4\ x_5$	-33.12	.31	-1.74	-3.54	-12.28	-5.68	.17
22	$x_1\ x_1\ x_3/2$	0.00	0.00	23.56	14.44	-3.67	-79.52	0.00
23	$x_1\ x_1\ x_5/2$	0.00	-51.56	4.43	27.26	67.90	41.75	0.00
24	$x_1\ x_3\ x_3/2$	0.00	0.00	2.85	7.28	-22.91	-68.32	-43.88
25	$x_1\ x_3\ x_4$	0.00	0.00	-25.37	38.64	15.03	103.03	0.00
26	$x_1\ x_3\ x_5$	0.00	0.00	7.39	-.14	-25.53	-26.80	-18.93
27	$x_1\ x_4\ x_5$	0.00	0.00	-24.99	37.73	2.31	26.87	0.00
28	$x_1\ x_5\ x_5/2$	0.00	0.00	-6.14	-24.67	-30.80	21.39	-23.25
29	$x_3\ x_3\ x_3/6$	0.00	21.93	3.32	35.00	93.37	55.56	-37.64
30	$x_3\ x_3\ x_4/2$	0.00	-53.50	17.20	-31.01	-67.11	-66.72	0.00
31	$x_3\ x_3\ x_5/2$	0.00	-1.44	.70	17.49	-3.57	3.56	-28.65
32	$x_3\ x_4\ x_4/2$	0.00	79.25	.40	11.73	-9.13	-13.06	0.00
33	$x_3\ x_4\ x_5$	0.00	-1.08	6.44	-5.40	23.62	-13.87	0.00
34	$x_3\ x_5\ x_5/2$	0.00	7.52	9.15	16.30	-24.65	-26.73	-10.78
35	$x_4\ x_4\ x_5/2$	0.00	3.99	-6.95	-32.98	-36.57	-45.42	-23.67
36	$x_4\ x_5\ x_5/2$	0.00	12.71	-10.21	9.01	29.39	17.86	0.00

TABLE VI. - Concluded.

Derivative Index, j	Derivative Multiplier, X_j	$RSL_{,j}$ (180,-1.5)	$RSL_{,j}$ (180,-1.0)	$RSL_{,j}$ (180,-0.5)	$RSL_{,j}$ (180,0.0)	$RSL_{,j}$ (180,0.5)	$RSL_{,j}$ (180,1.0)	$RSL_{,j}$ (180,1.5)
					Circular and Coaxial Jet			
1	1	6.13	3.28	-1.66	-9.46	-13.73	-17.83	-5.16
2	x_1	8.21	-15.04	-11.38	36.90	38.22	25.34	17.61
3	x_2	-27.22	-3.27	-4.87	-7.76	-9.06	2.92	47.67
4	$x_1\ x_1/2$	0.00	-56.74	-20.87	165.10	229.84	206.89	0.00
5	$x_1\ x_2$	0.00	14.15	63.07	91.22	54.84	157.94	132.35
6	$x_2\ x_2/2$	301.38	64.74	-37.06	-141.02	-142.23	-83.90	0.00
7	$x_1\ x_1\ x_2/2$	0.00	29.51	268.47	436.49	335.42	825.13	0.00
8	$x_1\ x_2\ x_2/2$	0.00	201.87	-150.70	-887.25	-759.51	-510.85	0.00
					Coaxial Jet Only			
9	x_3	-4.75	8.79	7.06	2.43	36.60	1.49	-29.70
10	x_4	-2.31	1.91	2.04	-10.21	-29.55	-4.60	3.56
11	$x_1\ x_3$	0.00	17.85	16.31	-23.56	-97.40	-114.67	-96.11
12	$x_1\ x_4$	0.00	-45.07	10.33	12.97	31.14	18.73	0.00
13	$x_1\ x_5$	0.00	12.86	-16.91	66.40	111.36	28.15	-13.06
14	$x_2\ x_3$	0.00	-38.36	2.67	28.36	129.73	-1.39	0.00
15	$x_2\ x_4$	0.00	-30.24	-18.53	15.12	-77.39	-25.45	0.00
16	$x_2\ x_5$	0.00	6.90	-5.87	-12.50	-12.68	-29.86	11.73
17	$x_3\ x_3/2$	0.00	6.71	16.54	1.82	88.47	-6.30	-20.05
18	$x_3\ x_4$	-59.56	-2.31	-37.03	29.44	49.66	65.14	-31.08
19	$x_3\ x_5$	12.66	-29.84	1.55	-31.55	-12.22	5.36	4.64
20	$x_4\ x_4/2$	183.17	57.93	37.41	-22.43	-85.53	-53.26	5.13
21	$x_4\ x_5$	-144.23	2.79	11.86	11.33	-13.83	-28.29	-13.92
22	$x_1\ x_1\ x_3/2$	0.00	0.00	56.87	-89.17	-95.05	-228.34	0.00
23	$x_1\ x_1\ x_5/2$	0.00	27.43	35.98	-54.51	184.80	48.70	0.00
24	$x_1\ x_3\ x_3/2$	0.00	0.00	-9.77	28.36	-145.77	-222.84	-122.21
25	$x_1\ x_3\ x_4$	0.00	0.00	-5.69	-8.15	91.04	226.45	0.00
26	$x_1\ x_3\ x_5$	0.00	0.00	17.37	-11.99	-112.43	-59.14	21.94
27	$x_1\ x_4\ x_5$	0.00	0.00	-60.67	60.97	-33.31	5.14	0.00
28	$x_1\ x_5\ x_5/2$	0.00	0.00	81.75	-141.60	-218.76	-11.09	45.86
29	$x_3\ x_3\ x_3/6$	0.00	-37.94	-26.52	105.37	322.06	28.70	-81.44
30	$x_3\ x_3\ x_4/2$	0.00	102.07	32.66	-131.42	-371.95	-28.07	0.00
31	$x_3\ x_3\ x_5/2$	0.00	-13.03	-37.87	33.14	14.40	-20.46	-77.55
32	$x_3\ x_4\ x_4/2$	0.00	-134.85	-151.19	137.04	394.27	213.23	0.00
33	$x_3\ x_4\ x_5$	0.00	-69.43	29.27	-42.15	50.64	80.24	0.00
34	$x_3\ x_5\ x_5/2$	0.00	-21.05	-15.31	47.86	35.66	-22.57	-50.13
35	$x_4\ x_4\ x_5/2$	0.00	158.03	-1.66	46.07	48.81	39.88	-78.17
36	$x_4\ x_5\ x_5/2$	0.00	61.37	-73.92	40.43	56.84	84.53	0.00

TABLE VII. - TOTAL NUMBER OF TEST POINTS IN DATA BASE

SOURCE	SET	NUMBER OF ANGLES	NUMBER OF FREQUENCIES	NUMBER OF CASES	TOTAL NUMBER OF SPL VALUES
NGTE	A	7	23	204	32,844
NGTE	C	8	27	277	59,832
NGTE	D	7	26	21	3,822
PWA	A	8	30	50	12,000
SNECMA	A	15	28	34	14,280
SNECMA	B	15	28	44	18,480
GELAC	A	19	24	59	26,904
GELAC	B	10	22	32	7,040
NASA LEWIS	A	8	27	96	20,736
	TOTAL			817	195,938

TABLE VIII. - NUMBER OF PREDICTION CONSTANTS

DERIVATIVE TERM	NUMBER OF DERIVATIVE MULTIPLIERS	NUMBER OF DIRECTIVITY ANGLES	NUMBER FREQUENCY TERMS	TOTAL NUMBER OF DERIVATIVE CONSTANTS
		CIRCULAR JET		
$PWL_{,j}$	8	1	1	8
$DI_{,j}(\theta_c)$	8	7	1	56
$F_{,j}(n_c)$	8	1	7	56
$RSL_{,j}(\theta_c,n_c)$	8	7	7	392
TOTAL				512
		COAXIAL JET		
$PWL_{,j}$	36	1	1	36
$DI_{,j}(\theta_c)$	36	7	1	252
$F_{,j}(n_c)$	36	1	7	252
$RSL_{,j}(\theta_c,n_c)$	36	7	7	1,764
TOTAL				2,304

TABLE IX. - STANDARD DEVIATIONS FOR PREDICTED SOUND PRESSURE LEVEL VALUES

Normalized Frequency Parameter	Directivity Angle, θ_c						
η_c	0°	30°	60°	90°	120°	150°	180°
-1.5	1.99	1.58	1.50	1.15	1.13	1.12	2.01
-1.0	2.23	1.75	1.62	1.29	1.29	1.30	2.16
-0.5	1.67	1.38	1.28	0.99	0.97	0.95	1.97
0.0	1.60	1.28	1.21	0.95	0.93	0.99	2.82
0.5	2.11	1.65	1.49	1.11	1.15	1.37	4.02
1.0	2.24	1.76	1.59	1.37	1.41	1.69	4.33
1.5	2.14	1.75	1.61	1.36	1.34	1.43	3.16

The mean error is 0.0 dB for all values of η_c and θ_c.

TABLE X. - STANDARD ERROR PREDICTION SUMMARY FOR SELECTED TESTS

DIRECTIVITY ANGLE degrees	MINIMUM STD. ERROR dB	MAXIMUM STD. ERROR dB	AVERAGE STD. ERROR dB
CIRCULAR JET (12 CASES)			
90	0.593	2.861	1.559
120	0.813	2.891	1.757
150	1.140	3.134	1.875
COANNULAR JET (26 CASES)			
90	0.618	3.135	1.588
120	0.549	3.583	1.465
150	1.181	5.491	2.542

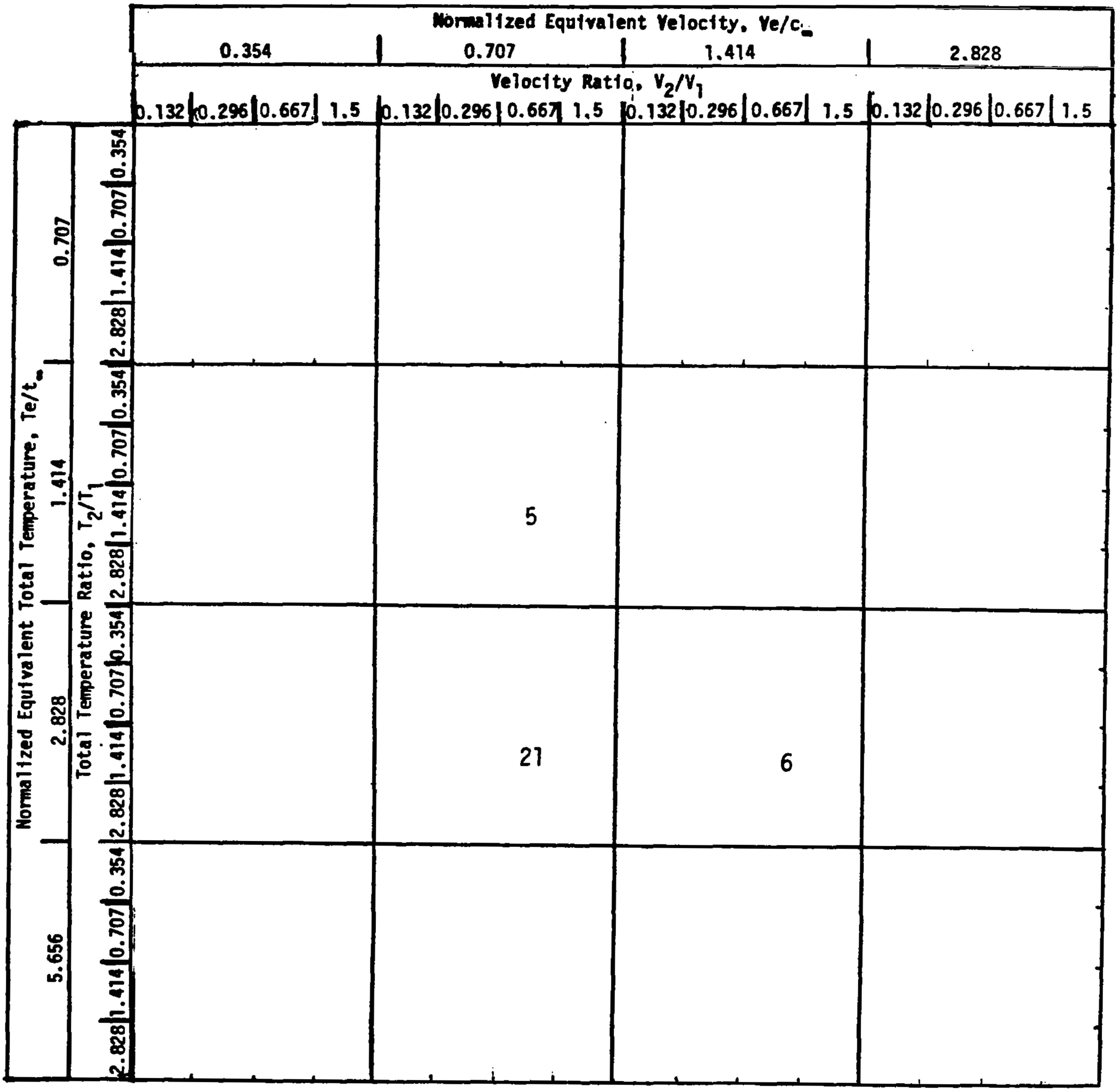

(a) Circular jet.

Figure 1. - Jet noise test points for NGTE set A.

		Normalized Equivalent Velocity, V_e/c_∞															
		0.354				0.707				1.414				2.828			
		Velocity Ratio, V_2/V_1															
Normalized Equivalent Total Temperature, T_e/t_∞	Total Temperature Ratio, T_2/T_1	0.132	0.296	0.667	1.5	0.132	0.296	0.667	1.5	0.132	0.296	0.667	1.5	0.132	0.296	0.667	1.5
0.707	0.354																
	0.707																
	1.414																
	2.828																
1.414	0.354	2	8	6			9	16	6								
	0.707		2	1			2	5									
	1.414																
	2.828																
2.828	0.354					1											
	0.707																
	1.414																
	2.828																
5.656	0.354																
	0.707																
	1.414																
	2.828																

(b) Coaxial jet, area ratio = 2.0.

Figure 1. - Continued.

		Normalized Equivalent Velocity, Ve/c_∞															
		0.354				0.707				1.414				2.828			
		Velocity Ratio, V_2/V_1															
Normalized Equivalent Total Temperature, Te/t_∞	Total Temperature Ratio, T_2/T_1	0.132	0.296	0.667	1.5	0.132	0.296	0.667	1.5	0.132	0.296	0.667	1.5	0.132	0.296	0.667	1.5
0.707	0.354																
	0.707																
	1.414																
	2.828																
1.414	0.354	4	12	8			4	14	6								
	0.707	1	1	2			2	4									
	1.414																
	2.828																
2.828	0.354																
	0.707																
	1.414																
	2.828																
5.656	0.354																
	0.707																
	1.414																
	2.828																

(c) Coaxial jet, area ratio = 4.0.

Figure 1. - Continued.

		Normalized Equivalent Velocity, V_e/c_∞															
		0.354				0.707				1.414				2.828			
		Velocity Ratio, V_2/V_1															
Normalized Equivalent Total Temperature, T_e/t_∞	Total Temperature Ratio, T_2/T_1	0.132	0.296	0.667	1.5	0.132	0.296	0.667	1.5	0.132	0.296	0.667	1.5	0.132	0.296	0.667	1.5
0.707	0.354																
	0.707																
	1.414																
	2.828																
1.414	0.354	4	14	7			2	15	5								
	0.707		2	1		1	1	4									
	1.414																
	2.828																
2.828	0.354																
	0.707																
	1.414																
	2.828																
5.656	0.354																
	0.707																
	1.414																
	2.828																

(d) Coaxial jet, area ratio = 6.0.

Figure 1. - Concluded.

		Normalized Equivalent Velocity, V_e/c_∞															
		0.354				0.707				1.414				2.828			
		Velocity Ratio, V_2/V_1															
Normalized Equivalent Total Temperature, T_e/t_∞	Total Temperature Ratio, T_2/T_1	0.132	0.296	0.667	1.5	0.132	0.296	0.667	1.5	0.132	0.296	0.667	1.5	0.132	0.296	0.667	1.5
0.707	0.354																
	0.707																
	1.414																
	2.828																
1.414	0.354																
	0.707																
	1.414																
	2.828																
2.828	0.354																
	0.707																
	1.414							36				15					
	2.828																
5.656	0.354																
	0.707																
	1.414																
	2.828																

(a) Circular jet.

Figure 2. - Jet noise test points for NGTE set C.

Normalized Equivalent Total Temperature, Te/t_∞	Total Temperature Ratio, T_2/T_1	Normalized Equivalent Velocity, Ve/c_∞: 0.354				0.707				1.414				2.828			
	Velocity Ratio, V_2/V_1:	0.132	0.296	0.667	1.5	0.132	0.296	0.667	1.5	0.132	0.296	0.667	1.5	0.132	0.296	0.667	1.5
0.707	0.354																
	0.707																
	1.414																
	2.828																
1.414	0.354			2			4	5	6			1					
	0.707																
	1.414																
	2.828																
2.828	0.354						1										
	0.707																
	1.414																
	2.828																
5.656	0.354																
	0.707																
	1.414																
	2.828																

(b) Coaxial jet, area ratio = 1.4.

Figure 2. - Continued.

Normalized Equivalent Total Temperature, T_e/t_∞	Total Temperature Ratio, T_2/T_1	Normalized Equivalent Velocity, V_e/c_∞: 0.354				0.707				1.414				2.828			
	Velocity Ratio, V_2/V_1	0.132	0.296	0.667	1.5	0.132	0.296	0.667	1.5	0.132	0.296	0.667	1.5	0.132	0.296	0.667	1.5
0.707	0.354																
	0.707																
	1.414																
	2.828																
1.414	0.354		7	12		1	17	31	23			7					
	0.707																
	1.414																
	2.828																
2.828	0.354	5	2			8	5			6							
	0.707																
	1.414																
	2.828																
5.656	0.354																
	0.707																
	1.414																
	2.828																

(c) Coaxial jet, area ratio = 1.5, 1.6, 1.9, and 2.0.

Figure 2. - Continued.

		Normalized Equivalent Velocity, V_e/c_∞															
		0.354				0.707				1.414				2.828			
Normalized Equivalent Total Temperature, T_e/t_∞	Total Temperature Ratio, T_2/T_1 \ Velocity Ratio, V_2/V_1	0.132	0.296	0.667	1.5	0.132	0.296	0.667	1.5	0.132	0.296	0.667	1.5	0.132	0.296	0.667	1.5
0.707	0.354																
	0.707																
	1.414																
	2.828																
1.414	0.354	3	5	4		1	5	11	12								
	0.707																
	1.414																
	2.828																
2.828	0.354	1								1							
	0.707																
	1.414																
	2.828																
5.656	0.354																
	0.707																
	1.414																
	2.828																

(d) Coaxial jet, area ratio = 4.0, 4.1, 4.3.

Figure 2. - Continued.

Normalized Equivalent Total Temperature, Te/t_∞	Total Temperature Ratio, T_2/T_1	Normalized Equivalent Velocity, Ve/c_∞: 0.354				0.707				1.414				2.828			
	Velocity Ratio, V_2/V_1	0.132	0.296	0.667	1.5	0.132	0.296	0.667	1.5	0.132	0.296	0.667	1.5	0.132	0.296	0.667	1.5
0.707	0.354																
	0.707																
	1.414																
	2.828																
1.414	0.354	5	9	4		1	6	8	2								
	0.707																
	1.414																
	2.828																
2.828	0.354	2				2				1							
	0.707																
	1.414																
	2.828																
5.656	0.354																
	0.707																
	1.414																
	2.828																

(e) Coaxial jet, area ratio = 7.9, 8.0, and 8.1.

Figure 2. - Concluded.

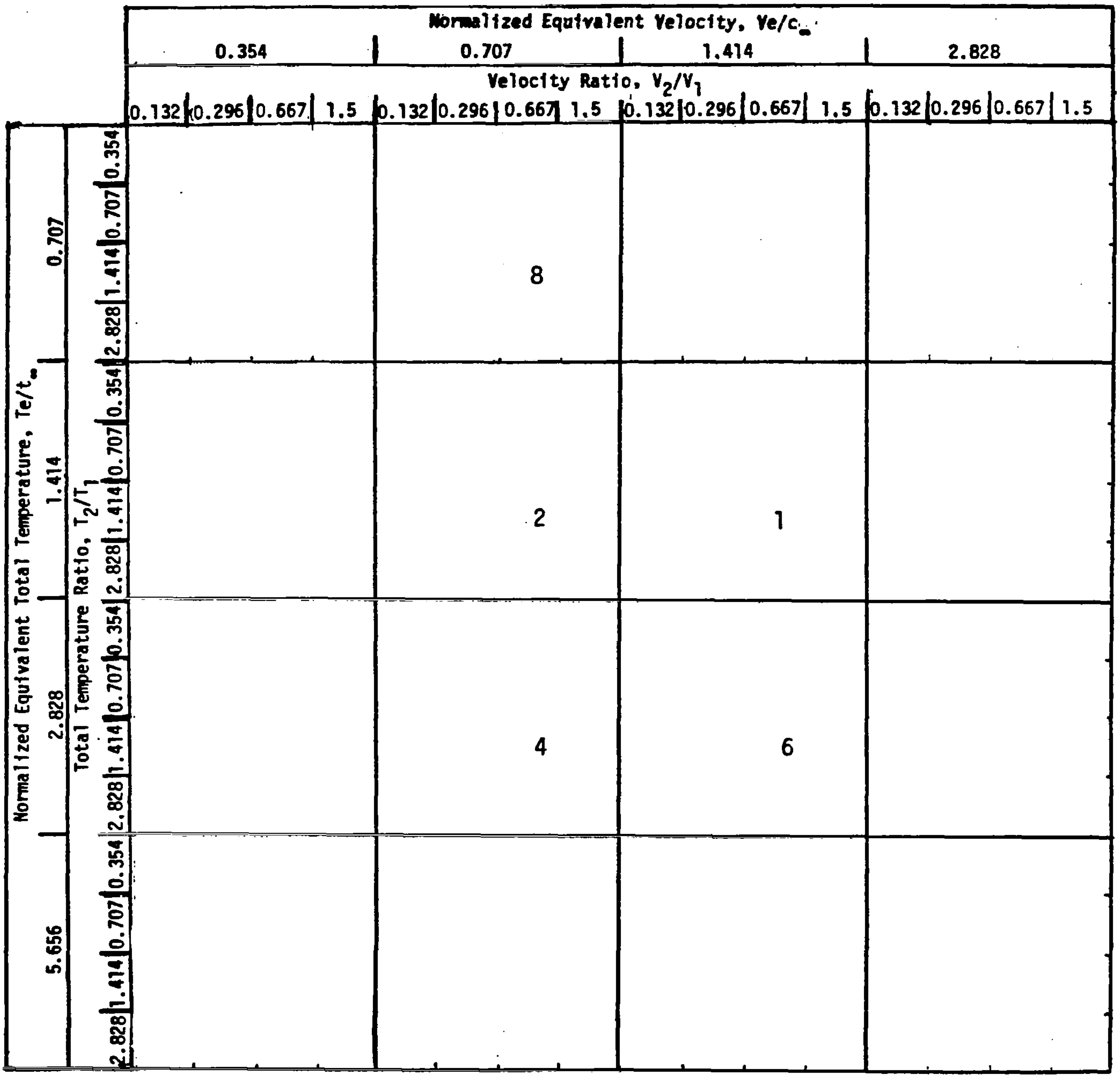

Figure 3. - Jet noise test points for NGTE set D circular jet.

Normalized Equivalent Total Temperature, Te/t_∞	Total Temperature Ratio, T_2/T_1	Normalized Equivalent Velocity, Ve/c_∞: 0.354 — Velocity Ratio, V_2/V_1: 0.132, 0.296, 0.667, 1.5	0.707 — 0.132, 0.296, 0.667, 1.5	1.414 — 0.132, 0.296, 0.667, 1.5	2.828 — 0.132, 0.296, 0.667, 1.5
0.707	2.828, 1.414, 0.707, 0.354				
1.414	2.828, 1.414, 0.707, 0.354		3	1	
2.828	2.828, 1.414, 0.707, 0.354		2	9	
5.656	2.828, 1.414, 0.707, 0.354				

(a) Circular jet.

Figure 4. - Jet noise test points for PWA set A.

		Normalized Equivalent Velocity, Ve/c_∞															
		0.354				0.707				1.414				2.828			
		Velocity Ratio, V_2/V_1															
Normalized Equivalent Total Temperature, Te/t_∞	Total Temperature Ratio, T_2/T_1	0.132	0.296	0.667	1.5	0.132	0.296	0.667	1.5	0.132	0.296	0.667	1.5	0.132	0.296	0.667	1.5
0.707	0.354																
	0.707																
	1.414																
	2.828																
1.414	0.354																
	0.707							2	1			1					
	1.414								2				2				
	2.828								1								
2.828	0.354											4					
	0.707											6	4				
	1.414											2	6				
	2.828								1				3				
5.656	0.354																
	0.707																
	1.414																
	2.828																

(b) Coaxial jet, area ratio = 0.75 and 1.2.

Figure 4. - Concluded.

Normalized Equivalent Total Temperature, Te/t_∞	Total Temperature Ratio, T_2/T_1	Normalized Equivalent Velocity, Ve/c_∞: 0.354	0.707	1.414	2.828
		Velocity Ratio, V_2/V_1: 0.132 | 0.296 | 0.667 | 1.5	0.132 | 0.296 | 0.667 | 1.5	0.132 | 0.296 | 0.667 | 1.5	0.132 | 0.296 | 0.667 | 1.5
0.707	0.354 | 0.707 | 1.414 | 2.828				
1.414	0.354 | 0.707 | 1.414 | 2.828				
2.828	0.354 | 0.707 | 1.414 | 2.828			4	
5.656	0.354 | 0.707 | 1.414 | 2.828				

(a) Circular jet.

Figure 5. - Jet noise test points for SNECMA set A.

Normalized Equivalent Total Temperature, Te/t_∞	Total Temperature Ratio, T_2/T_1	Normalized Equivalent Velocity, Ve/c_∞: 0.354				0.707				1.414				2.828			
	Velocity Ratio, V_2/V_1	0.132	0.296	0.667	1.5	0.132	0.296	0.667	1.5	0.132	0.296	0.667	1.5	0.132	0.296	0.667	1.5
0.707	0.354																
	0.707																
	1.414																
	2.828																
1.414	0.354			1				27									
	0.707																
	1.414								2								
	2.828																
2.828	0.354																
	0.707																
	1.414																
	2.828																
5.656	0.354																
	0.707																
	1.414																
	2.828																

(b) Coaxial jet, area ratio = 3.52.

Figure 5. - Concluded.

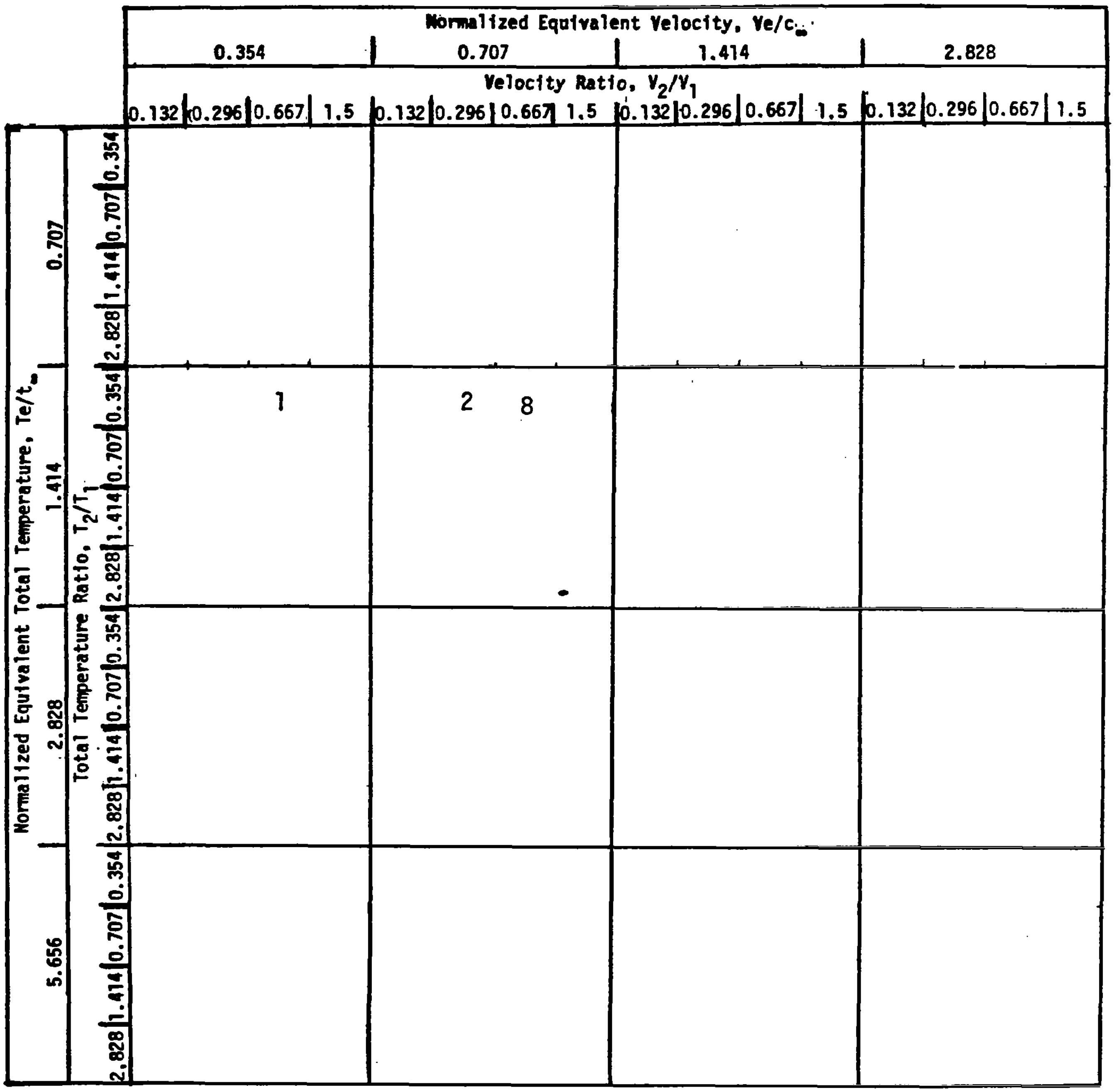

(a) Coaxial jet, area ratio = 2.25.

Figure 6. - Jet noise test points for SNECMA set B.

Normalized Equivalent Total Temperature, Te/t_∞	Total Temperature Ratio, T_2/T_1	Normalized Equivalent Velocity, Ve/c_∞: 0.354				0.707				1.414				2.828			
	Velocity Ratio, V_2/V_1	0.132	0.296	0.667	1.5	0.132	0.296	0.667	1.5	0.132	0.296	0.667	1.5	0.132	0.296	0.667	1.5
0.707	0.354																
	0.707																
	1.414																
	2.828																
1.414	0.354			2			2	11	1								
	0.707																
	1.414																
	2.828																
2.828	0.354																
	0.707																
	1.414																
	2.828																
5.656	0.354																
	0.707																
	1.414																
	2.828																

(b) Coaxial jet, area ratio = 3.92.

Figure 6. - Continued.

	Normalized Equivalent Velocity, Ve/c_∞	0.354				0.707				1.414				2.828			
Normalized Equivalent Total Temperature, Te/t_∞	Total Temperature Ratio, T_2/T_1 \ Velocity Ratio, V_2/V_1	0.132	0.296	0.667	1.5	0.132	0.296	0.667	1.5	0.132	0.296	0.667	1.5	0.132	0.296	0.667	1.5
0.707	0.354																
	0.707																
	1.414																
	2.828																
1.414	0.354			2			2	11	2								
	0.707																
	1.414																
	2.828																
2.828	0.354																
	0.707																
	1.414																
	2.828																
5.656	0.354																
	0.707																
	1.414																
	2.828																

(c) Coaxial jet, area ratio = 6.09.

Figure 6. - Concluded.

Normalized Equivalent Total Temperature, Te/t_∞	Total Temperature Ratio, T_2/T_1	Normalized Equivalent Velocity, Ve/c_∞: 0.354	0.707	1.414	2.828
		Velocity Ratio, V_2/V_1: 0.132, 0.296, 0.667, 1.5	0.132, 0.296, 0.667, 1.5	0.132, 0.296, 0.667, 1.5	0.132, 0.296, 0.667, 1.5
0.707	2.828, 1.414, 0.707, 0.354	3	4		
1.414	2.828, 1.414, 0.707, 0.354	6	14	1	
2.828	2.828, 1.414, 0.707, 0.354	9	12	10	
5.656	2.828, 1.414, 0.707, 0.354				

Figure 7. - Jet noise test points for GELAC set A circular jet.

Normalized Equivalent Total Temperature, Te/t_∞	Total Temperature Ratio, T_2/T_1	Normalized Equivalent Velocity, Ve/c_∞: 0.354				0.707				1.414				2.828			
	Velocity Ratio, V_2/V_1	0.132	0.296	0.667	1.5	0.132	0.296	0.667	1.5	0.132	0.296	0.667	1.5	0.132	0.296	0.667	1.5
0.707	0.354																
	0.707																
	1.414																
	2.828																
1.414	0.354						2	4									
	0.707						6	17	3								
	1.414																
	2.828																
2.828	0.354																
	0.707																
	1.414																
	2.828																
5.656	0.354																
	0.707																
	1.414																
	2.828																

Figure 8. - Jet noise test points for GELAC Set B coaxial jet with area ratio = 2.93.

Normalized Equivalent Total Temperature, Te/t_∞	Total Temperature Ratio, T_2/T_1	Normalized Equivalent Velocity, Ve/c_∞: 0.354	0.707	1.414	2.828
		Velocity Ratio, V_2/V_1: 0.132, 0.296, 0.667, 1.5	0.132, 0.296, 0.667, 1.5	0.132, 0.296, 0.667, 1.5	0.132, 0.296, 0.667, 1.5
0.707	2.828, 1.414, 0.707, 0.354				
1.414	2.828, 1.414, 0.707, 0.354	6	10		
2.828	2.828, 1.414, 0.707, 0.354			6	
5.656	2.828, 1.414, 0.707, 0.354			10	

(a) Circular jet.

Figure 9. - Jet noise test points for LERC set A.

Normalized Equivalent Total Temperature, Te/t_∞	Total Temperature Ratio, T_2/T_1	Normalized Equivalent Velocity, Ve/c_∞: 0.354				0.707				1.414				2.828			
	Velocity Ratio, V_2/V_1	0.132	0.296	0.667	1.5	0.132	0.296	0.667	1.5	0.132	0.296	0.667	1.5	0.132	0.296	0.667	1.5
0.707	0.354																
	0.707																
	1.414																
	2.828																
1.414	0.354							2									
	0.707							1									
	1.414							2	1								
	2.828																
2.828	0.354										3	1					
	0.707											1					
	1.414												4				
	2.828												1				
5.656	0.354																
	0.707																
	1.414																
	2.828																

(b) Coaxial jet, area ratio = 1.2.

Figure 9. - Continued.

		Normalized Equivalent Velocity, Ve/c_∞															
		0.354				0.707				1.414				2.828			
		Velocity Ratio, V_2/V_1															
Normalized Equivalent Total Temperature, Te/t_∞	Total Temperature Ratio, T_2/T_1	0.132	0.296	0.667	1.5	0.132	0.296	0.667	1.5	0.132	0.296	0.667	1.5	0.132	0.296	0.667	1.5
0.707	0.354																
	0.707																
	1.414																
	2.828																
1.414	0.354						4	4			3						
	0.707							1									
	1.414							3	4								
	2.828																
2.828	0.354										1						
	0.707											2					
	1.414												8				
	2.828												2				
5.656	0.354																
	0.707																
	1.414																
	2.828																

(c) Coaxial jet, area ratio = 1.5 and 2.0.

Figure 9. - Continued.

Normalized Equivalent Total Temperature, T_e/t_∞	Total Temperature Ratio, T_2/T_1	Normalized Equivalent Velocity, V_e/c_∞: 0.354				0.707				1.414				2.828			
	Velocity Ratio, V_2/V_1:	0.132	0.296	0.667	1.5	0.132	0.296	0.667	1.5	0.132	0.296	0.667	1.5	0.132	0.296	0.667	1.5
0.707	0.354																
	0.707																
	1.414																
	2.828																
1.414	0.354						4	2									
	0.707							1									
	1.414							2	1								
	2.828																
2.828	0.354																
	0.707											1					
	1.414												4				
	2.828												1				
5.656	0.354																
	0.707																
	1.414																
	2.828																

(d) Coaxial jet, area ratio = 3.3.

Figure 9. - Concluded.

Normalized Equivalent Total Temperature, T_e/t_∞	Total Temperature Ratio, T_2/T_1	Normalized Equivalent Velocity, V_e/c_∞: 0.354	0.707	1.414	2.828
	Velocity Ratio, V_2/V_1	0.132, 0.296, 0.667, 1.5	0.132, 0.296, 0.667, 1.5	0.132, 0.296, 0.667, 1.5	0.132, 0.296, 0.667, 1.5
0.707	2.828, 1.414, 0.707, 0.354	3	12		
1.414	2.828, 1.414, 0.707, 0.354	12	34	3	
2.828	2.828, 1.414, 0.707, 0.354	9	75	56	
5.656	2.828, 1.414, 0.707, 0.354			10	

(a) Circular jet.

Figure 10. - Jet noise test points for all data sets combined.

Normalized Equivalent Total Temperature, Te/t_∞	Total Temperature Ratio, T_2/T_1	Normalized Equivalent Velocity, Ve/c_∞: 0.354				0.707				1.414				2.828			
	Velocity Ratio, V_2/V_1	0.132	0.296	0.667	1.5	0.132	0.296	0.667	1.5	0.132	0.296	0.667	1.5	0.132	0.296	0.667	1.5
0.707	0.354																
	0.707																
	1.414																
	2.828																
1.414	0.354			2			4	7	6			1					
	0.707							3	1			1					
	1.414							2	3				2				
	2.828								1								
2.828	0.354						1				3	5					
	0.707											7	4				
	1.414											2	10				
	2.828								1				4				
5.656	0.354																
	0.707																
	1.414																
	2.828																

(b) Coaxial jet, area ratio range from 0.707 to 1.414.

Figure 10. - Continued.

Normalized Equivalent Total Temperature, Te/t_∞	Total Temperature Ratio, T_2/T_1	Normalized Equivalent Velocity, Ve/c_∞: 0.354				0.707				1.414				2.828			
	Velocity Ratio, V_2/V_1	0.132	0.296	0.667	1.5	0.132	0.296	0.667	1.5	0.132	0.296	0.667	1.5	0.132	0.296	0.667	1.5
0.707	0.354																
	0.707																
	1.414																
	2.828																
1.414	0.354	2	15	19		1	32	59	29		3	7					
	0.707		2	1			2	6									
	1.414							3	4								
	2.828																
2.828	0.354	5	2			9	5			6	1						
	0.707											2					
	1.414												8				
	2.828												2				
5.656	0.354																
	0.707																
	1.414																
	2.828																

(c) Coaxial jet, area ratio range from 1.414 to 2.828.

Figure 10. - Continued.

Normalized Equivalent Total Temperature, Te/t_∞	Total Temperature Ratio, T_2/T_1	Normalized Equivalent Velocity, Ve/c_∞: 0.354				0.707				1.414				2.828			
	Velocity Ratio, V_2/V_1	0.132	0.296	0.667	1.5	0.132	0.296	0.667	1.5	0.132	0.296	0.667	1.5	0.132	0.296	0.667	1.5
0.707	0.354																
	0.707																
	1.414																
	2.828																
1.414	0.354	7	17	15		1	17	69	19								
	0.707	1	1	2			8	22	3								
	1.414							2	3								
	2.828																
2.828	0.354	1								1							
	0.707											1					
	1.414												4				
	2.828												1				
5.656	0.354																
	0.707																
	1.414																
	2.828																

(d) Coaxial jet, area ratio range from 2.828 to 5.656.

Figure 10. - Continued.

Normalized Equivalent Total Temperature, T_e/t_∞	Total Temperature Ratio, T_2/T_1	Normalized Equivalent Velocity, V_e/c_∞: 0.354				0.707				1.414				2.828			
	Velocity Ratio, V_2/V_1	0.132	0.296	0.667	1.5	0.132	0.296	0.667	1.5	0.132	0.296	0.667	1.5	0.132	0.296	0.667	1.5
0.707	0.354																
	0.707																
	1.414																
	2.828																
1.414	0.354	9	23	13		1	10	34	9								
	0.707		2	1		1	1	4									
	1.414																
	2.828																
2.828	0.354	2				2				1							
	0.707																
	1.414																
	2.828																
5.656	0.354																
	0.707																
	1.414																
	2.828																

(e) Coaxial jet, area ratio range from 5.656 to 11.312.

Figure 10. - Concluded.

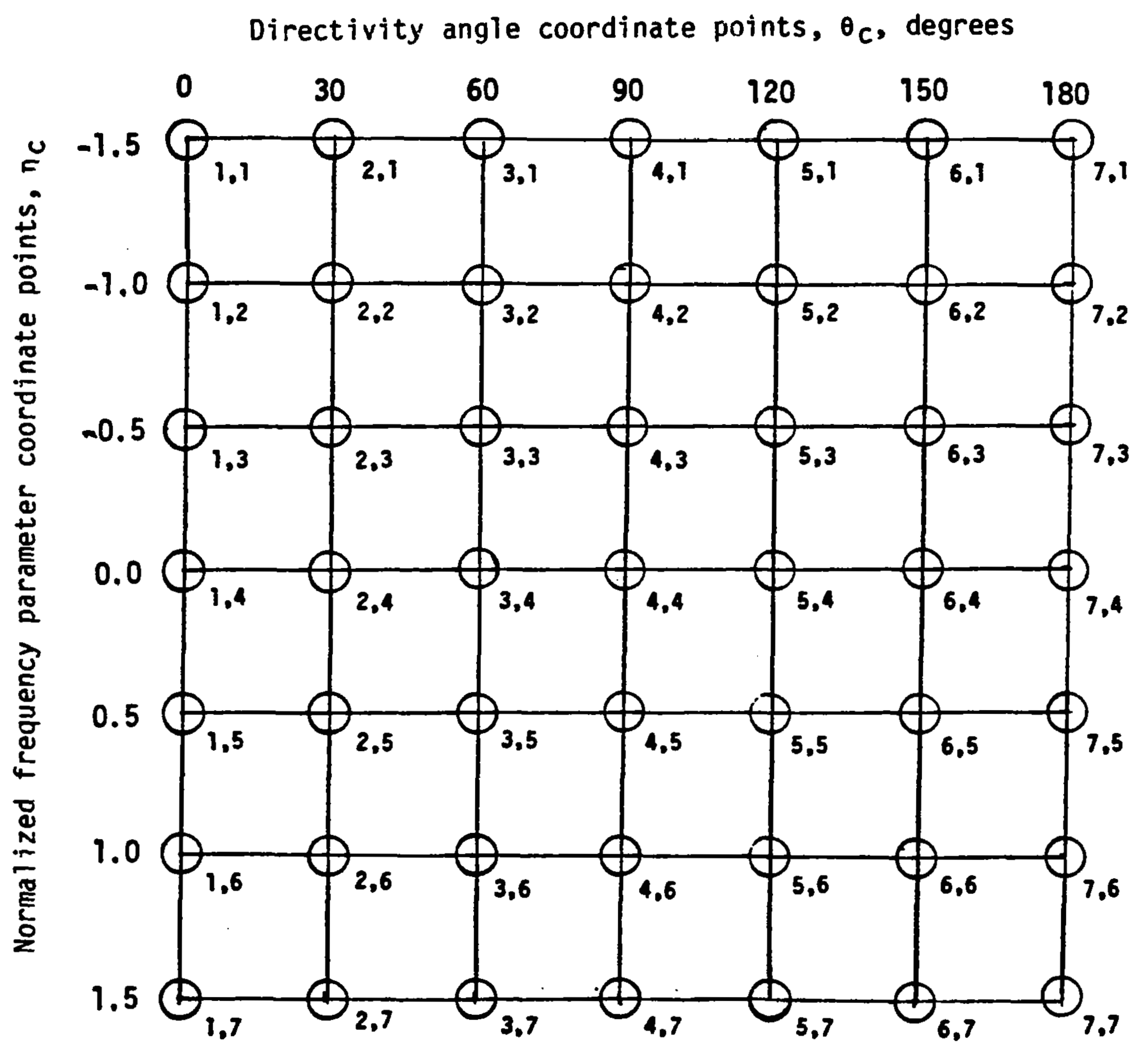

Figure 11. Standard computational grid for cubic spline to jet noise data.

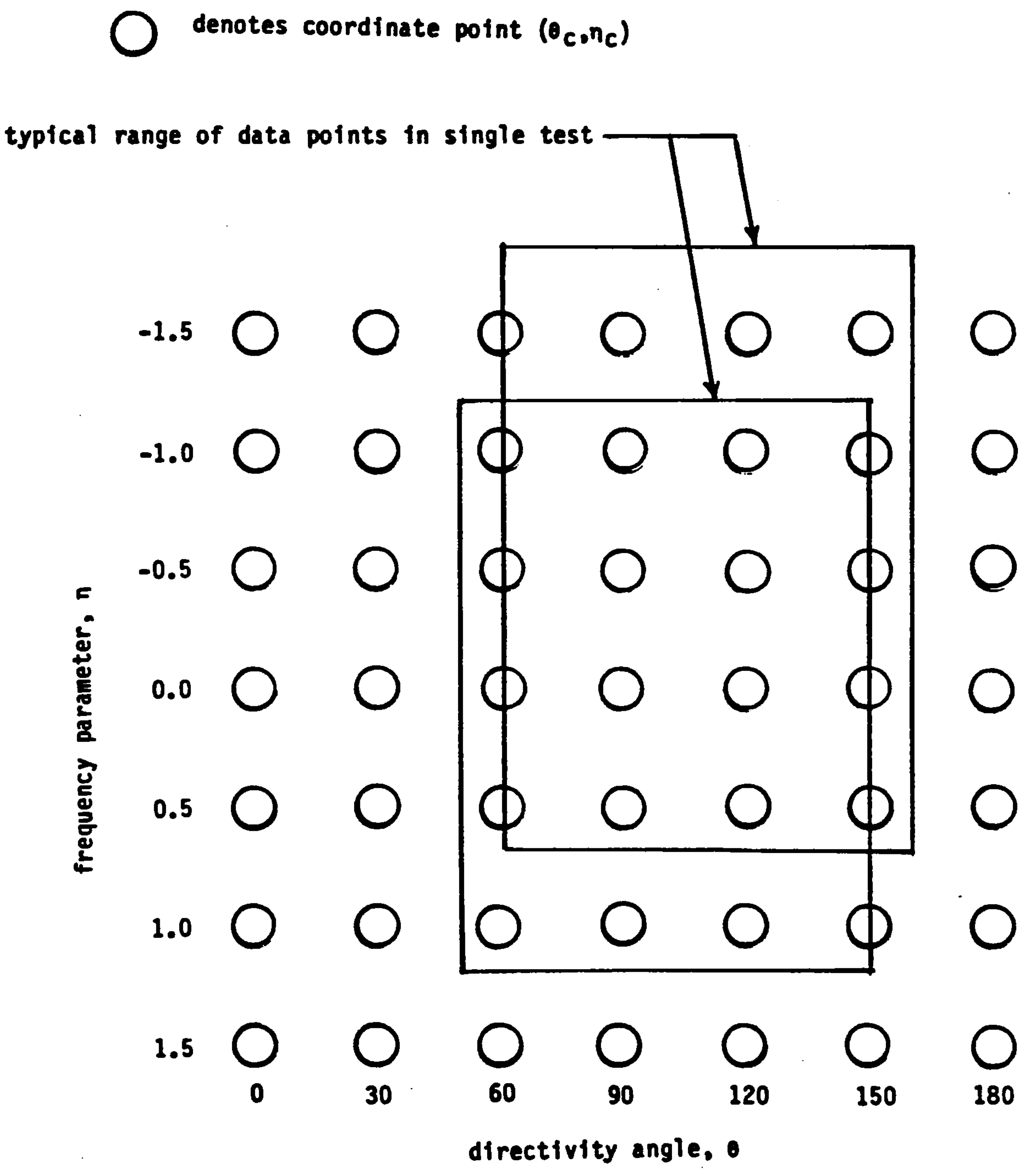

Figure 12. Single test data ranges relative to grid coordinate points.

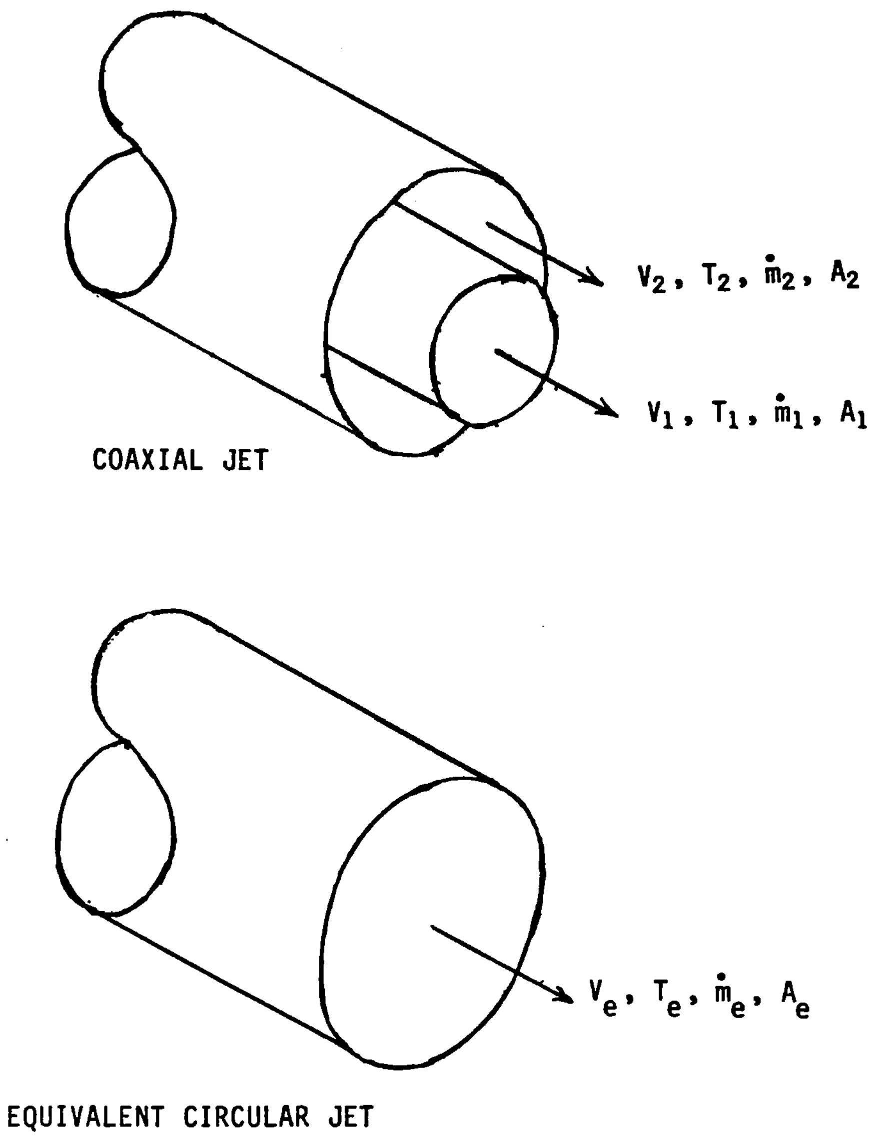

MASS FLOW	$\dot{m}_e = \dot{m}_1 + \dot{m}_2$
MOMENTUM	$\dot{m}_e V_e = \dot{m}_1 V_1 + \dot{m}_2 V_2$
ENERGY	$\dot{m}_e C_{p_e} T_e = \dot{m}_1 C_{p_1} T_1 + \dot{m}_2 C_{p_2} T_2$

Figure 13. Jet flow state parameters.

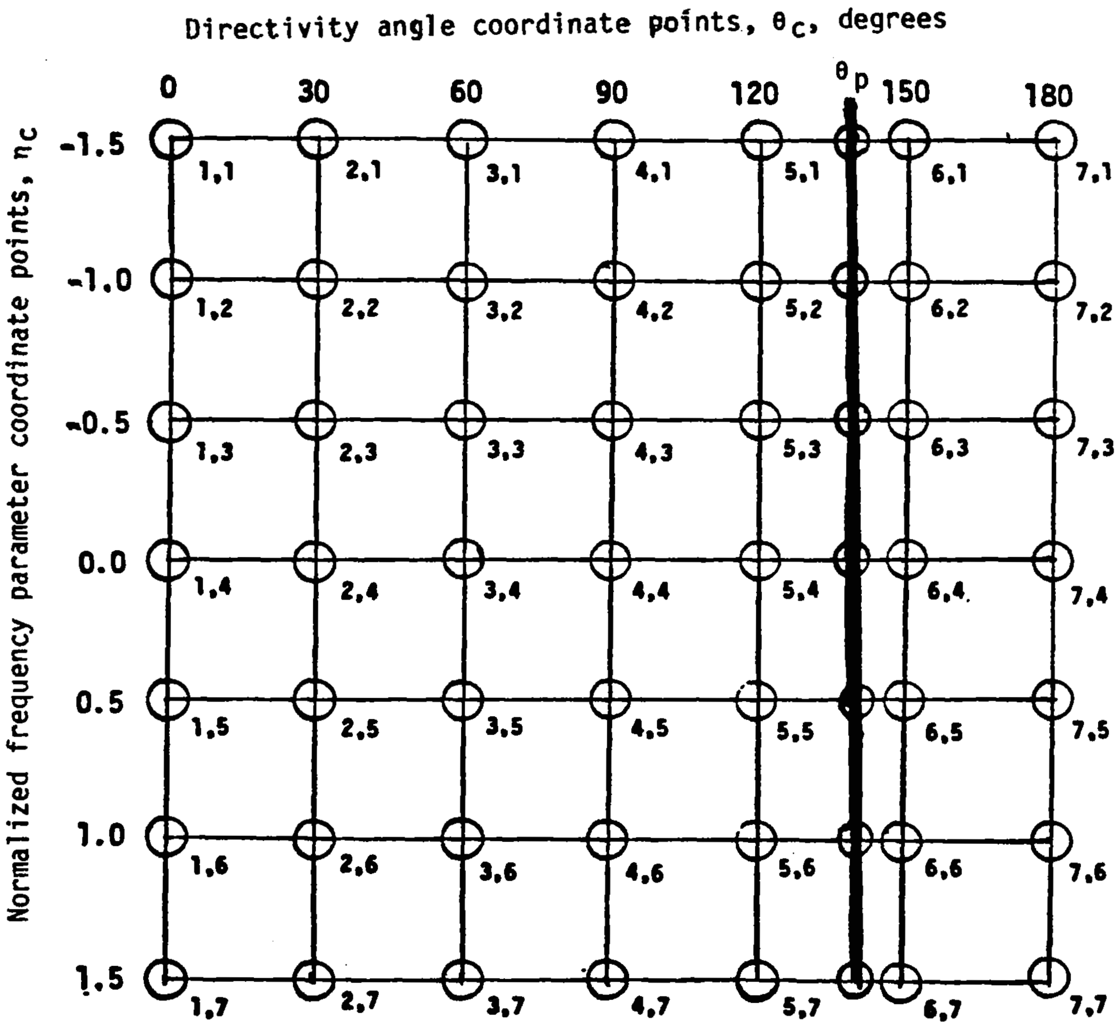

Figure 14. - Interpolation on directivity angle at θ_p to obtain OASPL(θ_p) and RSL(n_c, θ_p) values.

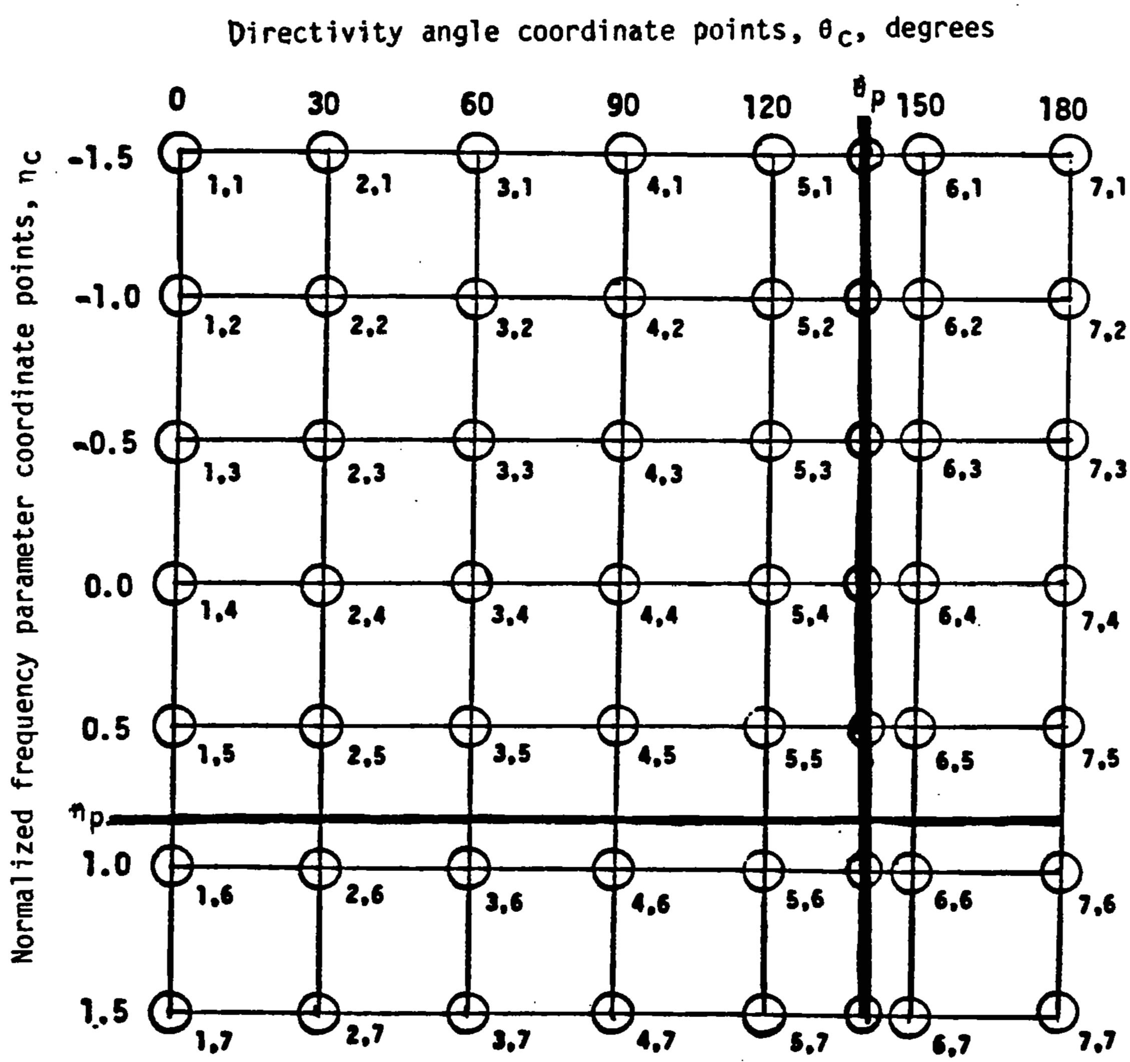

Figure 15. - Interpolation of normalized frequency parameter at η_p to obtain $F(\eta_p)$ and $RSL(\eta_p, \theta_p)$ values.

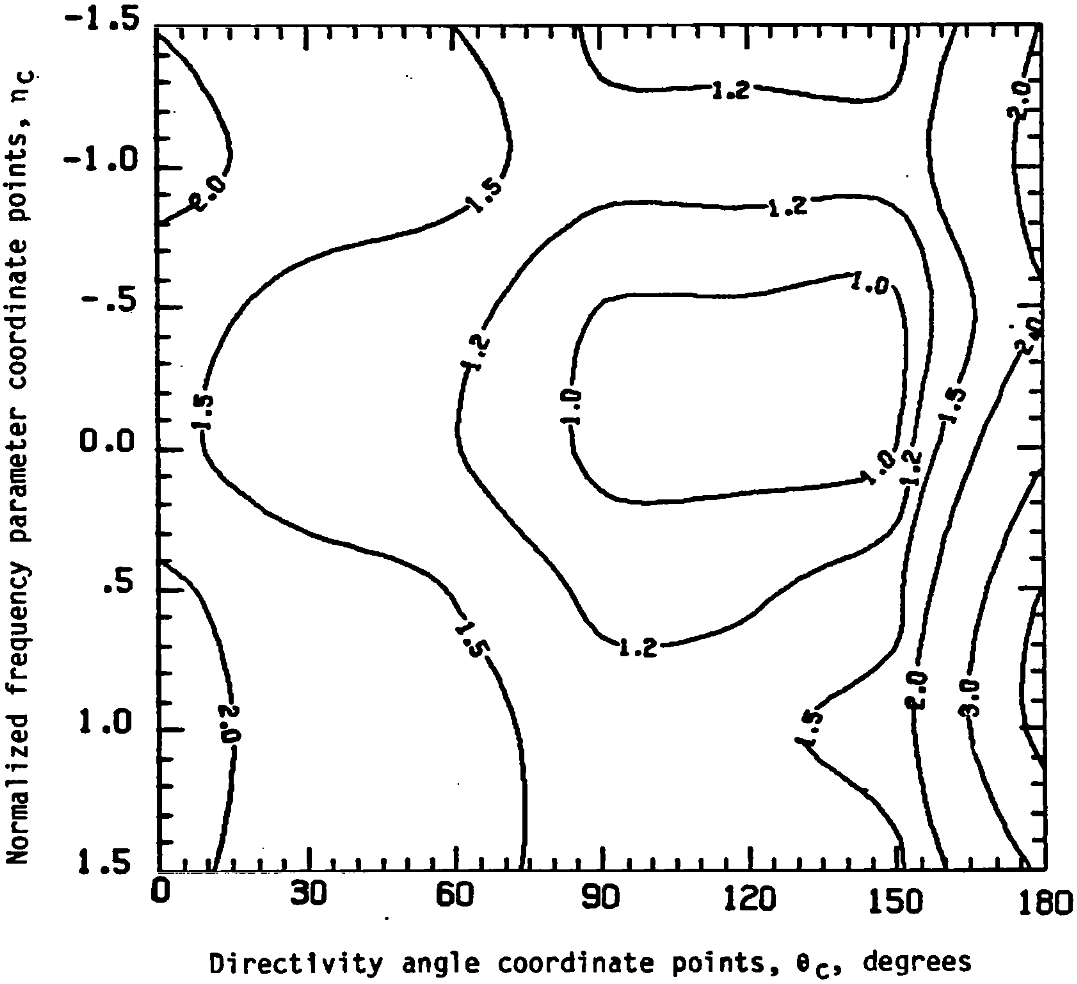

Figure 16. - Contour plot of standard deviations for prediction sound pressure levels.

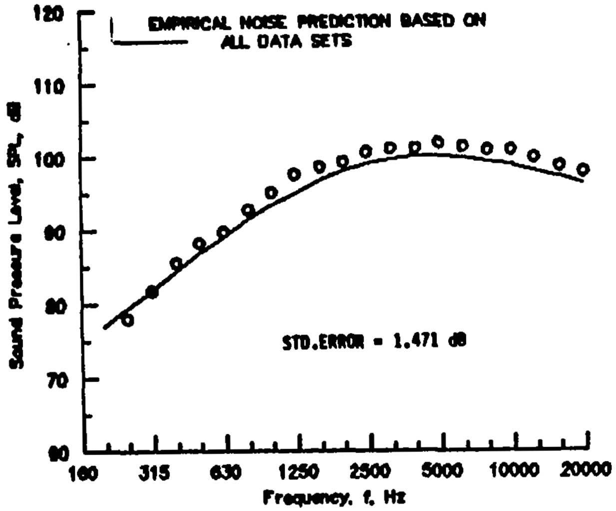

(b) Directivity angle = 120 degrees.

$V_e/C_\infty = 1.120 \qquad T_{t_e}/T_\infty = 2.430$

$V_2/V_1 = 1.000 \qquad T_{t_2}/T_{t_1} = 1.000$

$A_2/A_1 = 1.000$

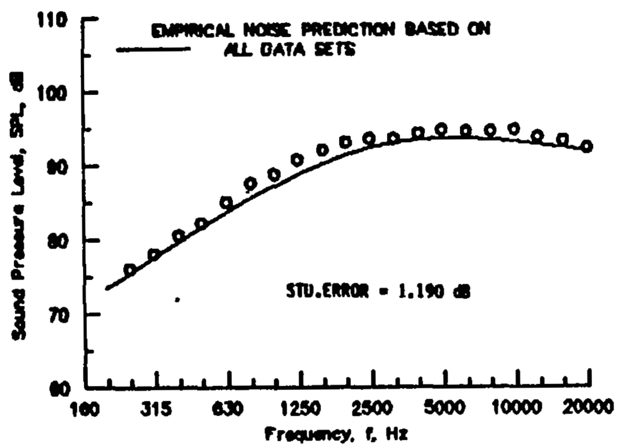

(a) Directivity angle = 90 degrees.

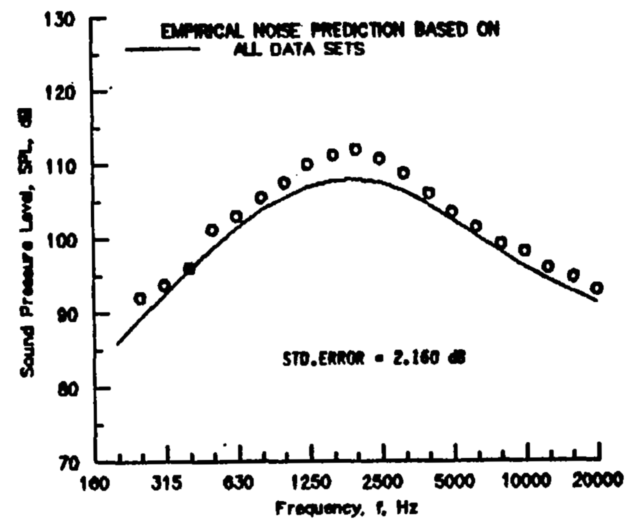

(c) Directivity angle = 150 degrees.

Figure 17. - Prediction method comparison for case NGTA0114.

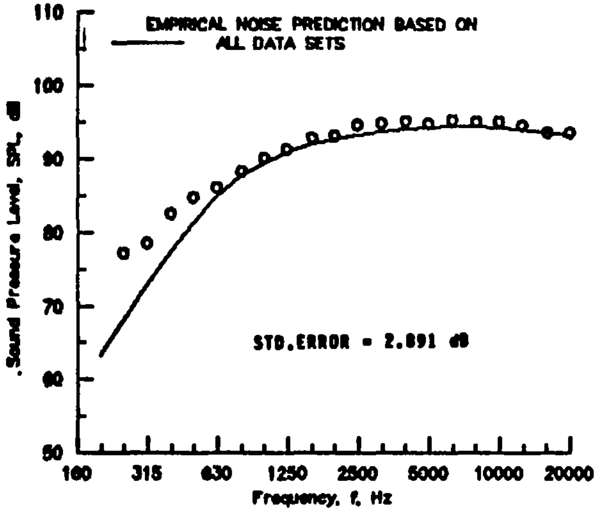

(b) Directivity angle = 120 degrees.

$V_e/C_\infty = .895$ $\quad T_{t_e}/T_\infty = 1.004$

$V_2/V_1 = 1.000$ $\quad T_{t_2}/T_{t_1} = 1.000$

$A_2/A_1 = 1.000$

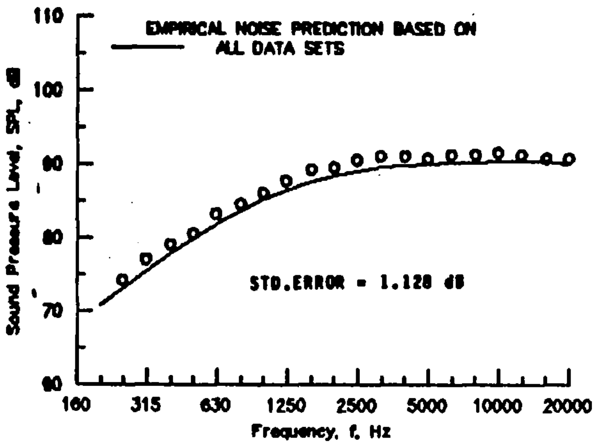

(a) Directivity angle = 90 degrees.

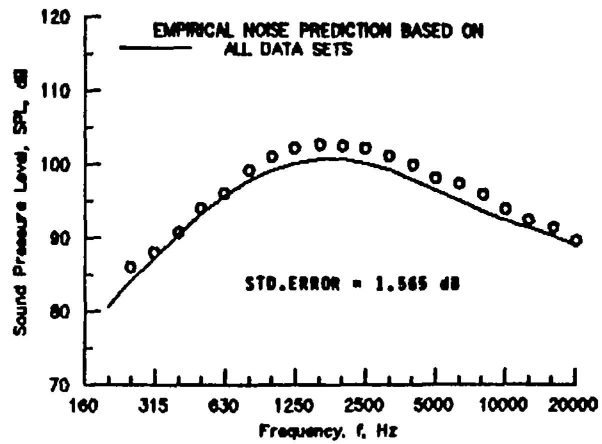

(c) Directivity angle = 150 degrees.

Figure 18. - Prediction method comparison for case NGTA0138.

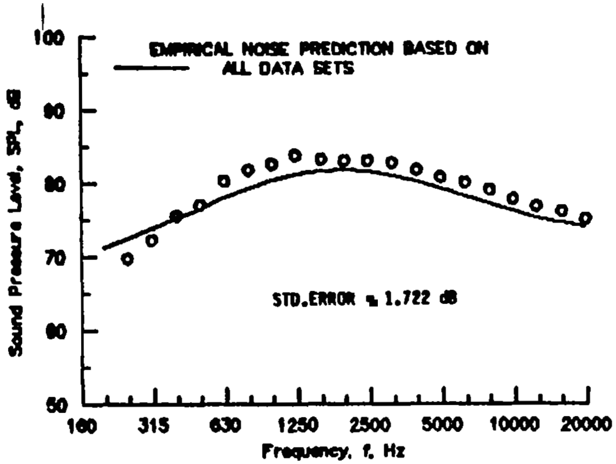

(b) Directivity angle = 120 degrees.

$V_e/C_\infty = .583 \qquad T_{t_e}/T_\infty = 3.125$

$V_2/V_1 = 1.000 \qquad T_{t_2}/T_{t_1} = 1.000$

$A_2/A_1 = 1.000$

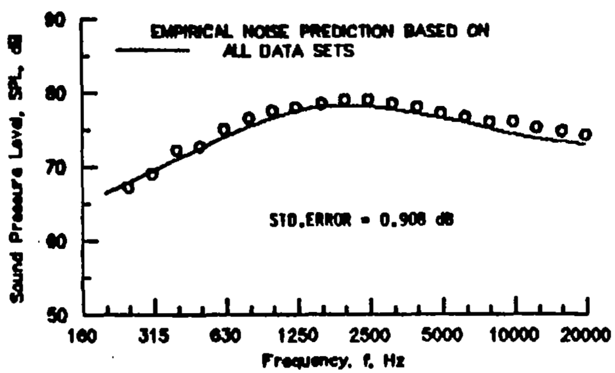

(a) Directivity angle = 90 degrees.

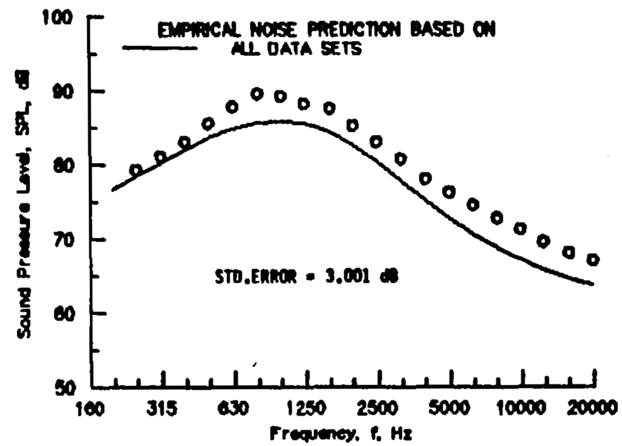

(c) Directivity angle = 150 degrees.

Figure 19. - Prediction method comparison for case NGTA0168.

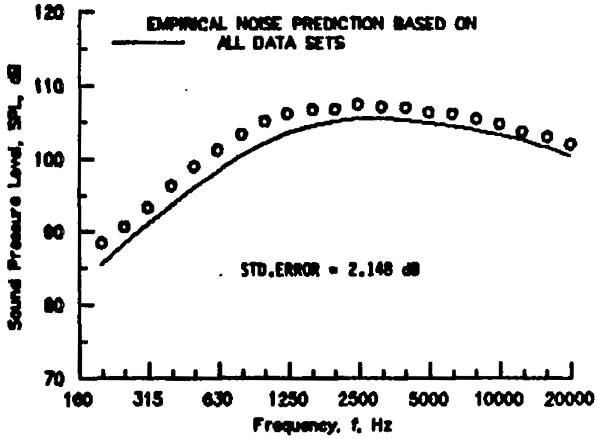

(b) Directivity angle = 120 degrees.

$V_e/C_\infty = 1.497$ $T_{t_e}/T_\infty = 2.864$

$V_2/V_1 = 1.000$ $T_{t_2}/T_{t_1} = 1.000$

$A_2/A_1 = 1.000$

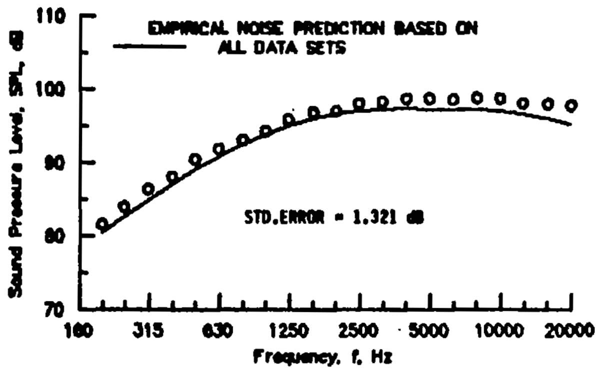

(a) Directivity angle = 90 degrees.

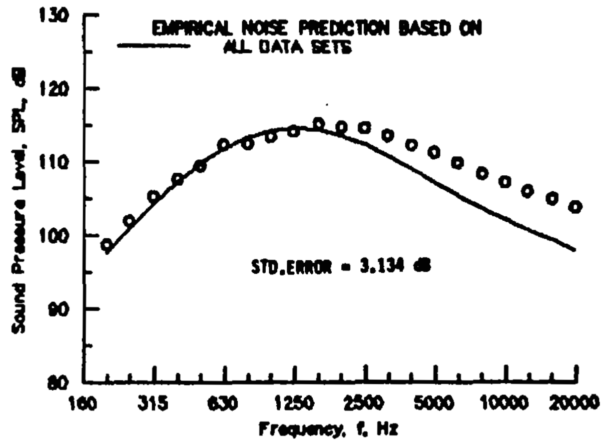

(c) Directivity angle = 150 degrees.

Figure 20. - Prediction method comparison for case NGTC0115.

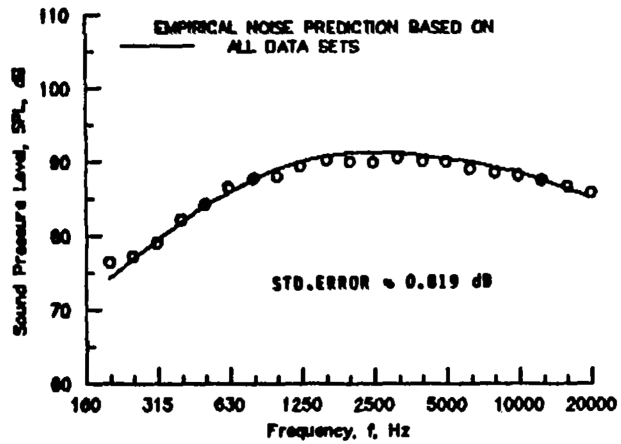

(b) Directivity angle = 120 degrees.

$$V_e/C_\infty = 1.117 \qquad T_{t_e}/T_\infty = 2.052$$

$$V_2/V_1 = 1.000 \qquad T_{t_2}/T_{t_1} = 1.000$$

$$A_2/A_1 = 1.000$$

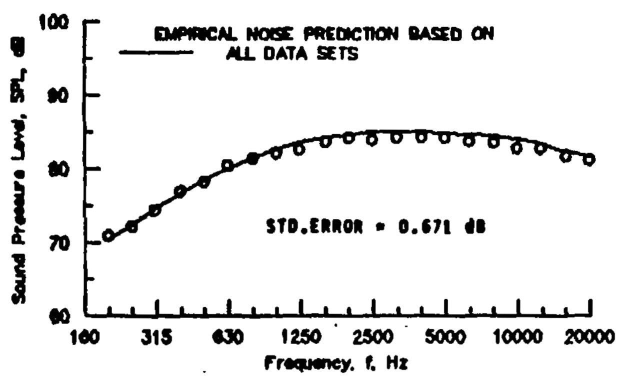

(a) Directivity angle = 90 degrees.

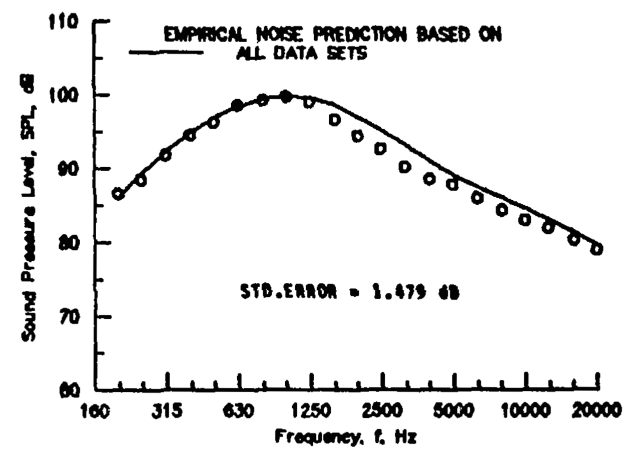

(c) Directivity angle = 150 degrees.

Figure 21. - Prediction method comparison for case NGTD0018.

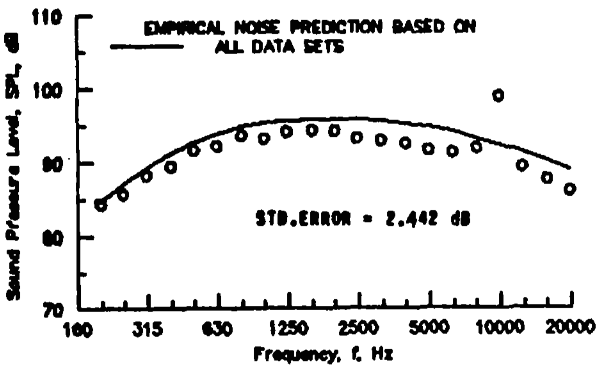

(b) Directivity angle = 120 degrees.

$V_e/C_\infty = .883 \qquad T_{t_e}/T_\infty = 1.352$

$V_2/V_1 = 1.000 \qquad T_{t_2}/T_{t_1} = 1.000$

$A_2/A_1 = 1.000$

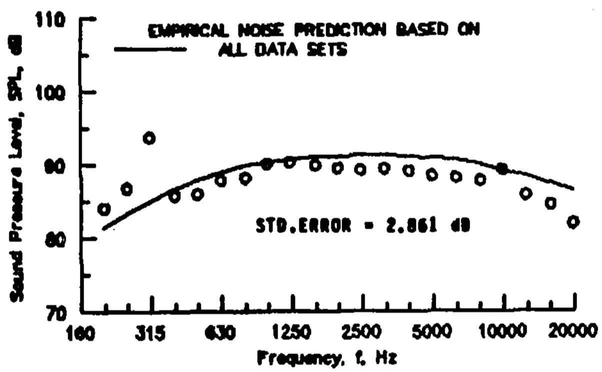

(a) Directivity angle = 90 degrees.

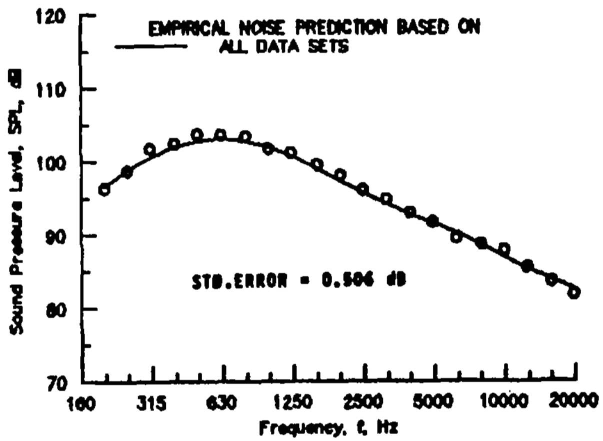

(c) Directivity angle = 150 degrees.

Figure 22. - Prediction method comparison for case PWA00404.

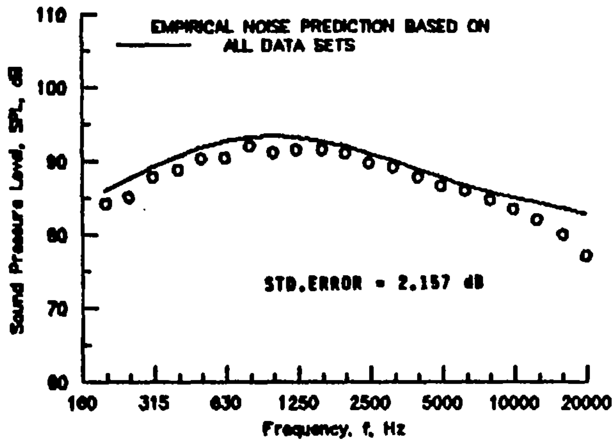

(b) Directivity angle = 120 degrees.

$$V_e/C_\infty = .792 \qquad T_{t_e}/T_\infty = 3.069$$

$$V_2/V_1 = 1.000 \qquad T_{t_2}/T_{t_1} = 1.000$$

$$A_2/A_1 = 1.000$$

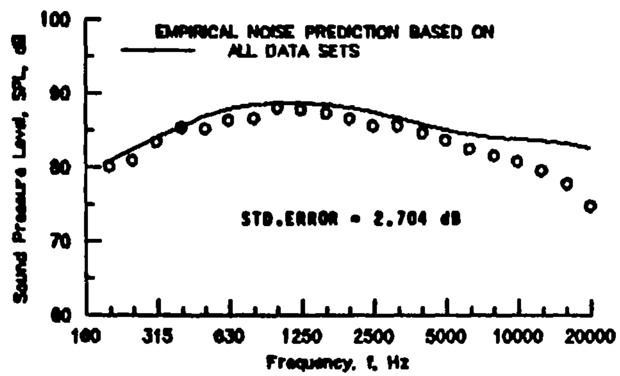

(a) Directivity angle = 90 degrees.

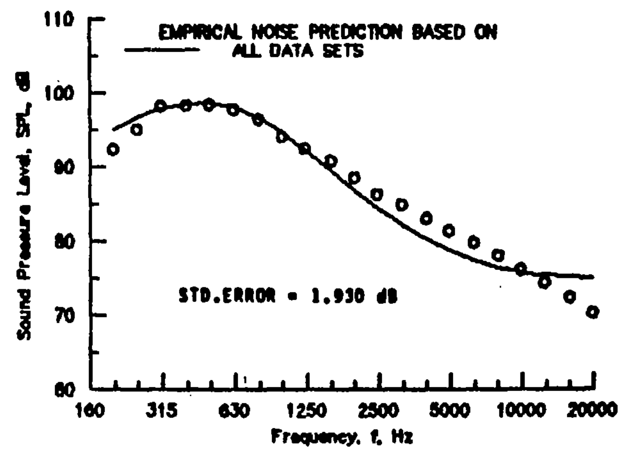

(c) Directivity angle = 150 degrees.

Figure 23. - Prediction method comparison for case PWA02205.

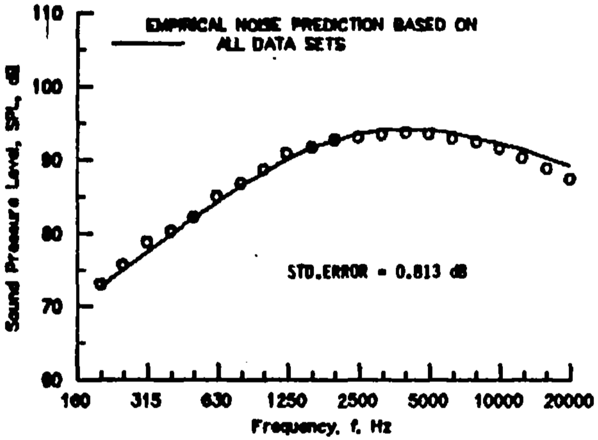

(b) Directivity angle = 120 degrees.

$$V_e/C_\infty = 1.179 \qquad T_{t_e}/T_\infty = 3.012$$

$$V_2/V_1 = 1.000 \qquad T_{t_2}/T_{t_1} = 1.000$$

$$A_2/A_1 = 1.000$$

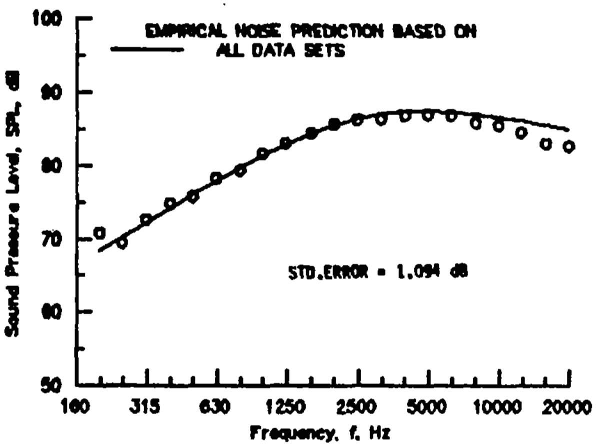

(a) Directivity angle = 90 degrees.

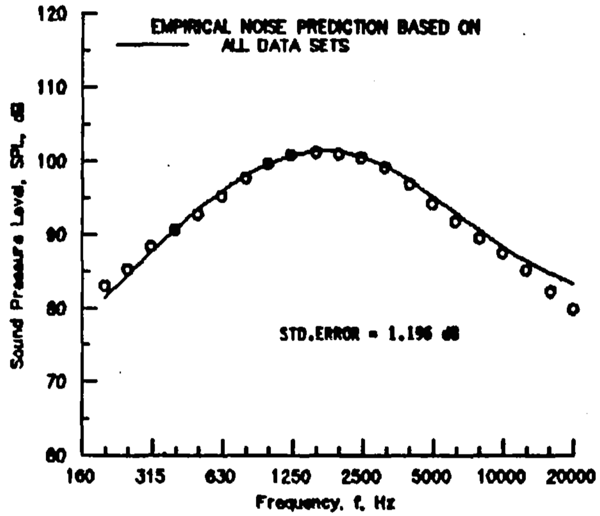

(c) Directivity angle = 150 degrees.

Figure 24. - Prediction method comparison for case SNCA0092.

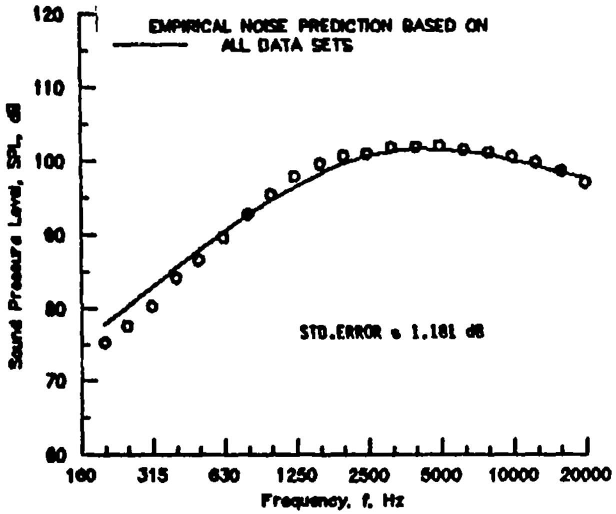

(b) Directivity angle = 120 degrees.

$$V_e/C_\infty = 1.324 \qquad T_{t_e}/T_\infty = 3.131$$

$$V_2/V_1 = 1.000 \qquad T_{t_2}/T_{t_1} = 1.000$$

$$A_2/A_1 = 1.000$$

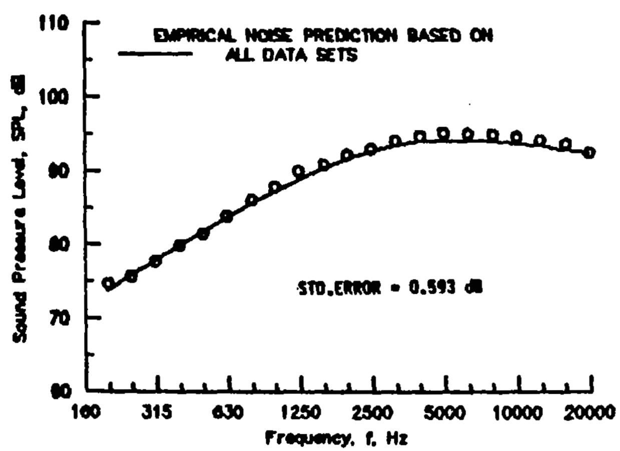

(a) Directivity angle = 90 degrees.

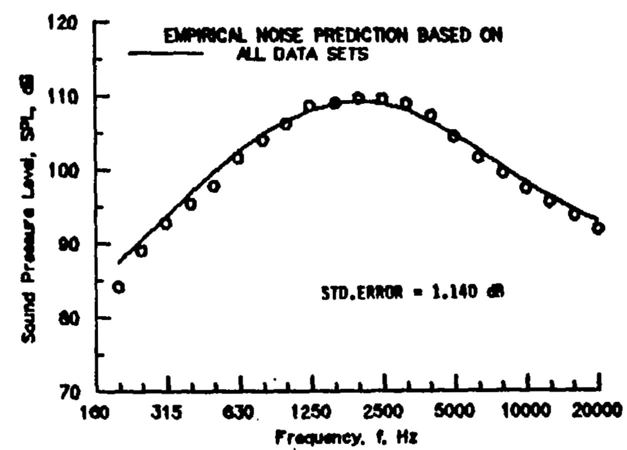

(c) Directivity angle = 150 degrees.

Figure 25. - Prediction method comparison for case LGCA0048.

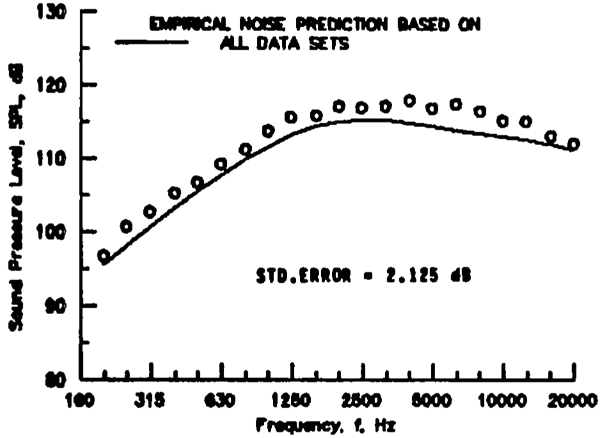

(b) Directivity angle = 115 degrees.

$V_e/C_\infty = 1.775 \qquad T_{t_e}/T_\infty = 4.094$

$V_2/V_1 = 1.000 \qquad T_{t_2}/T_{t_1} = 1.000$

$A_2/A_1 = 1.000$

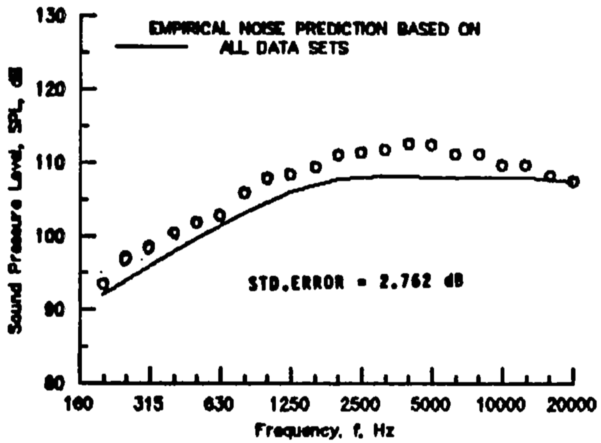

(a) Directivity angle = 95 degrees.

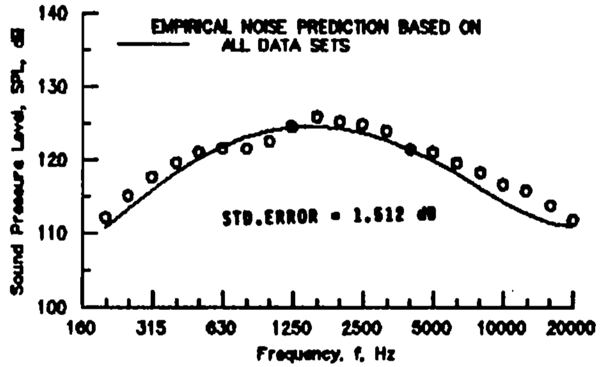

(c) Direcitvity angle = 151 degrees.

Figure 26. - Prediction method comparison for case LEW0137.

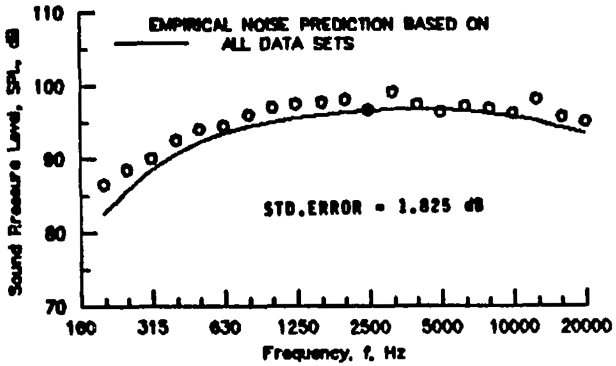

(b) Directivity angle = 113 degrees.

$V_e/C_\infty = .880$ $T_{t_e}/T_\infty = 1.029$

$V_2/V_1 = 1.000$ $T_{t_2}/T_{t_1} = 1.000$

$A_2/A_1 = 1.000$

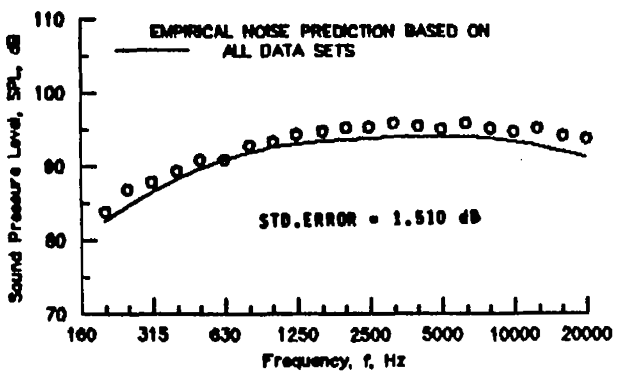

(a) Directivity angle = 93 degrees.

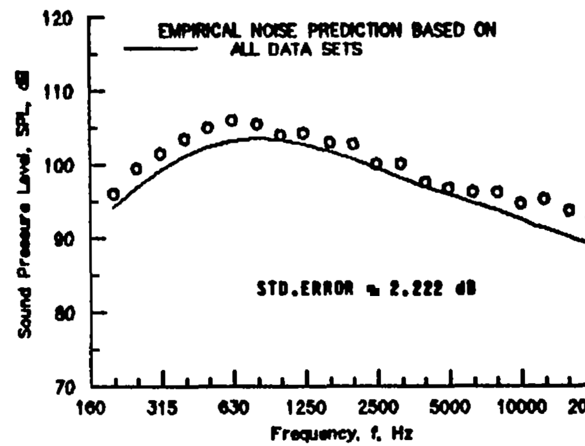

(c) Directivity angle = 147 degrees.

Figure 27. - Prediction method comparison for case LEW0224.

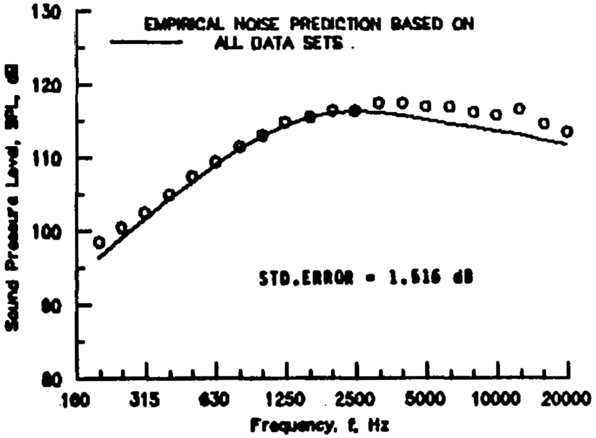

(b) Directivity angle = 118 degrees.

$$V_e/C_\infty = 1.782 \qquad T_{t_e}/T_\infty = 4.126$$

$$V_2/V_1 = 1.000 \qquad T_{t_2}/T_{t_1} = 1.000$$

$$A_2/A_1 = 1.000$$

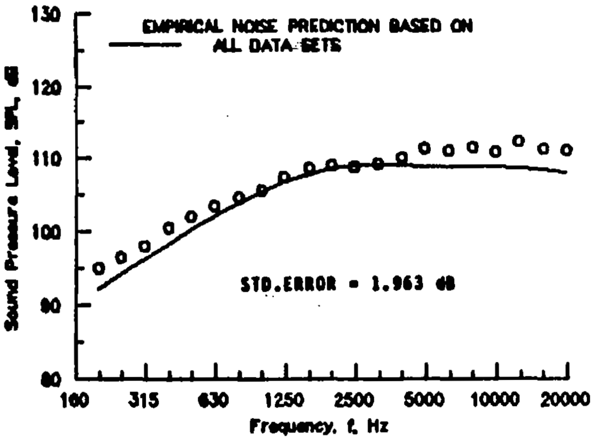

(a) Directivity angle = 98 degrees.

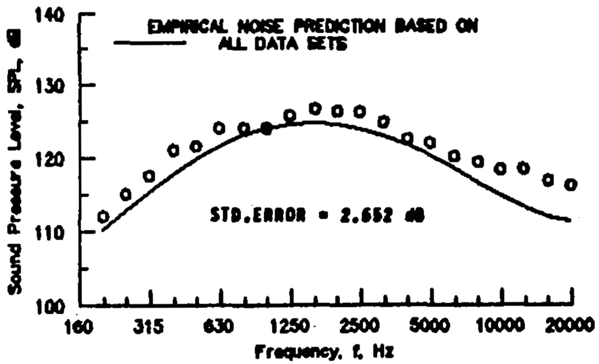

(c) Directivity angle = 149 degrees.

Figure 28. - Prediction method comparison for case LEW0229.

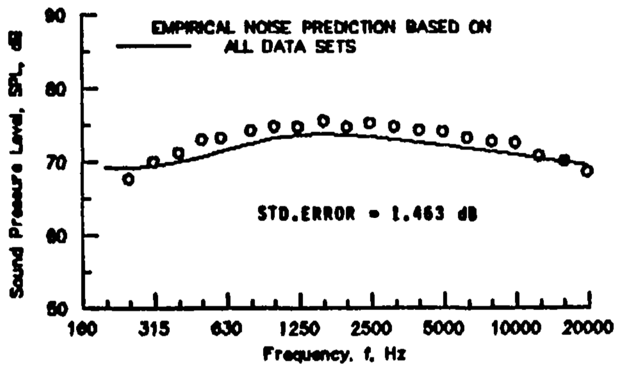

(b) Directivity angle = 120 degrees.

$$V_e/C_\infty = .340 \qquad T_{t_e}/T_\infty = 1.004$$

$$V_2/V_1 = .399 \qquad T_{t_2}/T_{t_1} = 1.000$$

$$A_2/A_1 = 6.001$$

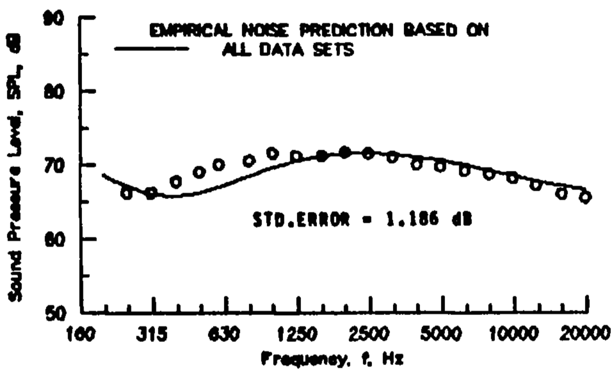

(a) Directivity angle = 90 degrees.

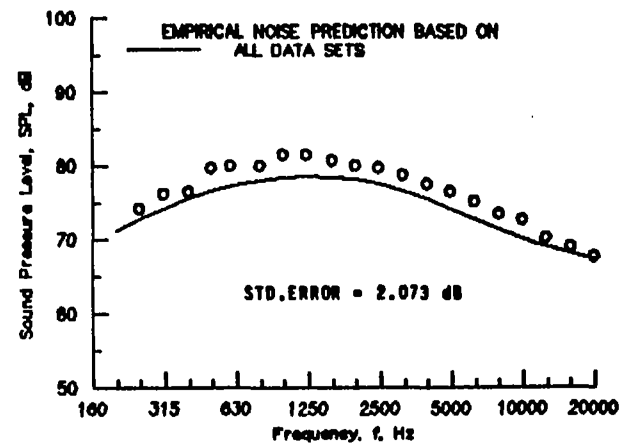

(c) Directivity angle = 150 degrees.

Figure 29. - Prediction method comparison for case NGTA0038.

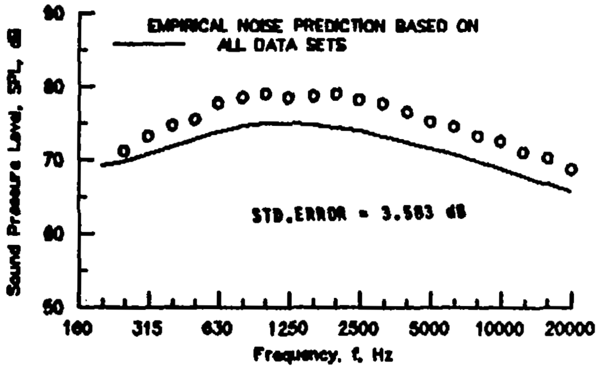

(b) Directivity angle = 120 degrees.

$V_e/C_\infty = .284$ $\quad T_{t_e}/T_\infty = 1.227$

$V_2/V_1 = .398$ $\quad T_{t_2}/T_{t_1} = .412$

$A_2/A_1 = 6.001$

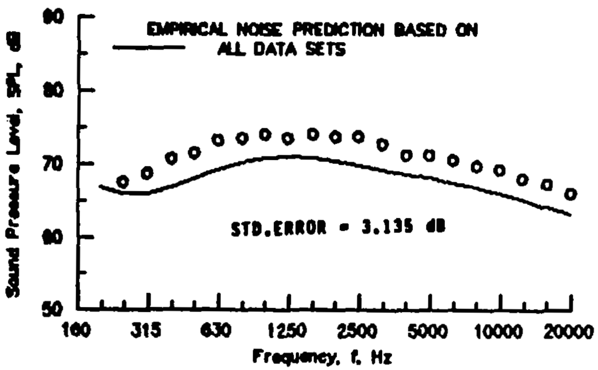

(a) Directivity angle = 90 degrees.

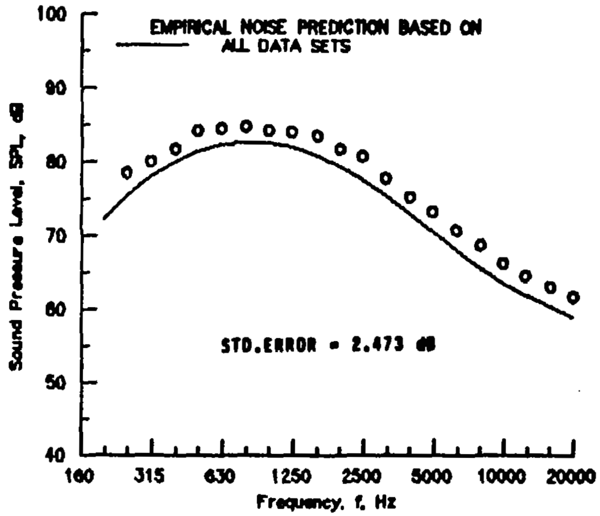

(c) Directivity angle = 150 degrees.

Figure 30. - Prediction method comparison for case NGTA0050.

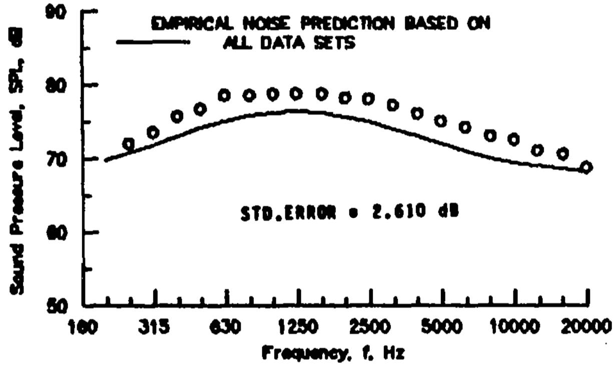

(c) Directivity angle = 150 degrees.

$V_e/C_\infty = .274 \qquad T_{t_e}/T_\infty = 1.294$

$V_2/V_1 = .399 \qquad T_{t_2}/T_{t_1} = .324$

$A_2/A_1 = 6.001$

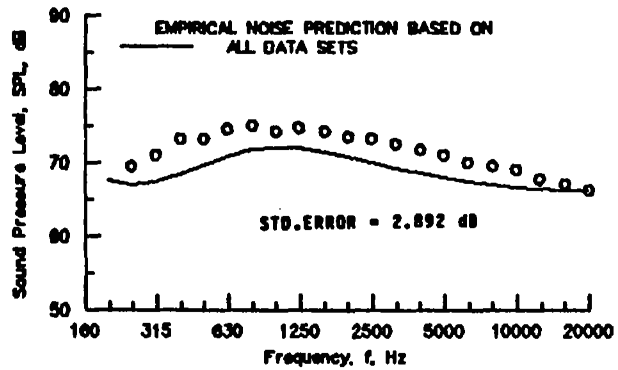

(a) Directivity angle = 90 degrees.

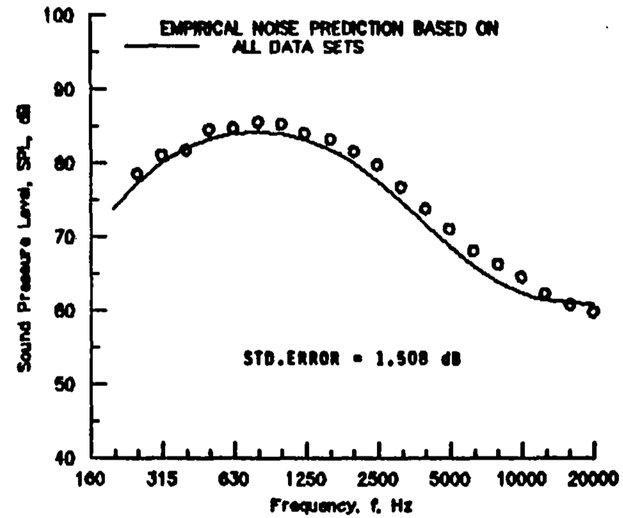

(b) Directivity angle = 120 degrees.

Figure 31. - Prediction method comparison for case NGTA0074.

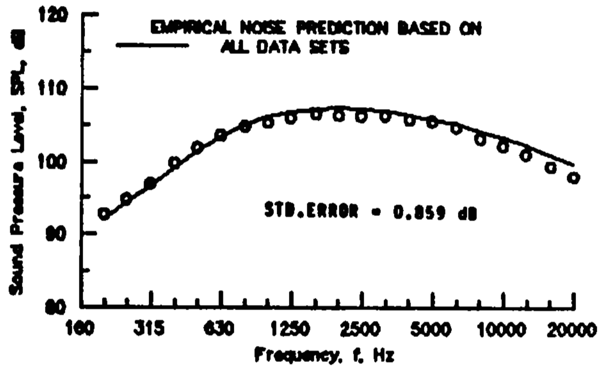

(b) Directivity angle = 120 degrees.

$V_e/C_\infty = 1.050$ $T_{t_e}/T_\infty = 1.466$

$V_2/V_1 = .602$ $T_{t_2}/T_{t_1} = .359$

$A_2/A_1 = 2.000$

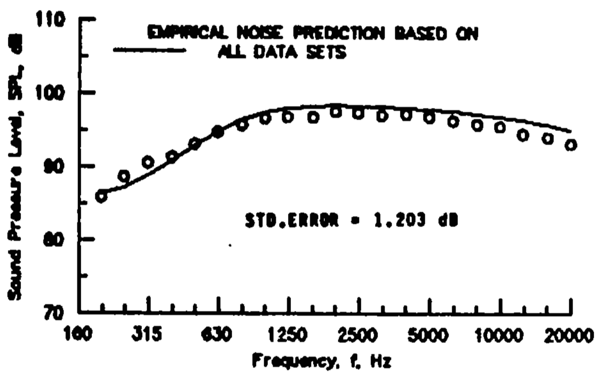

(a) Directivity angle = 90 degrees.

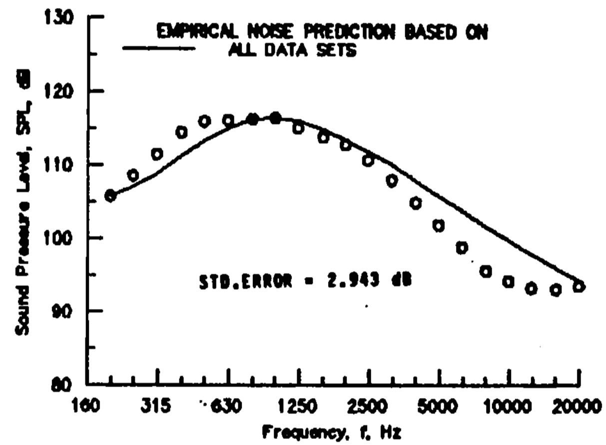

(c) Directivity angle = 150 degrees.

Figure 32. - Prediction method comparison for case NGTC0004.

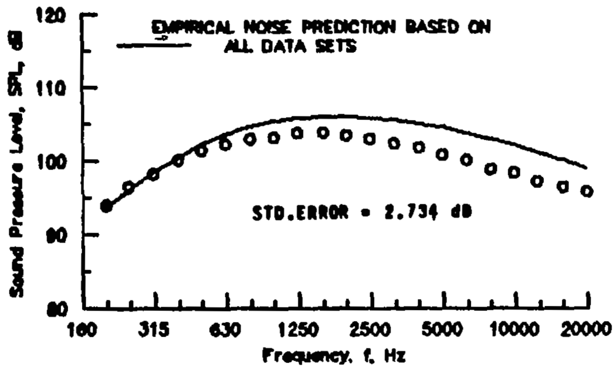

(b) Directivity angle = 120 degrees.

$V_e/C_\infty = .977$ $\quad T_{t_e}/T_\infty = 1.256$

$V_2/V_1 = .598$ $\quad T_{t_2}/T_{t_1} = .355$

$A_2/A_1 = 4.300$

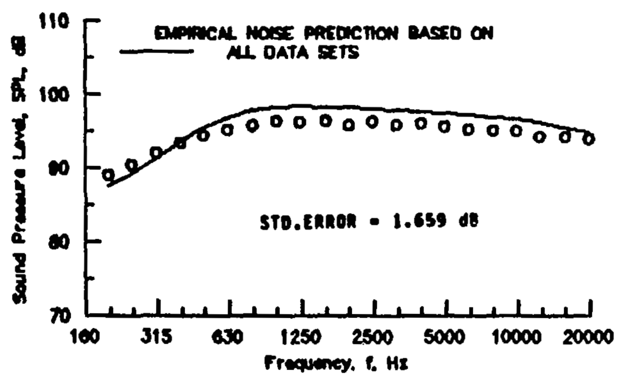

(a) Directivity angle = 90 degrees.

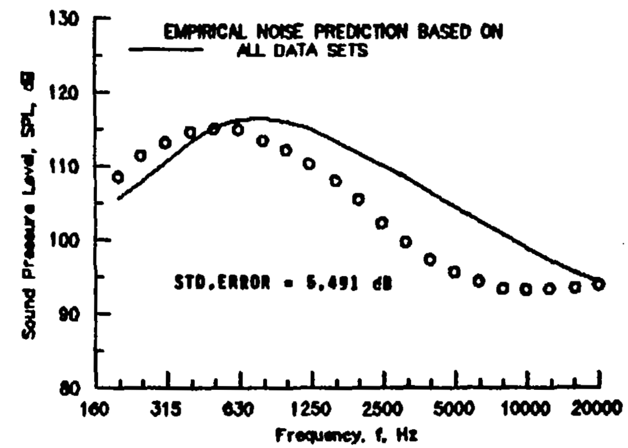

(c) Directivity angle = 150 degrees.

Figure 33. - Prediction method comparison for case NGTC0039.

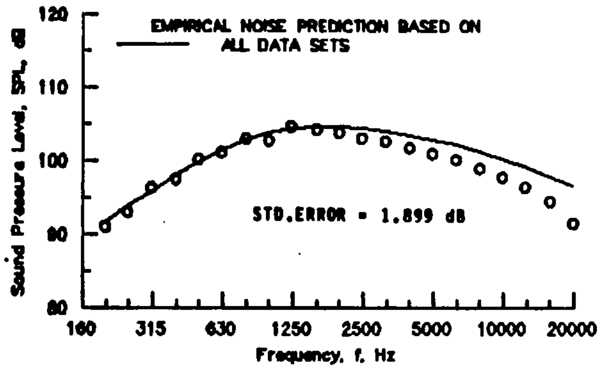

(b) Directivity angle = 120 degrees.

$V_e/C_\infty = 1.134$ $T_{t_e}/T_\infty = 2.006$

$V_2/V_1 = .802$ $T_{t_2}/T_{t_1} = .482$

$A_2/A_1 = .750$

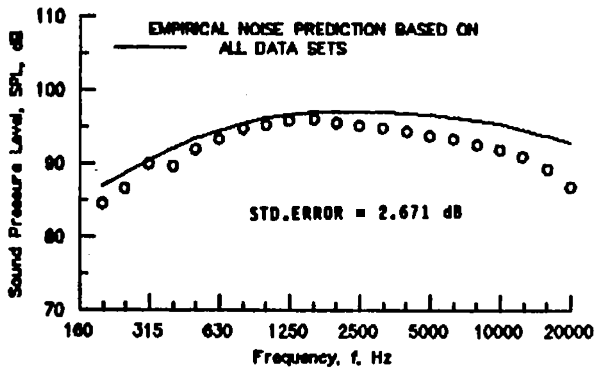

(a) Directivity angle = 90 degrees.

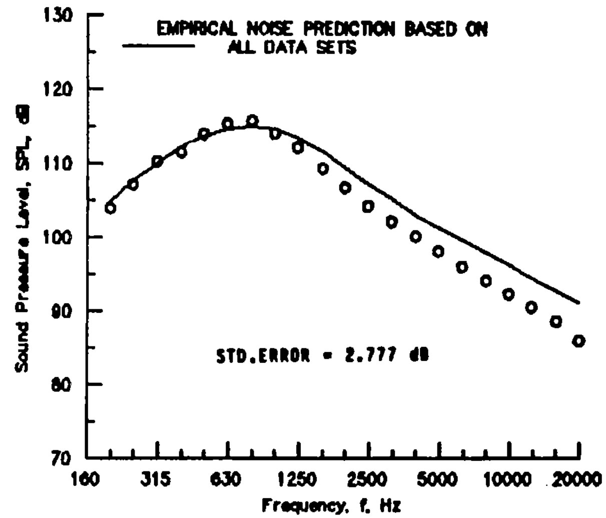

(c) Directivity angle = 150 degrees.

Figure 34. - Prediction method comparison for case PWA00703.

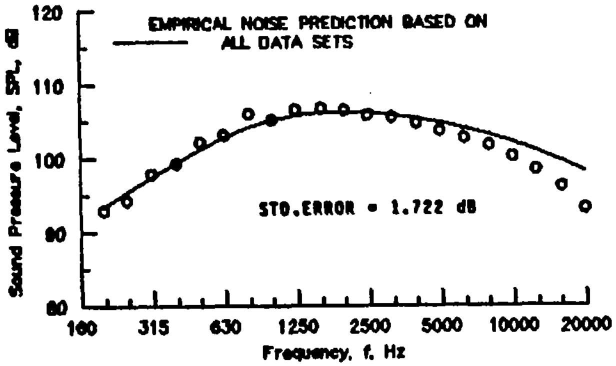

(b) Directivity angle = 120 degrees.

$V_e/C_\infty = 1.189 \qquad T_{t_e}/T_\infty = 2.347$

$V_2/V_1 = .704 \qquad T_{t_2}/T_{t_1} = .376$

$A_2/A_1 = .750$

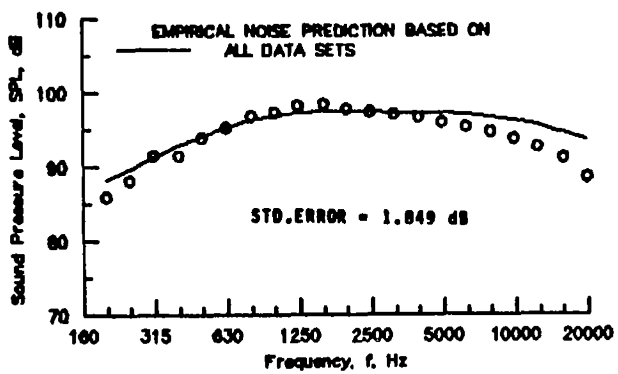

(a) Directivity angle = 90 degrees.

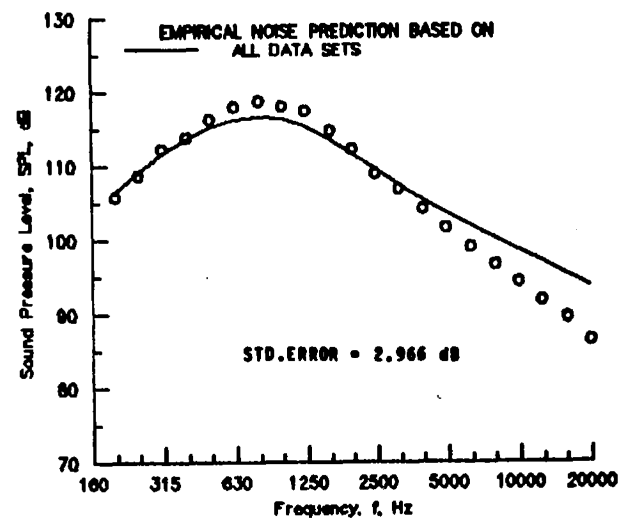

(c) Directivity angle = 150 degrees.

Figure 35. - Prediction method comparison for case PWA00803.

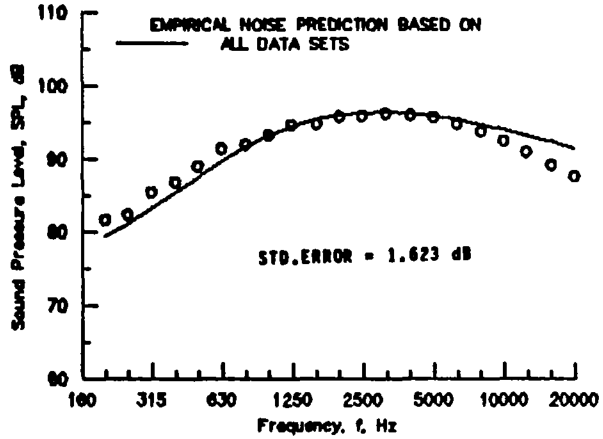

(b) Directivity angle = 120 degrees.

$V_e/C_\infty = .827 \qquad T_{t_e}/T_\infty = 1.257$

$V_2/V_1 = .595 \qquad T_{t_2}/T_{t_1} = .350$

$A_2/A_1 = 3.521$

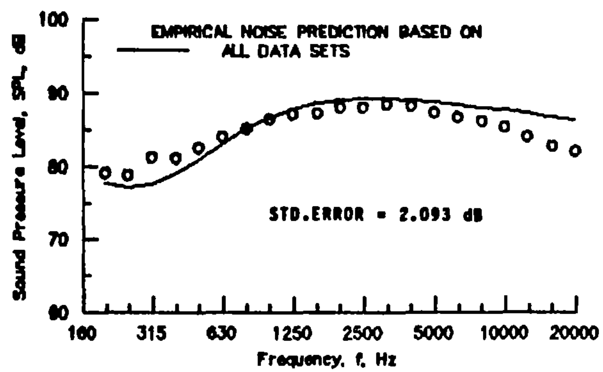

(a) Directivity angle = 90 degrees.

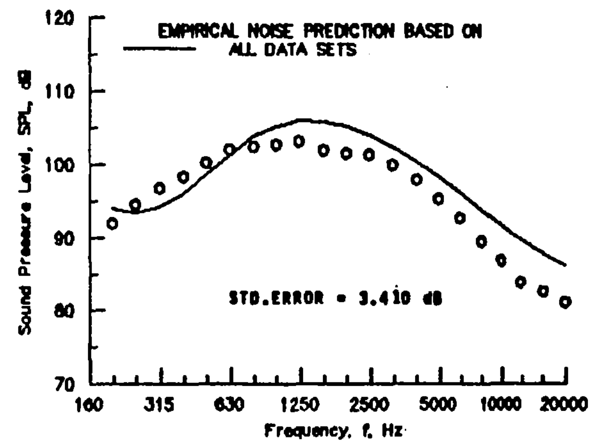

(c) Directivity angle = 150 degrees.

Figure 36. - Prediction method comparison for case SNCA0155.

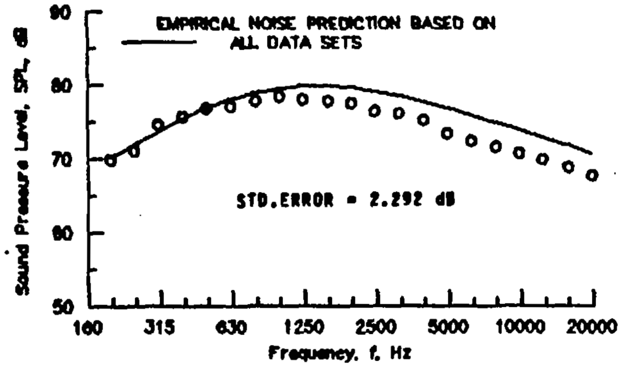

(b) Directivity angle = 120 degrees.

$V_e/C_\infty = .540 \qquad T_{t_e}/T_\infty = 1.321$

$V_2/V_1 = .701 \qquad T_{t_2}/T_{t_1} = .473$

$A_2/A_1 = 3.917$

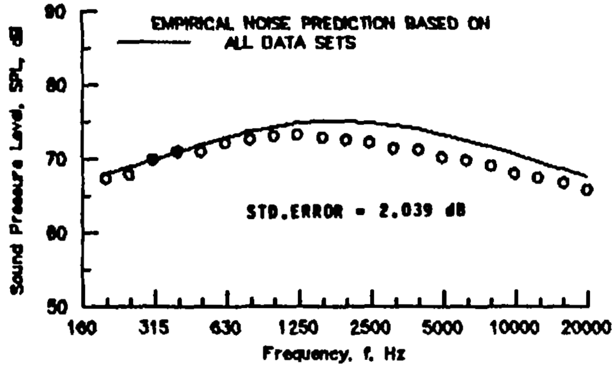

(a) Directivity angle = 90 degrees.

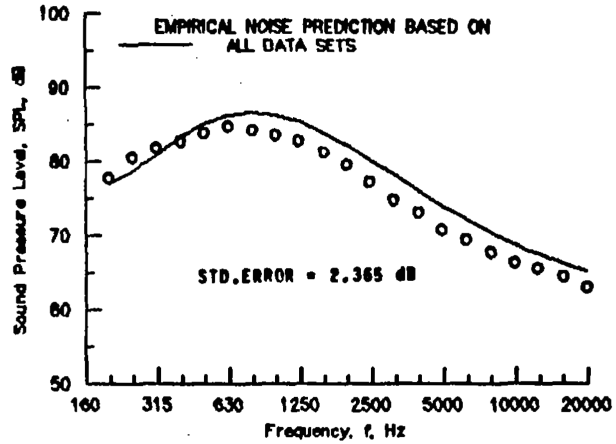

(c) Directivity angle = 150 degrees.

Figure 37. - Prediction method comparison for case SNCB0010.

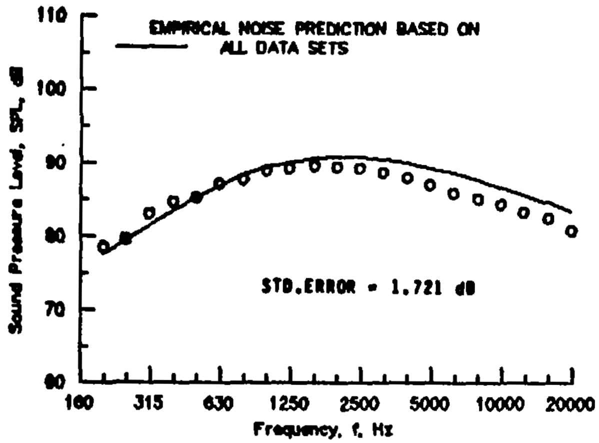

(b) Directivity angle = 120 degrees.

$V_e/C_\infty = .756 \qquad T_{t_e}/T_\infty = 1.372$

$V_2/V_1 = .706 \qquad T_{t_2}/T_{t_1} = .431$

$A_2/A_1 = 3.917$

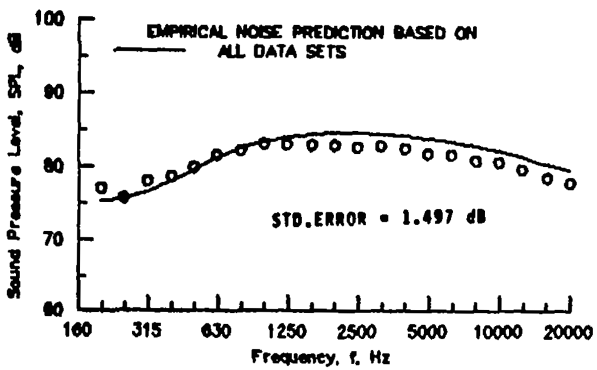

(a) Directivity angle = 90 degrees.

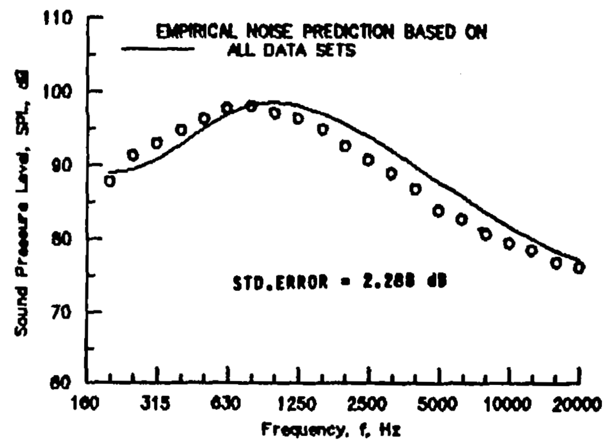

(c) Directivity angle = 150 degrees.

Figure 38. - Prediction method comparison for case SNCB0017.

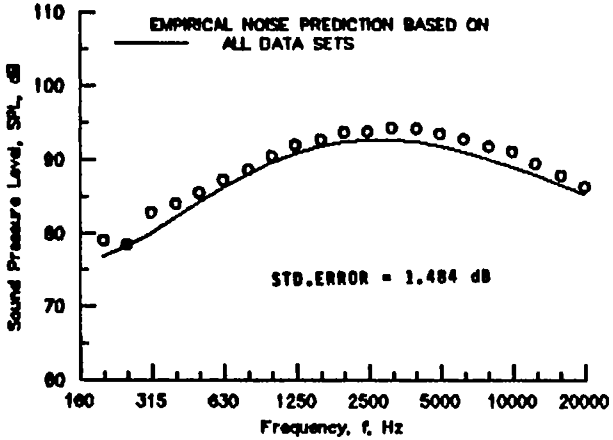

(b) Directivity angle = 120 degrees.

$V_e/C_\infty = .685 \qquad T_{t_e}/T_\infty = 1.563$

$V_2/V_1 = .402 \qquad T_{t_2}/T_{t_1} = .386$

$A_2/A_1 = 3.917$

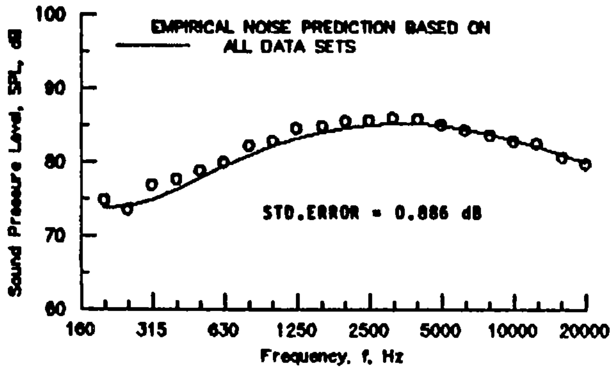

(a) Directivity angle = 90 degrees.

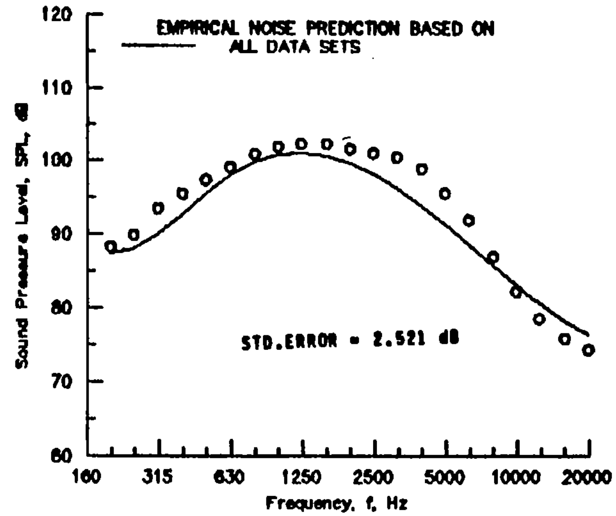

(c) Directivity angle = 150 degrees.

Figure 39. - Prediction method comparison for case SNCB0027.

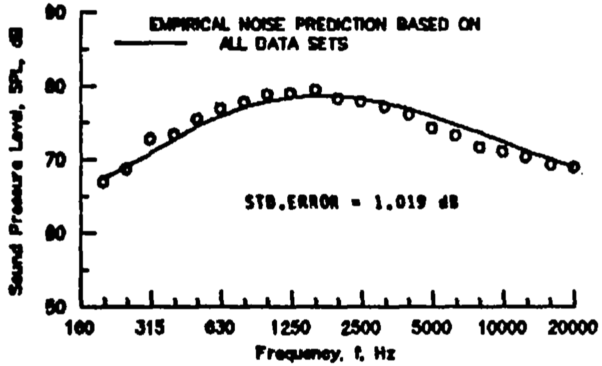

(b) Directivity angle = 120 degrees.

$V_e/C_\infty = .513 \qquad T_{t_e}/T_\infty = 1.466$

$V_2/V_1 = .597 \qquad T_{t_2}/T_{t_1} = .467$

$A_2/A_1 = 2.249$

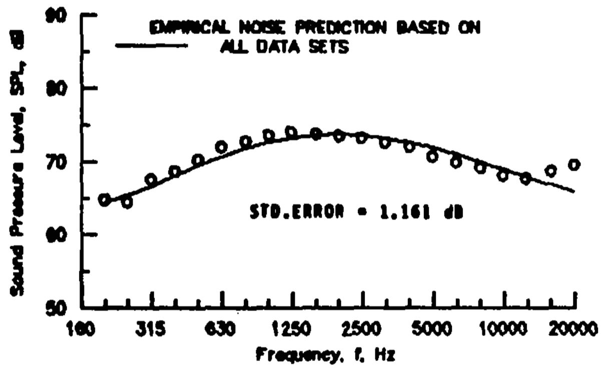

(a) Directivity angle = 90 degrees.

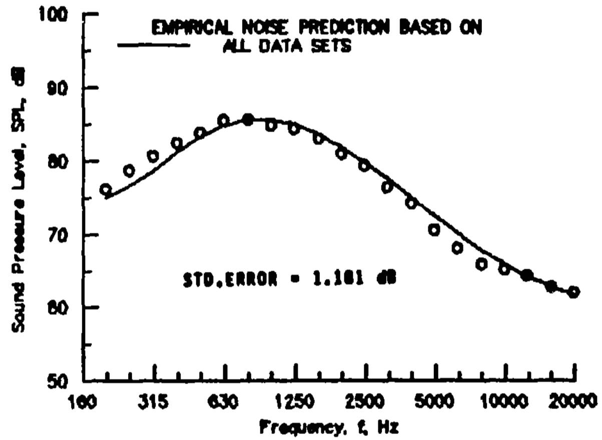

(c) Directivity angle = 150 degrees.

Figure 40. - Prediction method comparison for case SNCB0030.

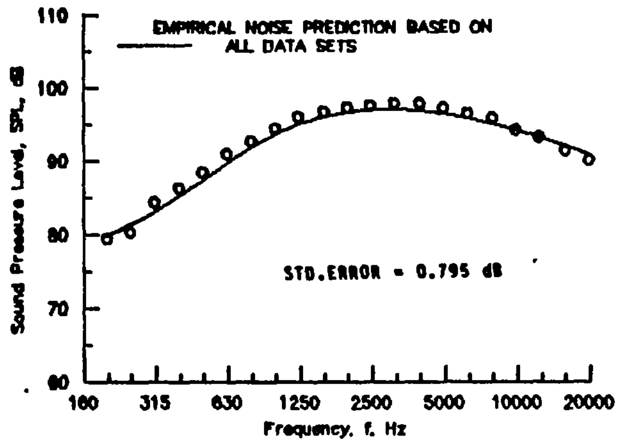

(b) Directivity angle = 120 degrees.

$V_e/C_\infty = .897$ $T_{t_e}/T_\infty = 1.588$

$V_2/V_1 = .601$ $T_{t_2}/T_{t_1} = .383$

$A_2/A_1 = 2.249$

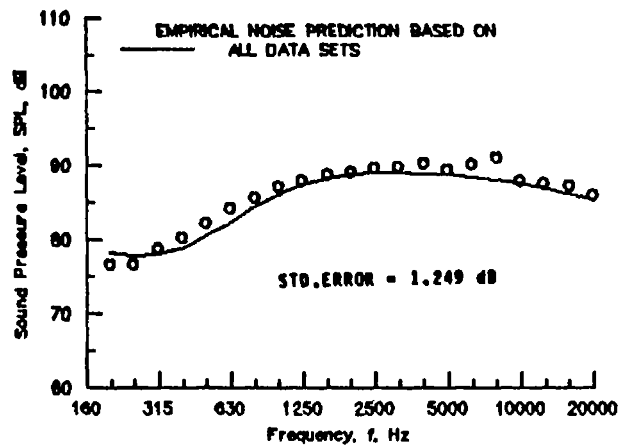

(a) Directivity angle = 90 degrees.

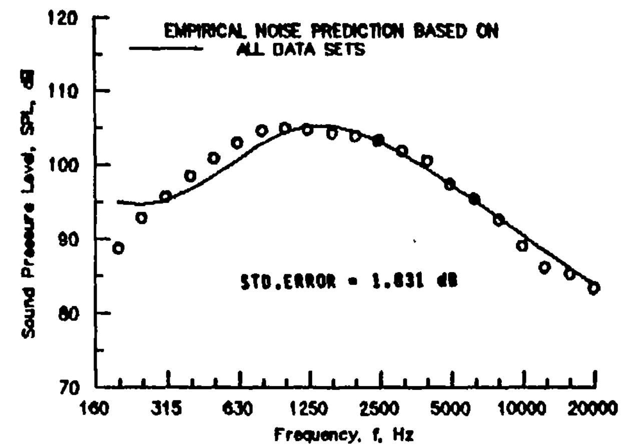

(c) Directivity angle = 150 degrees.

Figure 41. - Prediction method comparison for case SNCB0040.

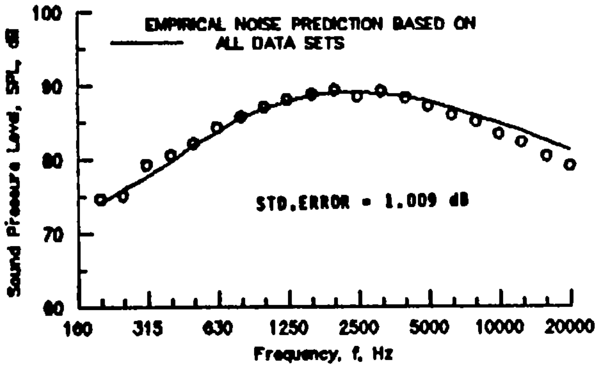

(b) Directivity angle = 120 degrees.

$V_e/C_\infty = .702 \qquad T_{t_e}/T_\infty = 1.524$

$V_2/V_1 = .591 \qquad T_{t_2}/T_{t_1} = .418$

$A_2/A_1 = 2.249$

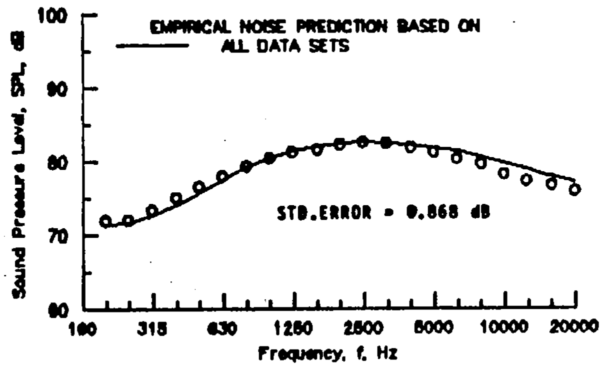

(a) Directivity angle = 90 degrees.

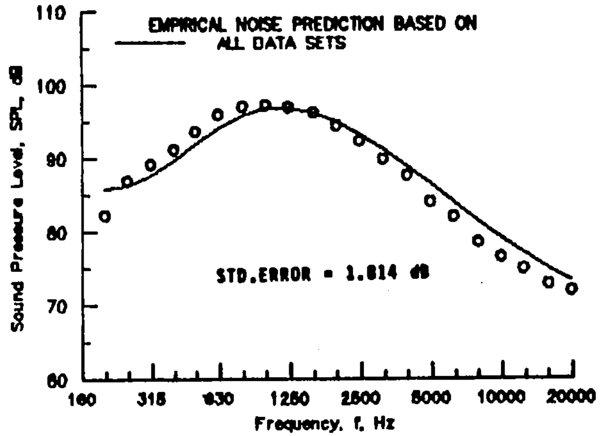

(c) Directivity angle = 150 degrees.

Figure 42. - Prediction method comparison for case SNCB0047.

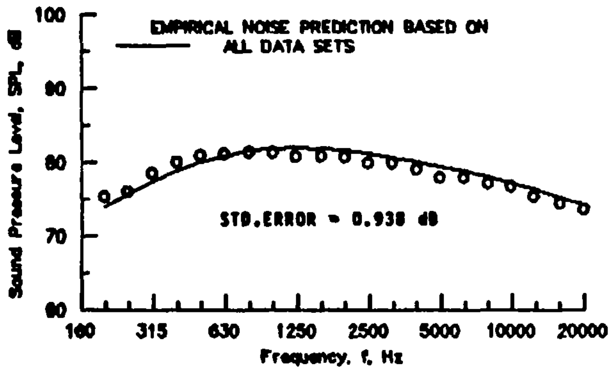

(b) Directivity angle = 120 degrees.

$$V_e/C_\infty = .594 \qquad T_{t_e}/T_\infty = 1.233$$

$$V_2/V_1 = .799 \qquad T_{t_2}/T_{t_1} = .470$$

$$A_2/A_1 = 6.093$$

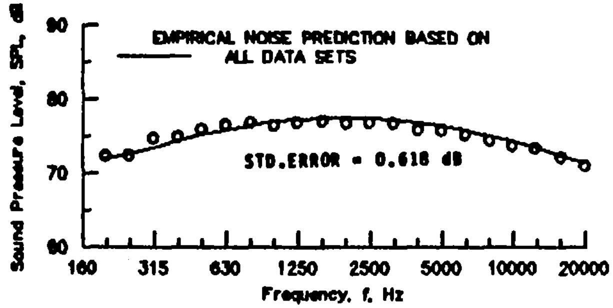

(a) Directivity angle = 90 degrees.

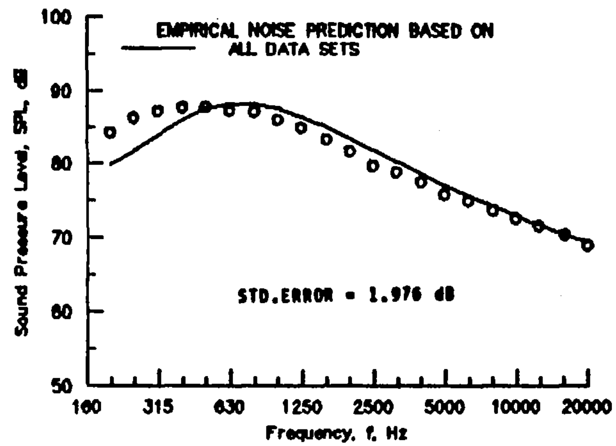

(c) Directivity angle = 150 degrees.

Figure 43. - Prediction method comparison for case SNCB0054.

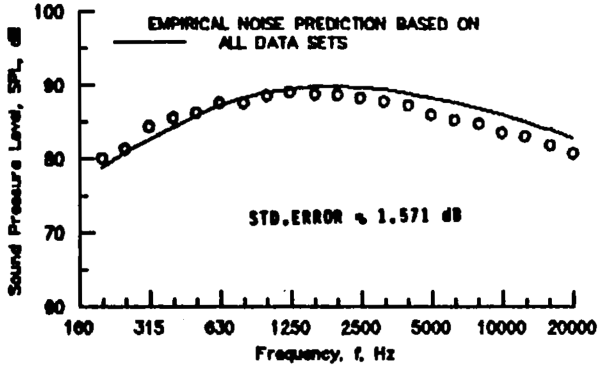

(b) Directivity angle = 120 degrees.

$V_e/C_\infty = .733$ $T_{t_e}/T_\infty = 1.275$

$V_2/V_1 = .695$ $T_{t_2}/T_{t_1} = .420$

$A_2/A_1 = 6.093$

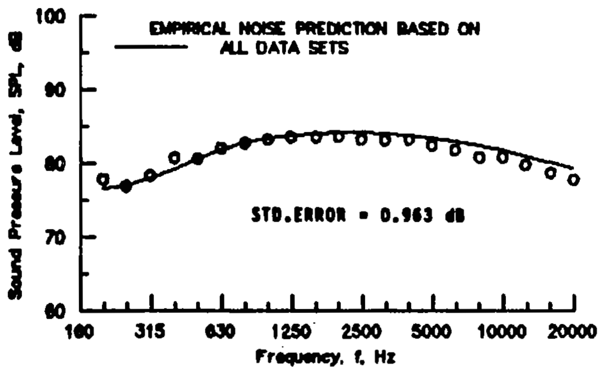

(a) Directivity angle = 90 degrees.

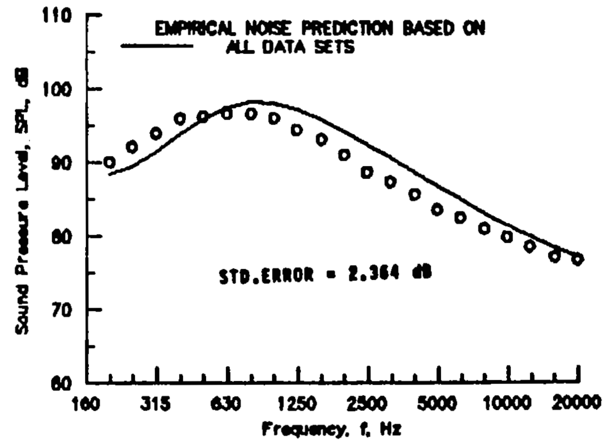

(c) Directivity angle = 150 degrees.

Figure 44. - Prediction method comparison for case SNCB0065.

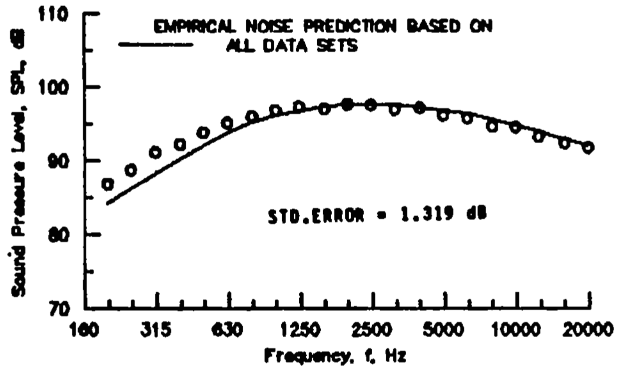

(b) Directivity angle = 120 degrees.

$$V_e/C_\infty = .943 \qquad T_{t_e}/T_\infty = 1.305$$

$$V_2/V_1 = .702 \qquad T_{t_2}/T_{t_1} = .384$$

$$A_2/A_1 = 6.093$$

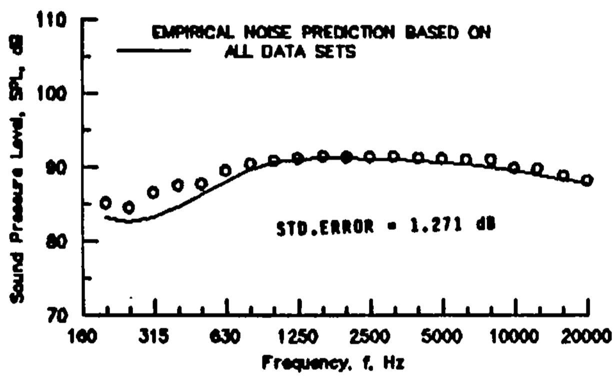

(a) Directivity angle = 90 degrees.

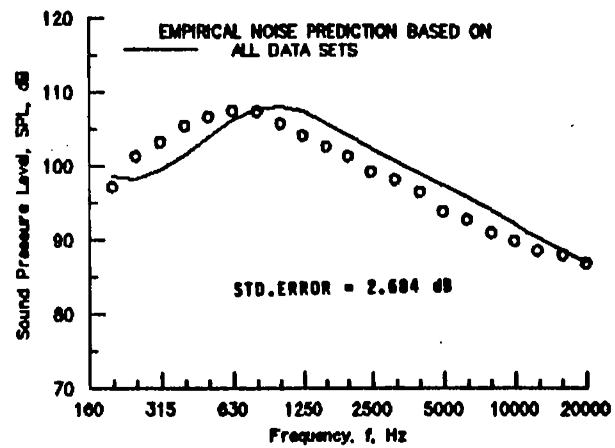

(c) Directivity angle = 150 degrees.

Figure 45. - Prediction method comparison for case SNCB0068.

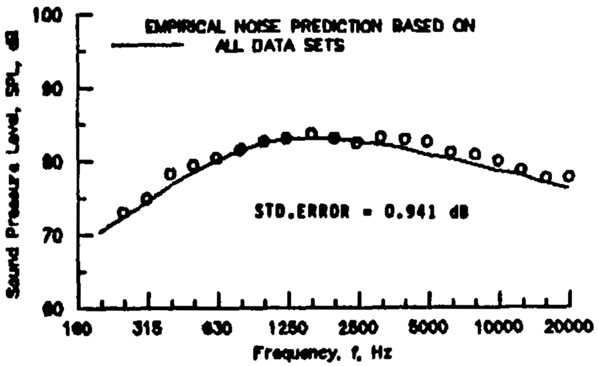

(b) Directivity angle = 120 degrees.

$V_e/C_\infty = .658 \qquad T_{t_e}/T_\infty = 1.687$

$V_2/V_1 = 1.016 \qquad T_{t_2}/T_{t_1} = 1.000$

$A_2/A_1 = 2.930$

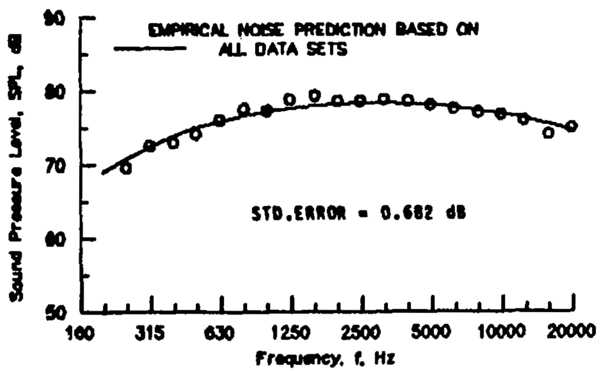

(a) Directivity angle = 90 degrees.

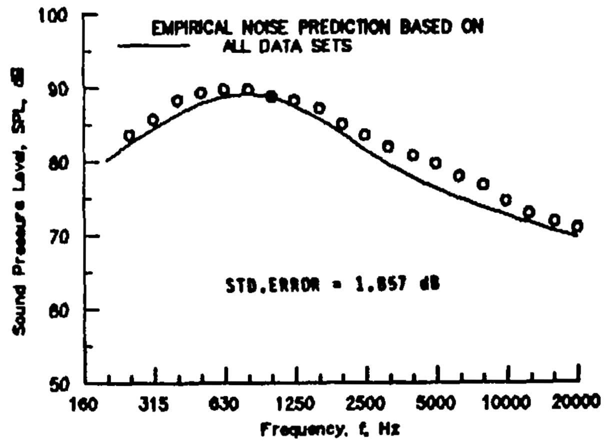

(c) Directivity angle = 150 degrees.

Figure 46. - Prediction method comparison for case LGCB0001.

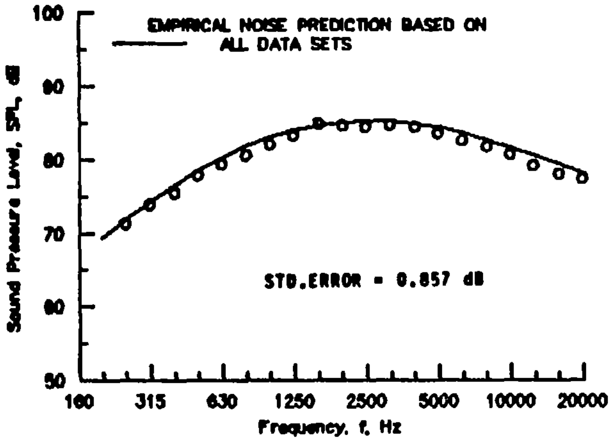

(b) Directivity angle = 120 degrees.

$V_e/C_\infty = .647$ $T_{t_e}/T_{\infty} = 1.497$

$V_2/V_1 = .491$ $T_{t_2}/T_{t_1} = .895$

$A_2/A_1 = 2.930$

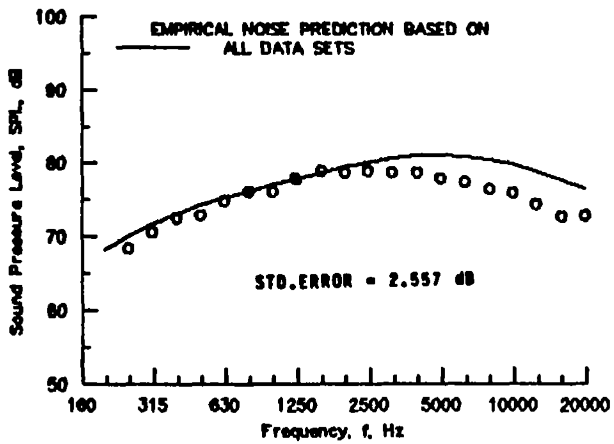

(a) Directivity angle = 90 degrees.

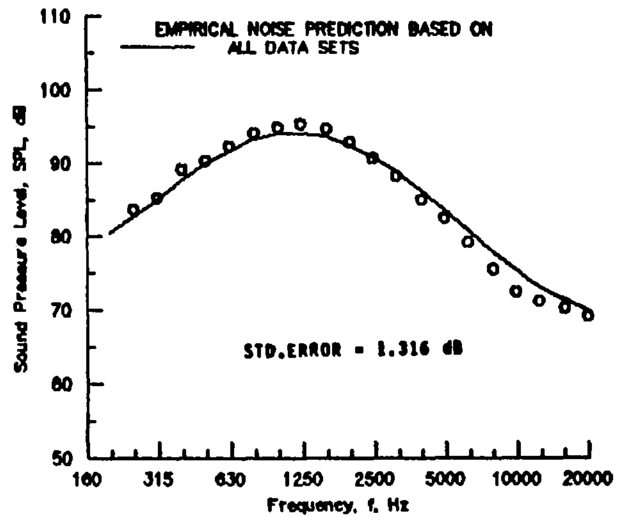

(c) Directivity angle = 150 degrees.

Figure 47. - Prediction method comparison for case LGCB0006.

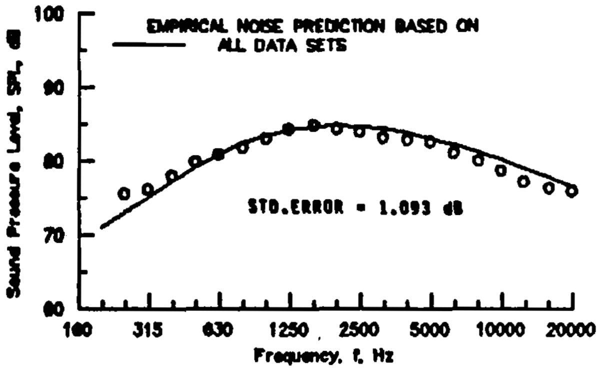

(b) Directivity angle = 120 degrees.

$V_e/C_\infty = .651 \qquad T_{t_e}/T_\infty = 1.648$

$V_2/V_1 = .671 \qquad T_{t_2}/T_{t_1} = .813$

$A_2/A_1 = 2.930$

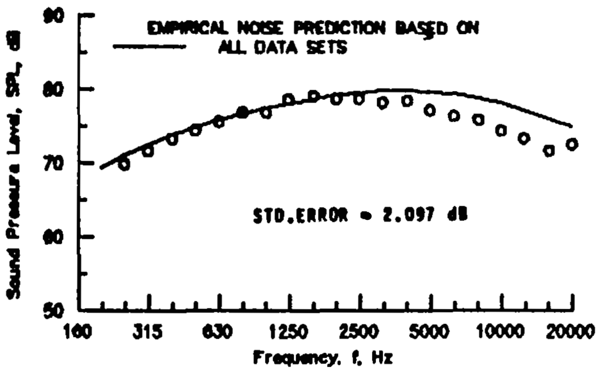

(a) Directivity angle = 90 degrees.

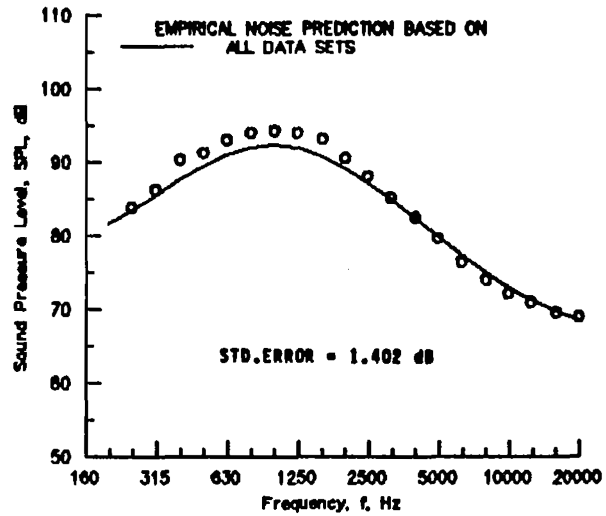

(c) Directivity angle = 150 degrees.

Figure 48. - Prediction method comparison for case LGCB0012.

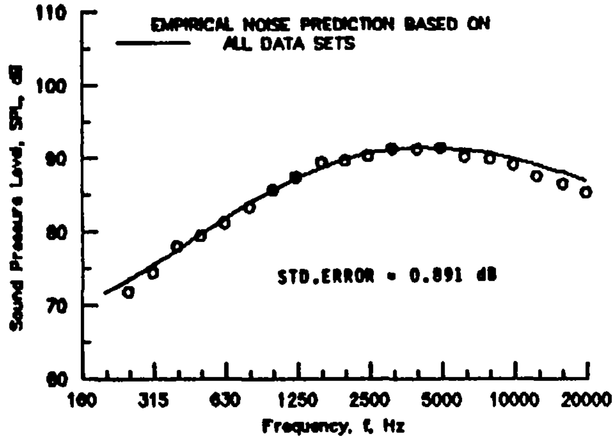

(b) Directivity angle = 120 degrees.

$V_e/C_\infty = .647$ $T_{t_e}/T_\infty = 1.365$

$V_2/V_1 = .284$ $T_{t_2}/T_{t_1} = .609$

$A_2/A_1 = 2.930$

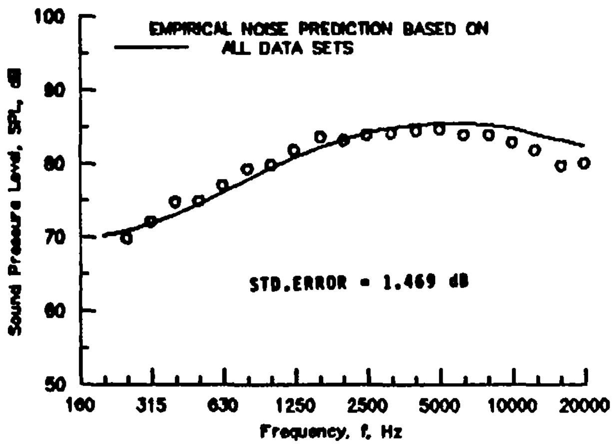

(a) Directivity angle = 90 degrees.

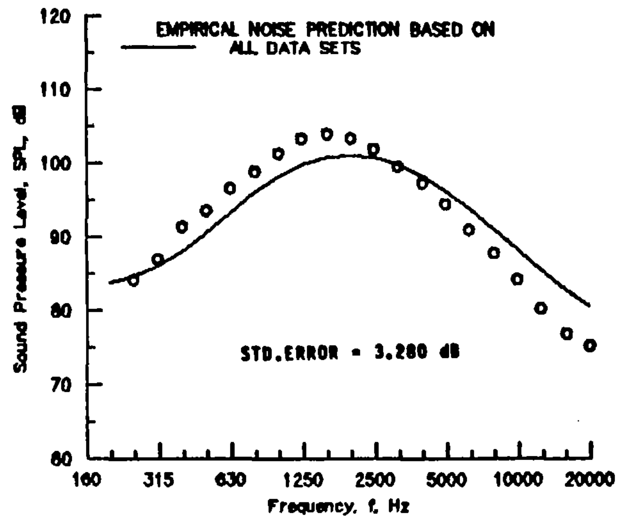

(c) Directivity angle = 150 degrees.

Figure 49. - Prediction method comparison for case LGCB0024.

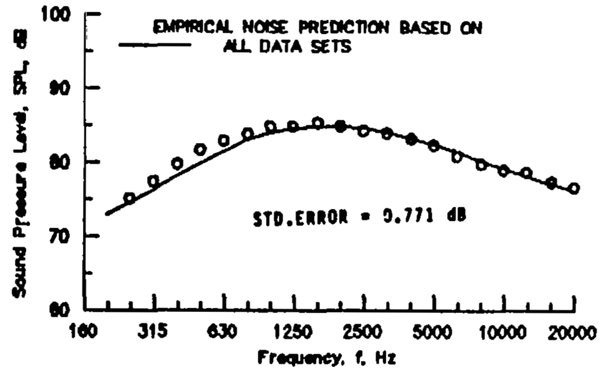

(b) Directivity angle = 120 degrees.

$V_e/C_\infty = .648$ $T_{t_e}/T_\infty = 1.691$

$V_2/V_1 = .919$ $T_{t_2}/T_{t_1} = .511$

$A_2/A_1 = 2.930$

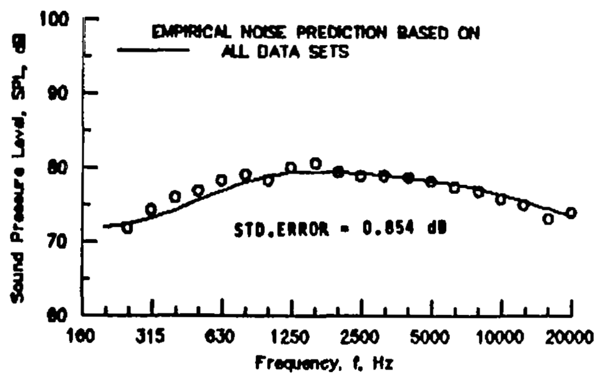

(a) Directivity angle = 90 degrees.

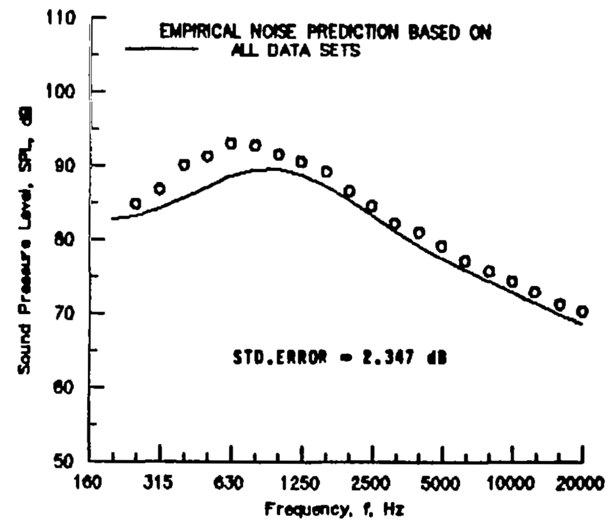

(c) Directivity angle = 150 degrees.

Figure 50. - Prediction method comparison for case LGCB0026.

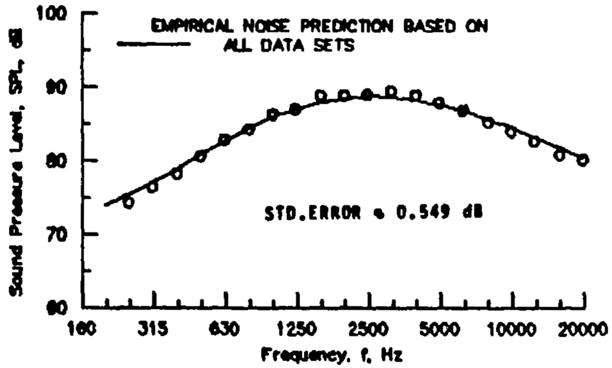

(b) Directivity angle = 120 degrees.

$$V_e/C_\infty = .642 \qquad T_{t_e}/T_\infty = 1.695$$

$$V_2/V_1 = .499 \qquad T_{t_2}/T_{t_1} = .478$$

$$A_2/A_1 = 2.930$$

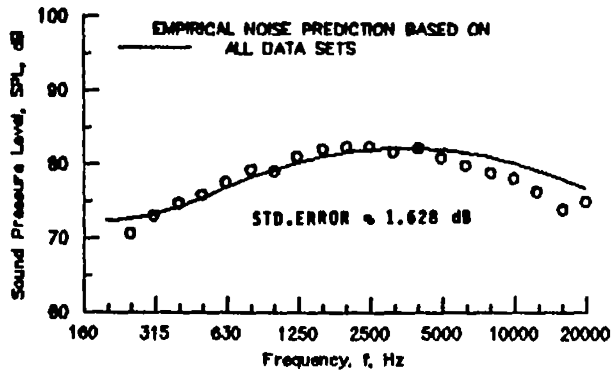

(a) Directivity angle = 90 degrees.

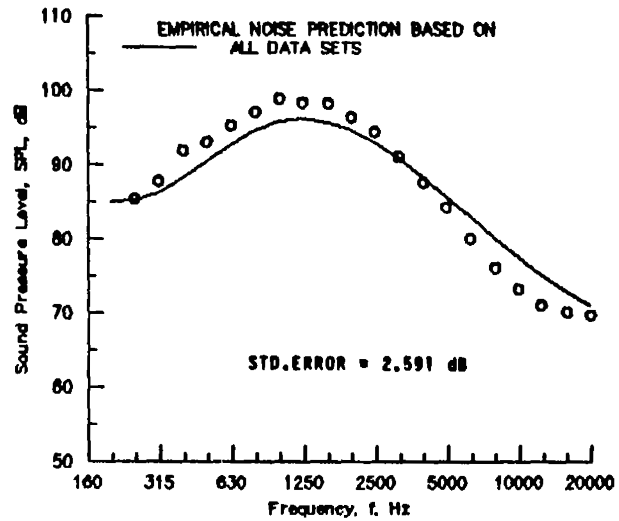

(c) Directivity angle = 150 degrees.

Figure 51. - Prediction method comparison for case LGCB0030.

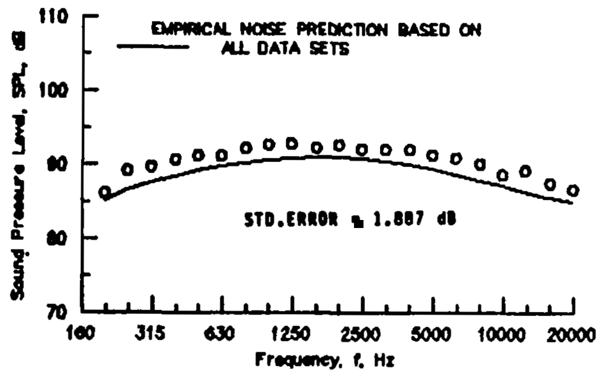

(b) Directivity angle = 115 degrees.

$V_e/C_\infty = .649$ $T_{t_e}/T_\infty = 1.003$

$V_2/V_1 = .992$ $T_{t_2}/T_{t_1} = 1.000$

$A_2/A_1 = 2.000$

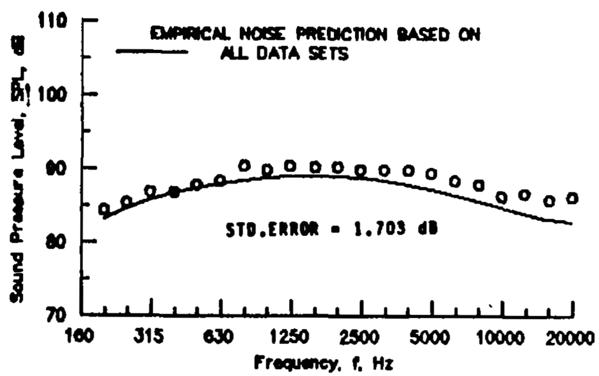

(a) Directivity angle = 95 degrees.

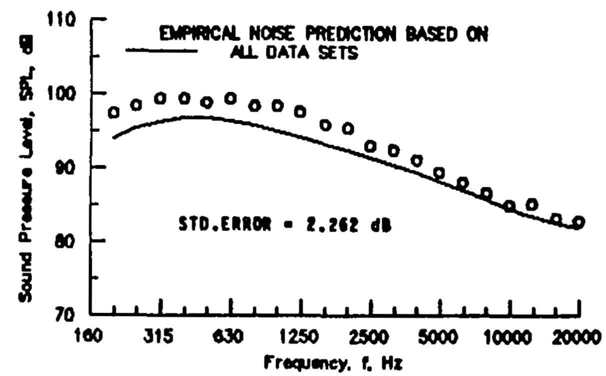

(c) Directivity angle = 148 degrees.

Figure 52. - Prediction method comparison for case LEW0243.

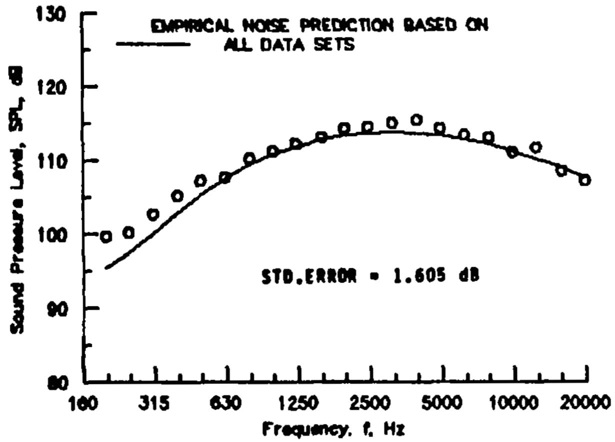

(b) Directivity angle = 115 degrees.

$V_e/C_\infty = .942 \qquad T_{t_e}/T_\infty = 1.926$

$V_2/V_1 = .365 \qquad T_{t_2}/T_{t_1} = .250$

$A_2/A_1 = 2.000$

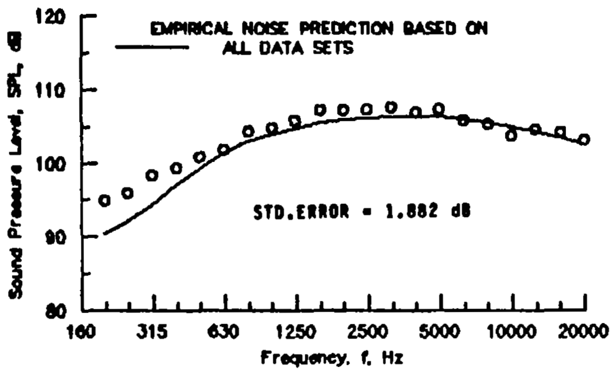

(a) Directivity angle = 95 degrees.

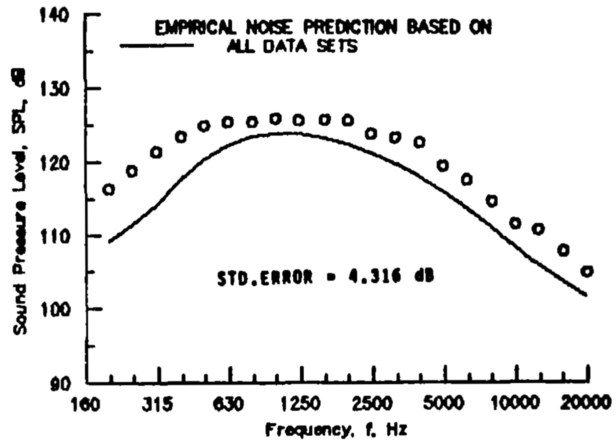

(c) Directivity angle = 148 degrees.

Figure 53. - Prediction method comparison for case LEW0245.

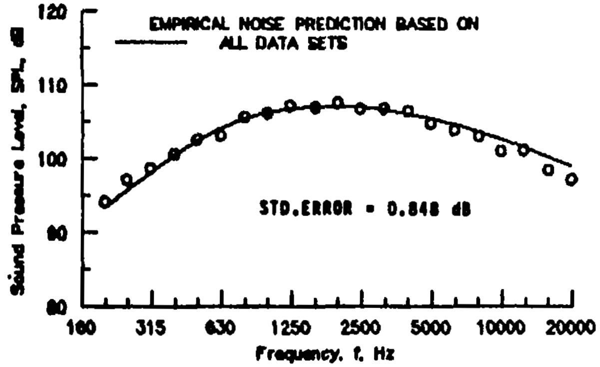

(b) Directivity angle = 115 degrees.

$V_e/C_\infty = .837$ $T_{t_e}/T_\infty = 1.577$

$V_2/V_1 = .478$ $T_{t_2}/T_{t_1} = .339$

$A_2/A_1 = 2.000$

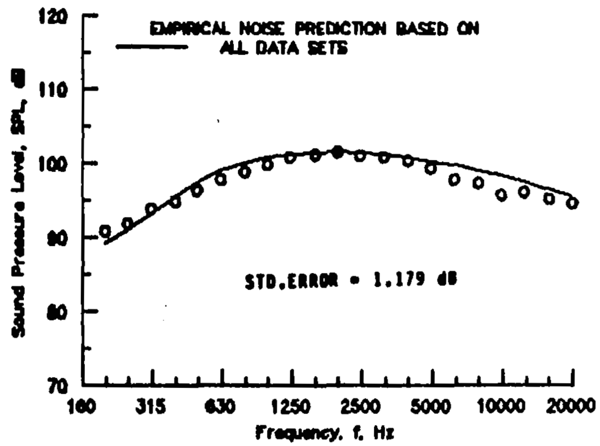

(a) Directivity angle = 95 degrees.

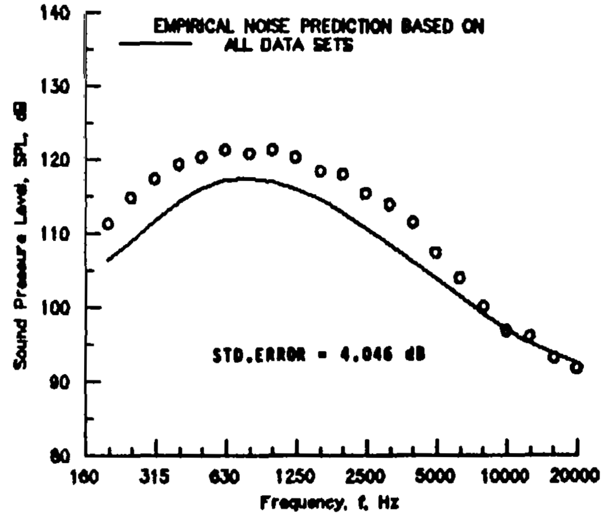

(c) Directivity angle = 148 degrees.

Figure 54. - Prediction method comparison for case LEW0248.

1. Report No.	2. Government Accession No.	3. Recipient's Catalog No.
NASA CR-3786		

4. Title and Subtitle	5. Report Date
AN EMPIRICAL METHOD FOR PREDICTING THE MIXING NOISE LEVELS OF SUBSONIC CIRCULAR AND COAXIAL JETS	February 1984
	6. Performing Organization Code
7. Author(s)	8. Performing Organization Report No.
James W. Russell	
	10. Work Unit No.
9. Performing Organization Name and Address	
Kentron International, Inc. Aerospace Technologies Division Hampton, Virginia 23666	11. Contract or Grant No. NAS1-16000
	13. Type of Report and Period Covered
12. Sponsoring Agency Name and Address	Contractor Report
National Aeronautics and Space Administration Washington, DC 20546	14. Sponsoring Agency Code

15. Supplementary Notes

Langley Technical Monitor: William E. Zorumski

16. Abstract

This report presents an empirical method for predicting the static free field source noise levels of subsonic circular and coaxial jet flow streams. The method was developed from an extensive data base of 817 jet tests obtained from five different government and industry sources in three nations.

The prediction method defines the jet noise in terms of four components which are overall power level, power spectrum level, directivity index, and relative spectrum level. The values of these noise level components are defined on a grid consisting of seven frequency parameter values (Strouhal numbers) and seven directivity angles. The value of the noise level at each of these grid points is called a noise level coordinate and were defined as a function of five jet exhaust flow state parameters which are equivalent jet velocity, equivalent jet total temperature, the velocity ratio (outer stream to inner stream), temperature ratio, and area ratio. The functions were obtained by curve fitting in a least squares sense the noise level coordinates from the data base in a five dimensional flow state space using a third order Taylor series. The noise level coordinates define the component noise levels for all frequencies and directivities through a bicubic spline function.

The empirical method here reduces the data base of approximately 200,000 sound pressure level measurements to a table of 2300 constants, which can be used for predicting the jet noise. Because this prediction method is derived from a least squares approximation to the data base, the mean error is 0 dB. The standard error of the prediction is less than 1.0 dB at the freqencies and directivities where the peak noise levels occur.

17. Key Words (Suggested by Author(s))	18. Distribution Statement
Jet noise Noise prediction Noise data base	Unclassified - Unlimited Subject Category 71

19. Security Classif. (of this report)	20. Security Classif. (of this page)	21. No. of Pages	22. Price*
Unclassified	Unclassified	123	A06

*For sale by the National Technical Information Service, Springfield, Virginia 22161